RIVISTA DEL NUOVO CIMENTO Vol. 38, N. 9 2015
DOI 10.1393/ncr/i2015-10116-x

Status and perspectives of experimental studies on hypernuclear weak decays

E. Botta(1)(2)(*), T. Bressani(2), S. Bufalino(1)(2) and A. Feliciello(2)

(1) *Dipartimento di Fisica, Università di Torino - Torino, Italy*
(2) *INFN, Sezione di Torino - Torino, Italy*

received 10 June 2015

Summary. — From the first beginning the weak decay of Λ-hypernuclei has been considered a very interesting physics case, since its study could shed light on several topics in nuclear and particle physics, among which the $\Lambda N \to NN$ four-baryon weak interaction not otherwise accessible. However, only in the last decade a substantial series of reliable experimental data samples has been produced thanks to the synergic effort of dedicated facilities at some laboratories in the world. The existing pattern of data on lifetimes, partial decay widths for mesonic and non-mesonic decay (both one- and two-nucleon induced) and energy spectra and correlations of the emitted particles is reviewed and compared with existing theoretical predictions. Updated tables and plots summarizing the existing experimental information are presented. For each item a brief account of possible new experimental efforts, approved, planned or futuristic is given. From these analyses the full pattern of partial decay widths for ${}^{4}_{\Lambda}$He, ${}^{5}_{\Lambda}$He, ${}^{11}_{\Lambda}$B and ${}^{12}_{\Lambda}$C is discussed. Rare decay channels and polarization studies are also briefly analyzed.

PACS 21.80.+a – Hypernuclei.
PACS 25.80.Pw – Hyperon-induced reactions.

(*) E-mail: elena.botta@to.infn.it

1. – Introduction

The first strange particle was observed in 1947 [1], the hypothesis of an associated production of the newly discovered particles was put forward in 1951-1952 [2, 3] and in 1953 M. Danysz and J. Pniewski, in the analysis of events recorded by a stack of photographic emulsions, interpreted an event with unusual features as signature of a nuclear fragment containing one of those still mysterious particles (known today as Λ-hyperon) [4]. It was the first example of what we call now a Λ-hypernucleus (shortened in hypernucleus in the following). In the same year, Gell-Mann introduced the concept and the name of strangeness [5]. We recall these quite well-known dates in the history of particle physics for the sake of emphasizing the intuition and the intellectual courage of the authors of ref. [4] in accepting very novel findings and concepts of particle physics and applying them to the study of other more complex systems, the nuclei.

It was clear from the first beginning that hypernuclear physics was interfacing particle and nuclear physics in a very challenging way, by making possible the observation of physical effects not otherwise clear in any of the two fields. As in many other cases, theoretical speculations and predictions anticipated their experimental evidence; actually, for hypernuclear physics several decades passed before their experimental verification. This was due to the necessary technological breakthroughs in particles accelerators, in detector performances and reliability and in computer tools.

Besides several interesting observations on light few-body systems, the most spectacular contribution to nuclear physics is, to our opinion, the experimental confirmation that bound nuclear systems do behave as the independent particle model predicts. The missing-mass spectroscopy with the (π^+, K^+) reaction on heavy nuclei showed the clear existence of all states corresponding to the Λ-hyperon bound in the potential well due

to the nucleons of the hypernucleus core nucleus. In ordinary nuclei, even with the best state-of-art experimental techniques, it was never possible to observe simultaneously the existence of nucleons in more than two well-defined states, corresponding moreover only to the most external orbits. This is a consequence of the fragmentation of the single-particle states intensity due to various effects; the experimental observation is then a continuous spectrum, without any structure. A detailed description of the results of hypernuclei missing-mass spectroscopy is given in the review paper of ref. [6]. We notice that these measurements were made possible by the operation of powerful magnetic spectrometers that will be outlined in sect. **3**.

With respect to particle physics, it was clear from the first beginning that a precise study of hypernuclei spectroscopy and of their decay modes was the only way to obtain quantitative information on both strong and weak interaction in the ΛN system. Direct measurements are in fact impossible due to the non-existence of suitable Λ-hyperon beams. Hypernuclei may then be considered as a laboratory for the study of the ΛN interaction. p-shell hypernuclei high-resolution γ-ray spectroscopy allowed for the first time the determination of the different spin components of the ΛN strong interaction, and the test of the theoretical approaches proposed on the subject. More details may be found in refs. [6-8]. From the experimental side, we remark that these measurements were possible by coupling large arrays of hyperpure Ge detectors to magnetic spectrometers needed to select and identify the hypernuclei under study.

It is remarkable that as early as in 1953 it was pointed out [9] that if the π emitted from the weak vertex Λ-$N\pi$ (in reality the Λ was still named V-particle!) is virtual, then it can be absorbed in the nuclear medium giving origin to $\Lambda N \to NN$ four-baryon weak interactions, very hard, if not impossible, to be studied in free space. The suggestion spurred considerable interest, mainly on the theoretical side, despite scarce and poor quality experimental information. The situation did not change for some decades, since it was necessary to produce abundantly and to identify hypernuclei and then to examine the spectra of charged and neutral particles emitted in their decay. This goal was achieved in the last ten years, allowing a first determination of the observables which provide a quite complete and consistent pattern. The experimental errors are still sometimes large, and further more precise experiments are needed.

This review contains an updated collection of all the available experimental data, with new summary tables and figures, and hints for future experiments. A review of experimental results and of theoretical models describing the Weak Decay (WD) of hypernuclei before 1990 can be found in ref. [10]. More recent review papers on the results obtained from 1990 on and on the development of the theoretical interpretations can be found in refs. [11-15].

The paper is organized as follows. In sect. **2** we summarize definitions and major issues concerning the WD of hypernuclei. Section **3** describes in short some experimental facilities, in particular the two that produced the largest amount (70%) of the available data. Sections **4**, **5** and **6** report in detail all the available experimental data respectively for the lifetimes of hypernuclei, their Mesonic Weak Decay (MWD) and Non-Mesonic Weak Decay (NMWD). For each item a short account of the relevant theoretical predictions is given, as well as some ideas about possible future experimental improvements. Section **7** describes in short some unusual decays of hypernuclei and sect. **8** is dedicated to a review of the data for the hypernuclei for which a complete mapping of the partial decay widths may be deduced. Section **9** is dealing with the experimental effort for the polarization measurements. Section **10** contains the summary and the conclusions of the review.

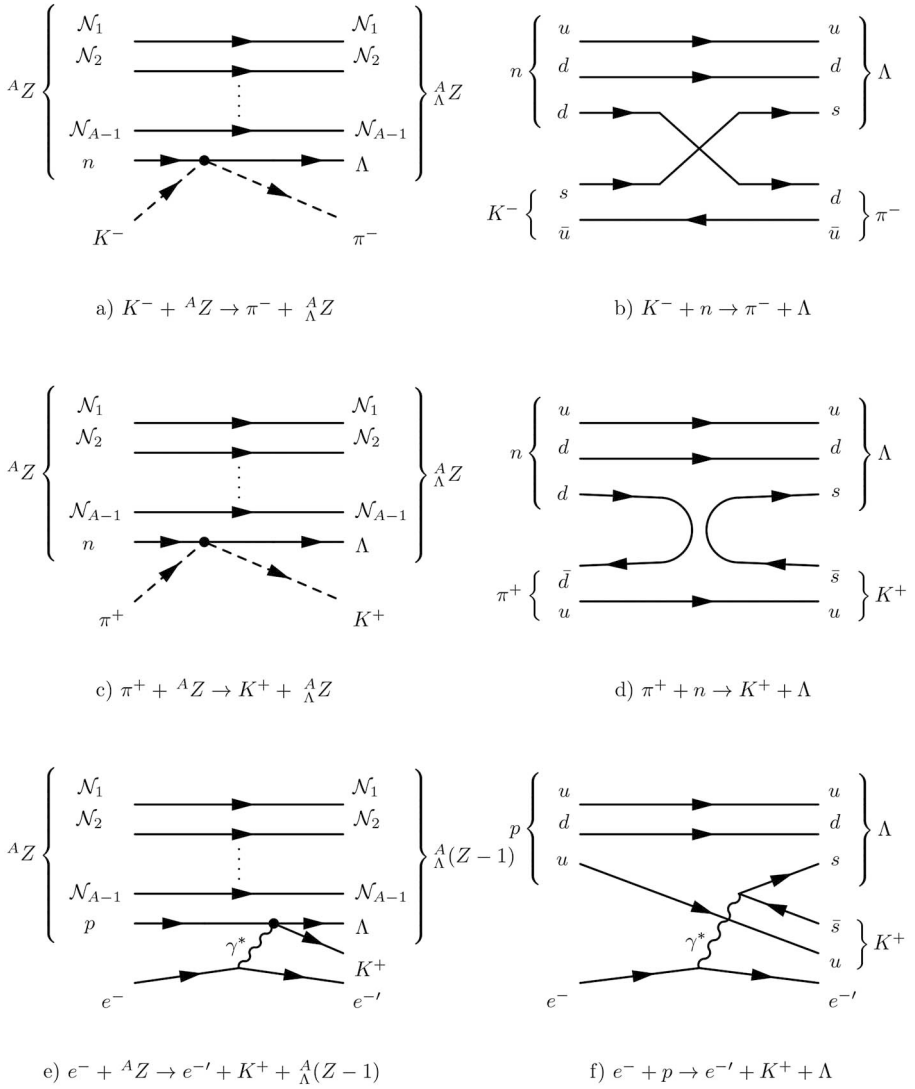

Fig. 1. – Diagrams for the production reactions of hypernuclei (left) and quark-flow diagrams for the corresponding elementary reactions (right). a) "strangeness exchange", b) $K^- + n \to \pi^- + \Lambda$; c) "associated production", d) $\pi^+ + n \to K^+ + \Lambda$; e) electroproduction, f) $e^- + p \to e^{-\prime} + K^+ + \Lambda$.

2. – Essentials of hypernuclear weak decays

Even though hypernuclei can be produced by a variety of reactions, the present bulk of experimental information on spectroscopy and WD of hypernuclei comes from two-body reactions producing a Λ on a nuclear target. They are, following the chronological realizations:

a) The "strangeness exchange" reaction:

$$K^- + {}^A Z \to \pi^- + {}^A_\Lambda Z, \tag{1}$$

in which ${}^A Z$ indicates the target nucleus of mass number A and atomic number Z and ${}^A_\Lambda Z$ the produced hypernucleus with the corresponding A and Z numbers. The associated diagram is represented in fig. 1a); the reaction can be seen as a transfer of the s-quark from the incident meson to the struck baryon, as represented in the quark-flow diagram of fig. 1b).

b) The "associated production" reaction:

$$\pi^+ + {}^A Z \to K^+ + {}^A_\Lambda Z, \tag{2}$$

with the same symbols meaning as in (1). The corresponding diagram is represented in fig. 1c); the reaction proceeds by the creation of a $(s\bar{s})$ pair by the incident meson, as represented in the quark-flow diagram of fig. 1d).

c) The electroproduction of strangeness on protons in the very forward direction:

$$e + {}^A Z \to e' + K^+ + {}^A_\Lambda (Z-1), \tag{3}$$

exploited quite recently. The corresponding diagram is shown in fig. 1e). It must be noticed that the virtual photon γ^* associated to the elementary reaction $e+p \to e' + K^+ + \Lambda$ can be regarded as quasi-real. The quark-flow diagram representing this last reaction is shown by fig. 1f).

More details on the features of these production reactions can be found in [15]. We recall here only that the strangeness-exchange reaction (1) is exoenergetic, with Q values of (170–180) MeV, depending on the binding energy of the specific $({}^A Z,\ {}^A_\Lambda Z)$ system. On the contrary, the associated production reaction (2) is endoenergetic, with Q-values of $(-530 \div -540)$ MeV. The electroproduction (3) has a similar feature.

When a hypernucleus is excited above the particle emission threshold it decays dominantly by the strong interaction via single or cluster nucleon emission, the remaining strange nuclear system then de-excites to its ground state through electromagnetic transitions. A hypernucleus in the ground state decays to non-strange systems through the MWD and NMWD mechanisms. In MWD the Λ-hyperon decays into $N\pi$ in the nuclear medium similarly to the main decay modes in free space ($\Lambda_{\text{free}} \to p + \pi^- + 37.8\,\text{MeV}$, branching ratio BR $= (63.9 \pm 0.5)\%$, $\Lambda_{\text{free}} \to n + \pi^0 + 41.1\,\text{MeV}$, BR $= (35.8 \pm 0.5)\%$, lifetime $\tau_\Lambda = (263.2 \pm 2.0)$ ps [16]) and the following decays occur:

$$ {}^A_\Lambda Z \to {}^A(Z+1) + \pi^- \quad (\Gamma_{\pi^-}), \tag{4}$$

$$ {}^A_\Lambda Z \to {}^A Z + \pi^0 \quad (\Gamma_{\pi^0}). \tag{5}$$

${}^A(Z+1)$ and ${}^A Z$ are the residual nuclear system(s) that may consist of a single nucleus in the ground state, in the simplest case, or in a low-lying excited state or in two or more bodies, eventually in excited states. The Γ's stand for the partial decay widths. The momenta carried by the nucleons emitted in the decay at rest of a free Λ are of the order of 100 MeV/c. Inside a hypernucleus the Binding Energy (BE) of the Λ (~ 3 MeV

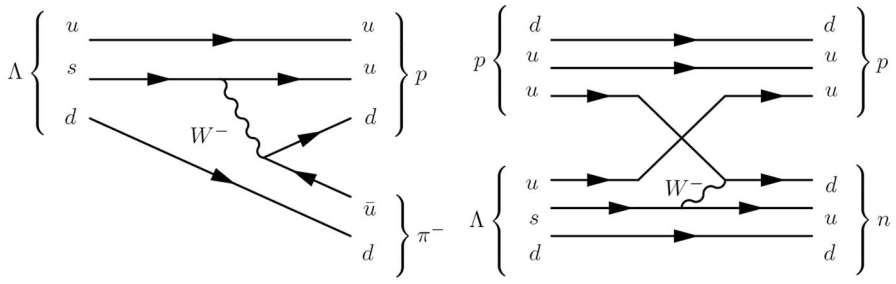

a) mesonic decay b) non-mesonic decay

Fig. 2. – Quark-flow diagrams for a) mesonic and b) non-mesonic decay of Λ in a hypernucleus.

for ${}^{5}_{\Lambda}$He, $\sim 11\,\mathrm{MeV}$ for ${}^{12}_{\Lambda}$C, $\sim 27\,\mathrm{MeV}$ for ${}^{208}_{\Lambda}$Pb) further reduces the energy available to the final-state particles. MWD is thus suppressed in hypernuclei with respect to the free-space decay due to the Pauli principle, since the momentum of the emitted nucleon is by far smaller than the nuclear Fermi momentum ($k_F \sim 270\,\mathrm{MeV}/c$) in all hypernuclei except for the lightest, s-shell, ones. The MWD width Γ_M is obviously defined as

$$\Gamma_M = \Gamma_{\pi^-} + \Gamma_{\pi^0}. \tag{6}$$

In principle it should be possible to add in eq. (6) a Γ_{π^+} term as the result of additional multibody processes such as $\Lambda p \to nn\pi^+$ (sometimes referred to as nucleon-induced pionic emission). Since this contribution is negligible, we will not consider it in the general approach, but we will briefly discuss it in sect. **7**.

Γ_M is the most important decay width for the s-shell hypernuclei, it remains quite important, at the level of (30–10)% of the total decay width, for p-shell hypernuclei and it becomes negligible for medium-, high-A hypernuclei where NMWD channels are dominant. These channels are instead linked to the occurrence of weak interactions of the constituent Λ hyperon with nucleons of the hypernucleus nuclear core. The simplest ones are $\Lambda N \to NN$ and usually are referred to as proton-induced, in the case of a $\Lambda p \to np$ elementary reaction, with decay width Γ_p, and neutron-induced in the case of $\Lambda n \to nn$, with the corresponding Γ_n.

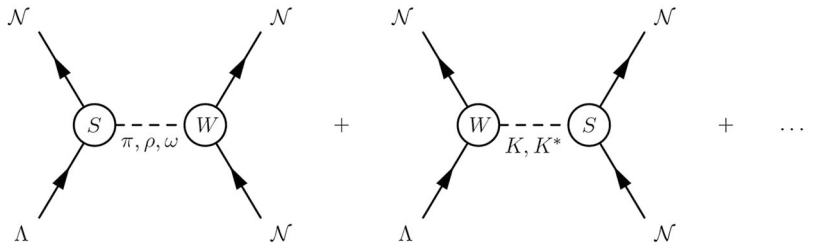

Fig. 3. – Feynman diagrams of the meson exchange description of one-nucleon–induced NMWD of hypernuclei.

Before continuing the survey of the definition of the quantities discussed in the following, we would like to put forward a few remarks concerning an elegant attempt to describe at an elementary level MWD and NMWD of hypernuclei. The MWD can be described as due to the exchange of a W boson between quarks, see fig. 2a). It is possible to envisage a similar mechanism for describing the weak interaction $\Lambda N \to NN$, see fig. 2b). However, severe strong interaction modifications to the $(V-A)$ form of the Hamiltonian describing the quark-W interaction, difficult to evaluate, drove the theoretical effort towards an alternative viewpoint for describing the NMWD in terms of mesons exchange. The relevant diagrams are reported in fig. 3 and the description will be discussed in sect. **6**.

By using the same naming conventions as for eqs. (4) and (5) the proton-induced NMWD may be written as

$$(7) \qquad {}^{A}_{\Lambda}Z \to {}^{A-2}(Z-1) + n + p \quad (\Gamma_p),$$

and the neutron-induced one as

$$(8) \qquad {}^{A}_{\Lambda}Z \to {}^{A-2}Z + n + n \quad (\Gamma_n).$$

Quite later, a further NMWD channel was predicted, corresponding to the elementary $\Lambda(NN) \to n(NN)$ weak interaction on a pair of correlated nucleons in the nuclear core of the hypernucleus [17], with a corresponding decay width Γ_{2N}. Γ_{2N} may be further split into three branches corresponding to the three projections of the total isospin $I = 1$ of the NN pair, with the related Γ_{pp}, Γ_{pn} and Γ_{nn}. Using always the same naming conventions, the $2N$-induced NMWD may be written as

$$(9) \qquad {}^{A}_{\Lambda}Z \to {}^{A-3}(Z-2) + n + p + p \qquad (\Gamma_{pp}),$$

$$(10) \qquad {}^{A}_{\Lambda}Z \to {}^{A-3}(Z-1) + n + n + p \qquad (\Gamma_{np}),$$

$$(11) \qquad {}^{A}_{\Lambda}Z \to {}^{A-3}Z + n + n + n \qquad (\Gamma_{nn}).$$

It must be underlined that microscopic calculations [18] predict that the decay (10) corresponding to the $I_3 = 0$ component (np) is the dominant one; the ratios among equations (9), (10) and (11) are in fact $(0.12 : 0.83 : 0.05)$. The existence of the $2N$-induced NMWD was assessed experimentally very recently, although with consistent errors. For this reason Γ_{np}, which is actually measured, is often approximated with Γ_{2N}. Contrarily to the multi-body Γ_{π^+} which does not contribute significantly to Γ_M, Γ_{2N} was found to be $\sim 40\%$ of Γ_p and its inclusion allowed to solve the so-called "Γ_n/Γ_p puzzle" existing a few years ago among theoretical predictions and experimental data. We will discuss in detail these issues in sect. **6**.

In conclusion, neglecting $3N$- or more nucleon-induced decays, we may define the NMWD width as

$$(12) \qquad \Gamma_{NM} = \Gamma_{1N} + \Gamma_{2N}$$

in which

$$(13) \qquad \Gamma_{1N} = \Gamma_p + \Gamma_n$$

and

$$\Gamma_{2N} = \Gamma_{pp} + \Gamma_{np} + \Gamma_{nn} \approx \Gamma_{np}. \tag{14}$$

The NMWD mode can occur only in nuclei; the Q-value of the elementary reactions $\Lambda N \to nN$ and $\Lambda(NN) \to n(NN)$ ($\sim 175\,\mathrm{MeV}$) is high enough to avoid any Pauli blocking effect on the final-state nucleons. For the $1N$-induced process, due to the point-like feature of the weak interaction, the outgoing nucleons are back-to-back emitted, with an angular dispersion due to the Fermi motion of the interacting Λ and nucleon and with momenta as high as $\sim 420\,\mathrm{MeV}/c$. For a $2N$-induced process the outgoing nucleons momenta are $\sim 340\,\mathrm{MeV}/c$, if the available energy is equally shared among the final-state particles; this way, the final nucleons have a great probability to escape from the nucleus. Indeed, the NMWD dominates over the MWD for all but the s-shell hypernuclei and only for light systems ($A \leq 7$) the two decay modes are competitive.

The total decay width of a hypernucleus $\Gamma_T({}^A_\Lambda Z)$ is given by the sum of the MWD and NMWD widths:

$$\Gamma_T = \Gamma_M + \Gamma_{NM} = \Gamma_{\pi^0} + \Gamma_{\pi^-} + \Gamma_p + \Gamma_n + \Gamma_{2N} \tag{15}$$

and is expressed in terms of the hypernuclear lifetime $\tau({}^A_\Lambda Z)$ by

$$\Gamma_T({}^A_\Lambda Z) = \hbar/\tau({}^A_\Lambda Z). \tag{16}$$

In order to compare data from different hypernuclei on a common time scale, partial Γ's are usually given in units of Γ_Λ, the total decay width of the free Λ, and eq. (15) is rewritten as

$$\Gamma_T/\Gamma_\Lambda = (\Gamma_M + \Gamma_{NM})/\Gamma_\Lambda = \Gamma_{\pi^-}/\Gamma_\Lambda + \Gamma_{\pi^0}/\Gamma_\Lambda + \Gamma_p/\Gamma_\Lambda + \Gamma_n/\Gamma_\Lambda + \Gamma_{2N}/\Gamma_\Lambda. \tag{17}$$

It is worthwhile to remind that

$$\Gamma_T/\Gamma_\Lambda = \tau(\Lambda)/\tau({}^A_\Lambda Z), \tag{18}$$

where $\tau(\Lambda)$ is the lifetime of the free Λ.

Then, it appears that it is necessary to measure six quantities to fully describe the decay features of a hypernucleus (the five Γ's and the lifetime; in principle it is possible to determine one of them by using eqs. (17) and (18) if the others are known). Furthermore, in addition to the experimental hardness, there is the difficulty due to the existence of Final State Interactions (FSI) that often obstructs the determination of the physical obervables from the experimental data. As remarked in ref. [19] the observables for NMWD are even not well-defined quantum mechanically. Each one of the possible elementary NMWD occurs in the nuclear environment, hence subsequent FSI modify the quantum numbers of the WD nucleons and new, secondary nucleons are emitted as well, also with the possibility of occurrence of interference phenomena. The decay observables which can be directly measured are $\tau({}^A_\Lambda Z)$, Γ_{π^-} and Γ_{π^0} (pions are not significantly affected by FSI due to their low energy) and the spectra of both MWD and NMWD light decay products (pions and nucleons). Daughter nuclei can hardly be detected. Γ_{NM} can thus be obtained in an indirect way as $\Gamma_{NM} = \Gamma_T - \Gamma_M$. The problem of comparing the experimental nucleon spectra (sometimes in coincidence) with the theoretical spectra

corresponding to the bare decays (7), (8), (9), (10), (11) was approached in two ways. On one side the experimentalists tried to extract from the spectra the contribution due to the bare NMWD by using intranuclear cascade (INC) model calculations or phenomenological approaches. One the other side some theoreticians embedded the INC model calculations in their theoretical spectra, for a direct comparison with the experimental ones. We will discuss in detail this item in sect. **6**.

3. – Experimental interlude

We summarize in this section the main features and experimental performance of the two recent complex detectors which provided the largest amount of data on the WD of hypernuclei: the SKS (acronym for Superconducting Kaon Spectrometer) at the KEK PS and the FINUDA (acronym for FIsica NUcleare a DAΦNE) spectrometer at the (e^+, e^-) collider DAΦNE at LNF. More details on the experimental effort at previous set-ups can be found in ref. [20, 21].

The experimental techniques and analysis methods for studying all the facets of hypernuclear physics, more specifically the WD, were pioneered at the BNL AGS. The magnetic spectrometer Moby Dick was used to select and to identify hypernuclei in well defined states produced via the (K^-, π^-) reaction at 700 MeV/c [22, 23]. However, only a reduced set of targets was employed for WD studies.

At the KEK PS the powerful spectrometer SKS, fully dedicated to hypernuclear physics, was installed and put into operation at the end of the last century. The reaction used to form hypernuclei was the associated strangeness production (π^+, K^+) at ~ 1.05 GeV/c, where the elementary cross section reaches its maximum. Due to a larger momentum transfer the reaction was more effective than the (K^-, π^-) one in producing hypernuclei in ground states, from which the WD preferentially occurs. Incident π^+ vector momenta were analyzed by means of a QQDQQ beam spectrometer. The produced K^+ vector momenta were analyzed by the SKS: it was designed to be specifically suitable for coincidence experiments, thanks to the large solid angle (100 msr), the large momentum acceptance, the short path length (~ 5 m, very suitable for precise time-of-flight (t.o.f.) measurements for particle identification (p.id.) purposes) and the good momentum resolution ($\sim 0.1\%$ at 720 MeV/c) [24].

Kaon events were selected in the mass spectrum of produced/scattered particles by means of the momentum-t.o.f. correlation functions. The mass of hypernuclei was calculated for selected (π^+, K^+) events by using the momentum vectors of incident π^+ and produced K^+ after correction for the different materials (detectors, targets) crossed by particles. The best resolution on the hypernuclear mass, obtained with a thin carbon target, was 1.5 MeV FWHM [25]. Figure 4 left shows a schematic layout of the beam spectrometer and SKS arrangement.

By taking advantage of the comfortable free space left around the target region, several detector arrays were installed to measure the spectra of particles emitted in coincidence with the hypernucleus formation in states identified in the ground state region within the energy resolution. They were arrays of high-purity Ge detectors for high-resolution γ-spectroscopy, as mentioned in the Introduction, or systems of detectors for the measurement of charged particles or neutrons emitted in the WD. A typical arrangement is shown in fig. 4, right, and consisted in timing scintillation counters, multiple cell drift chambers and range counters [26]. These arrays were located above and below the nuclear target, which was tilted by 10–15 degrees with respect to the beam direction to maximize the target thickness seen by the beam particles (6–10 gr/cm^2) and

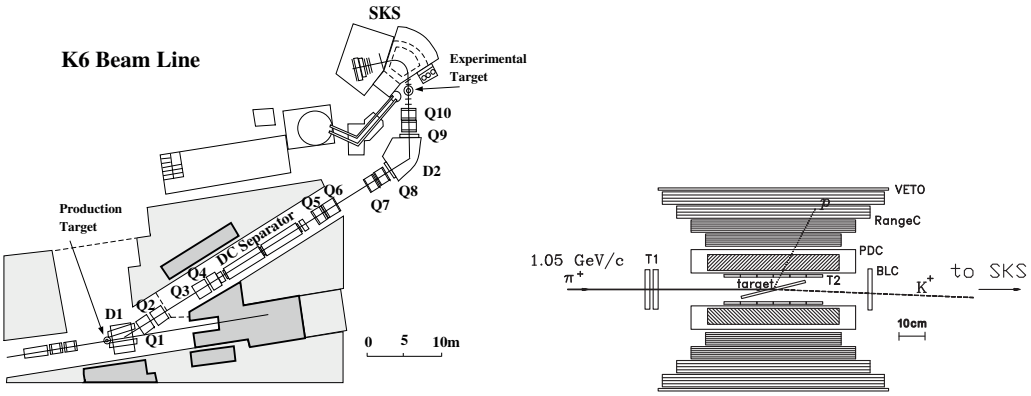

Fig. 4. – Left: Schematic view of the KEK-PS K6 beam line and SKS. Right: Schematic view of the decay counter system. Reprinted with permission from ref. [26], © 2005, the American Physical Society. http://dx.doi.org/10.1103/PhysRevC.71.025203.

to minimize the amount of material crossed by the particles emitted in the decay. The kinetic energy regions, covered by the range counter system, were 30–150 MeV for protons and 12–70 MeV for pions respectively.

Figure 5 (a) shows a typical mass spectrum obtained with the ^{12}C target. The resolution is more than three times worse than the nominal one due to the target thickness. It shows the well-known pattern characterized by two evident peaks. The first one is interpreted as the particle-hole shell-model configuration $(s(\Lambda),\ p-1(n))$, the ground state of $^{12}_{\Lambda}$C. The second one as the $(p(\Lambda),\ p-1(n))$, unbound and decaying strongly to $^{11}_{\Lambda}$B plus a low-energy proton (undetected). Out from a single nuclear target it is then possible to obtain information on two hypernuclear species. This feature was often used, in particular for WD studies.

Figures 5 (b) and 5 (c) show the mass spectrum in coincidence with WD protons and pions, respectively. From these spectra the physical quantities of interest for the WD were obtained by applying the suitable factors accounting for acceptances, efficiencies and so on.

Due to the concept of the set-up, measurements focused on different subjects of hypernuclear physics, like missing-mass spectroscopy, γ-rays spectroscopy in coincidence, WD studies, required different target thicknesses, different arrangements of the detectors arrays in coincidence and data had to be taken sequentially, at different times. Also for this reason the various measurements were identified by different experiment numbers; we will not quote them in this review, since they can be found in each cited reference, but in summarizing we will indicate only the laboratory (KEK).

Since the first beginning, K^-'s stopped in various materials were used to produce and to study the properties of hypernuclei by means of visualizing techniques and first-generation counter experiments (see ref. [21] for more details). A dedicated experiment at the KEK PS showed the great potentiality of the method, in particular for s-shell hypernuclei. The main results obtained are summarized in ref. [27] and stimulated the construction of a complex and performing detector dedicated to hypernuclear physics at the DAΦNE $(e^+,\ e^-)$ collider at LNF. It provides $\phi(1020)$ mesons with a luminosity of some $10^{32}\,\mathrm{cm}^{-2}\,\mathrm{s}^{-1}$. The $\phi(1020)$ decays about half of the times into a pair of slow ((16.5 ± 1.5) MeV), almost back-to-back charged kaons. FINUDA studied the hypernuclei

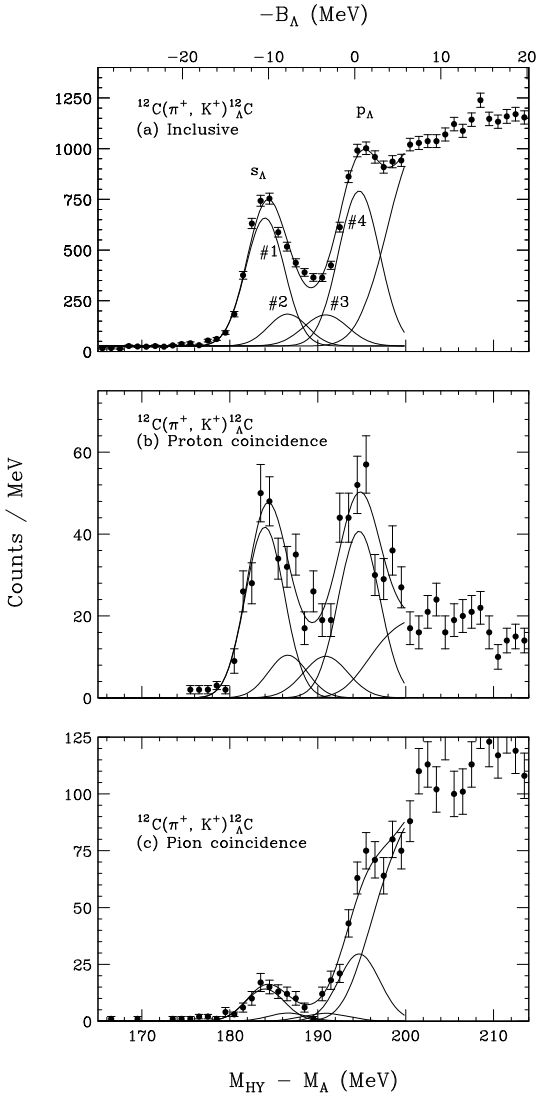

Fig. 5. – Hypernuclear mass spectra by the ^{12}C(π^+, K^+) reaction; (a) inclusive, (b) with coincident protons ($E_p > 40$ MeV), and (c) with coincident pions ($E_\pi > 12.5$ MeV). Reprinted with permission from ref. [26], © 2005, the American Physical Society.
http://dx.doi.org/10.1103/PhysRevC.71.025203.

production by K^- stopped in very thin nuclear targets ($\sim 0.25\,\mathrm{g/cm^2}$) arranged coaxially as tiles around the beams intersection region following the two-body reaction:

$$K^-_{\mathrm{stop}} + {}^A Z \to \pi^- + {}^A_\Lambda Z, \tag{19}$$

with the usual meaning of the symbols, and their subsequent WD.

In the years 2003–2007, in two periods, data corresponding to a total amount of $\sim 1.2\,\mathrm{fb}^{-1}$ of (e^+, e^-) collisions at the ϕ energy was collected. The apparatus, shown

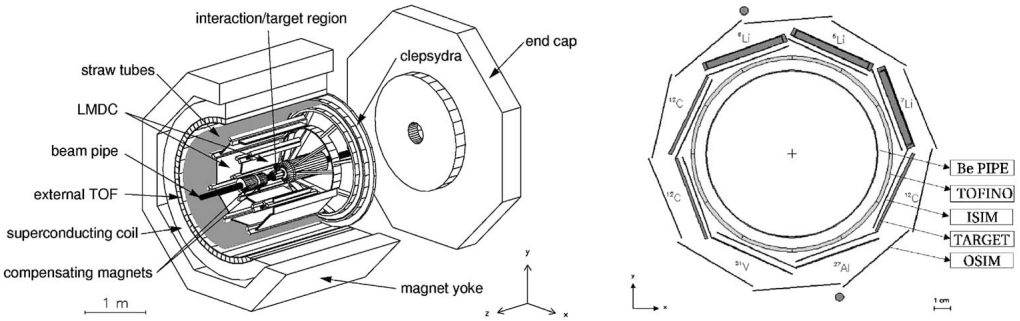

Fig. 6. – Left: Global view of the FINUDA detector. Right: Schematic view of the interaction/target region (targets of the 2003-2004 data taking period). Reprinted from ref. [28], © 2005, with permission from Elsevier.

in fig. 6, left, consisted of a magnetic spectrometer with cylindrical symmetry, of 125 cm radius and 225 cm maximum length, immersed in a 1 T solenoidal magnetic field provided by a superconducting magnet and uniform to better than 2%. The apparatus was able to detect the kaons before their interactions in the targets by means of a thin scintillator hodoscope surrounding the beam pipe (named TOFINO in short) and a vertex detector composed of one layer of eight double-sided silicon microstrip modules (named ISIM). A dedicated algorithm was developed to correctly identify the charge and momentum of the kaon before stopping in the target. Figure 6, right, shows a front view of the TOFINO-ISIM-targets assembly.

Beyond the target array, the momenta of the π^- emitted in the production reaction (19) and of the π^- emitted in the MWD decay, eq. (4), or the proton from the NMWD, eqs. (7), (9), (10), were determined by means of the tracking detector stack. It consisted of one layer of ten double-sided silicon microstrip modules (called OSIM) located at ~ 1.5 cm from the targets, two layers of eight planar low-mass drift chambers (LMDCs) at a distance, respectively, of ~ 37 and ~ 65 cm from the beam axis, and a six-layer array of stereo-staggered straw tubes, centered at ~ 110 cm from the beam axis. The tracking detectors were held by an aluminium clepsydra-shaped frame. The whole tracking system was filled and fluxed with He gas to minimize multiple scattering of the emitted particles. The silicon detectors and the drift chambers permitted p.id., through the measurement of the energy lost in their active volume. Information on the t.o.f. of particles was also used for p.id. It was provided by a system composed of the TOFINO scintillator array as start detector and a stop scintillator barrel, 10 cm thick, located outside the tracking region facing the magnet coil (named TOFONE). TOFONE allowed also the detection of neutrons with an efficiency of $\sim 10\%$ and an energy resolution of $\sim 13\%$ at 10 MeV and 20% at 100 MeV. Construction and experimental details can be found in refs. [21, 28-31]. The solid angle for detection of all particles was larger than 2π sr. The relative momentum resolution for π^- with momenta typical of formation reaction (19) (~ 270 MeV/c) was 0.6% FWHM, corresponding to an energy resolution on the hypernuclear states of 1.29 MeV, the best achieved at that time in hadron-induced reactions. For protons of 400 MeV/c, tipically emitted in NMWD like (7), it was 2% FWHM and for π^- from the WD (4), measured with a different combination of the tracking detectors, it was $\sim 6\%$ FWHM at 110 MeV/c. The threshold energy for the detection of protons was 15 MeV, due to the thinness of the targets and of the materials composing the tracking detectors, for π^- 20 MeV due to the magnetic rigidity.

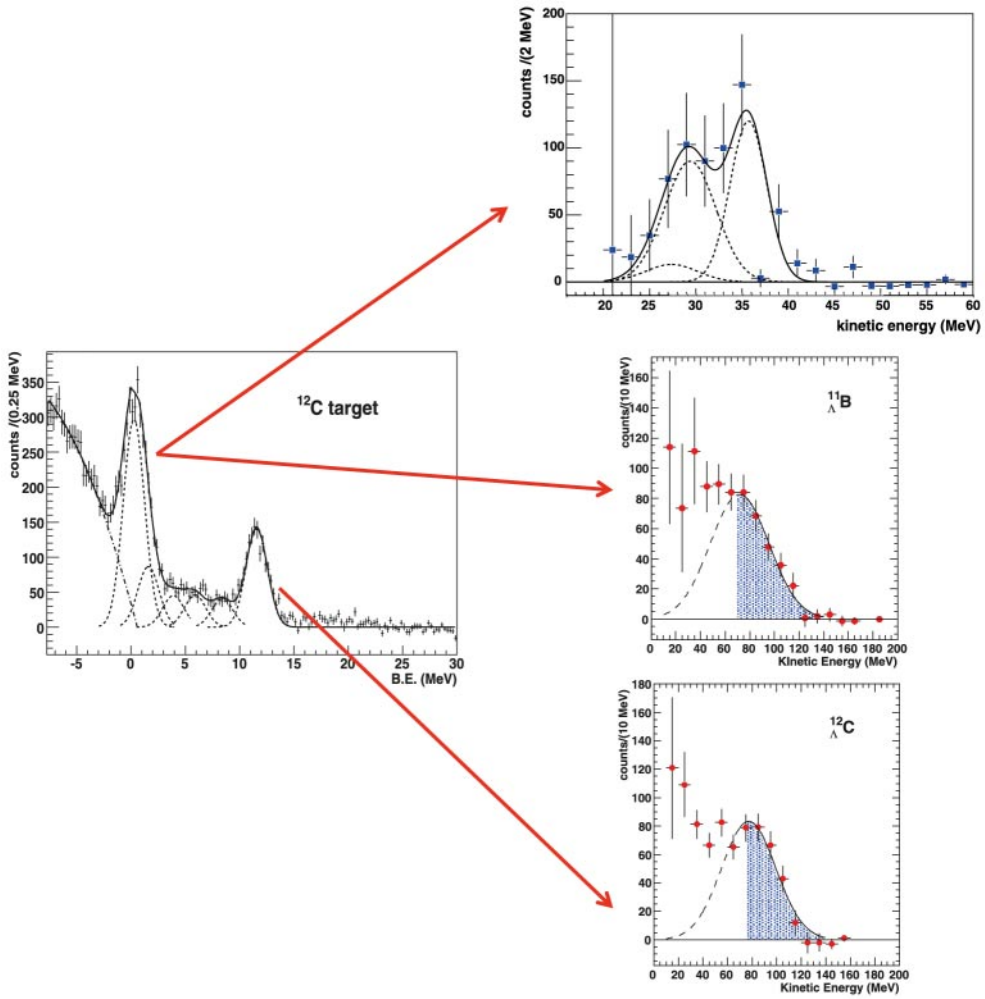

Fig. 7. – Schematic of the coincidence measurements for hypernucleus decay studies on ^{12}C target in FINUDA. Left panel: inclusive binding energy spectrum for π^- tracks coming from ^{12}C target. The continuous line is the best fit curve to the spectrum; the dashed and dot-dashed curves represent the contributions from known hypernuclear states production and from the Λ quasifree production background: from ref. [30]. Right upper panel: kinetic energy spectrum of MWD π^- from $^{11}_{\Lambda}$B after acceptance correction. The solid curve is a two-Gaussian fit to the peaks in the spectrum, dashed curves are single components: from ref. [30]. Right central panel: proton kinetic energy spectrum from the NMWD of $^{11}_{\Lambda}$B after acceptance correction. The solid curve is a Gaussian fit to the spectrum, the blue filled area indicates the one proton-induced NMWD contribution. From ref. [32]. Right lower panel: proton kinetic energy spectrum from the NMWD of $^{12}_{\Lambda}$C after acceptance correction. The solid curve is a Gaussian fit to the spectrum, the blue filled area indicates the one proton-induced NMWD contribution; from ref. [32].

FINUDA was optimized for the study of WD processes. Figure 7 shows an example of the experimental spectra from which the physical quantities discussed in the following were obtained for a ^{12}C stopping target. On the left the BE spectrum of $^{12}_{\Lambda}$C is shown, with the two characteristics peaks already discussed; note that the abscissa scale is

different from fig. 5 (−BE value is reported on the top of the figure), and the position of the two peaks is reversed. The proton energy spectra from the NMWD of the ground state of ${}^{12}_{\Lambda}$C (centered at BE $\sim$ 11.5 MeV) is shown in the right lower panel, whereas the one corresponding to the NMWD from ${}^{11}_{\Lambda}$B (centered at BE $\sim$ 0 MeV) in the right central panel. The right upper panel shows the π^- spectrum from MWD of ${}^{11}_{\Lambda}$B. Due to the involved BE, the π^- spectrum from MWD of ${}^{12}_{\Lambda}$C was falling below the detection threshold.

The resolution on the BE spectrum is 2.3 MeV, about twice the best achievable for spectroscopy measurements. The worsening was due to the relaxed quality cuts applied to increase the statistics for the sample available for coincidence measurements (a factor 6). This example shows how the concept of FINUDA was completely different from that of the SKS: various physical observables could be extracted from the same data bank by exploiting the performance of the experimental apparatus by defining optimized sets of analysis selections. A peculiar feature of FINUDA, not adopted before in the detectors designed for hypernuclear physics, was the presence of a powerful vertex reconstruction system (ISIM and OSIM arrays) that allowed the separation of the primary vertex of the K^- interaction from the secondary vertex due to the decay of the produced hyperons Λ and Σ with a spatial resolution of less than 3 mm.

The features of the apparatus allowed also the investigation, in the same data bank, of other final states produced in the interaction of stopped K^- with nuclei, leading to the discovery of the K^-pp deeply bound state [33], to investigate new features of the Σ^- interactions with nuclei [34] and to the first observation of the superheavy hyperisotope ${}^{6}_{\Lambda}$H [35].

4. – Lifetime of hypernuclei

4˙1. *Introductory remarks.* – The lifetime of a hypernucleus is the first observable that characterizes the WD of the system. Being an inclusive quantity, its determination is free from the difficulties arising from the unavoidable effects typical of the nuclear medium in which the Λ-hyperon is embedded, as it happens for the widths of specific NMWD channels.

For this reason, since the first beginning, all experiments focused on hypernuclear physics tried to determine the lifetime of a hypernucleus, after having ascertained its existence. There is then a variety of experimental techniques that were envisaged by different groups at different laboratories, adapted to the beams and facilities at disposal. The most straightforward and reliable experimental approach is that of producing and identifying a given hypernucleus in the ground state or in a low-lying excited state by means of a powerful magnetic spectrometer dedicated to the study of the production reaction, as discussed in sect. **3**. By installing near to the production target an array of fast timing detectors (typically plastic scintillators) featuring resolutions of less than 100 ps FWHM, it is possible to measure the time distribution of the charged particles (pions, protons) emitted in the WD of the hypernucleus selected by the magnetic spectrometer.

Typically, with a thousand of events in such a delay spectrum it is possible to determine the lifetime with a precision of some percent. Figure 8 shows a nice example of such a method, obtained for ${}^{12}_{\Lambda}$C with the (π^+, K^+) reaction on ^{12}C target [36]. A signal monitoring the stability of the time resolution function is mandatory in such a method. It was obtained by (π^+, pp) events recorded continuously during the data taking. However such a method was applied only in a restricted range of the mass number: up to $A \sim$ 60–70, with exclusion of the hydrogen hyperisotopes. Production of the last ones

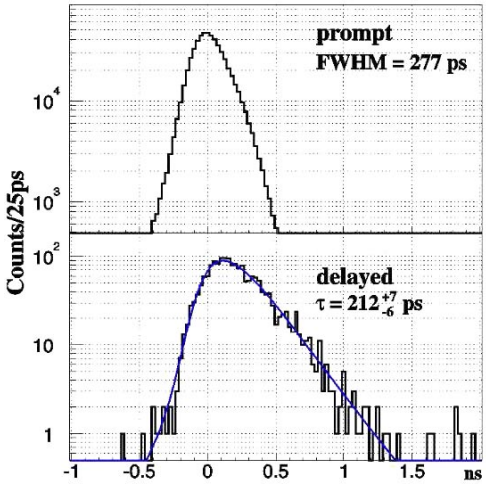

Fig. 8. – Upper part: prompt time spectrum of (π^+, pp) events on ^{12}C target. Lower part: decay time spectrum of $^{12}_{\Lambda}$C(g.s.). Reprinted with permission from ref. [36], © 2011, the Korean Physical Society.

is inhibited to double magnetic spectrometers optimized for the (π^+, K^+) or (K^-, π^-) reactions due to the non-availability of production targets. For targets of A larger than ~ 70, the produced hypernucleus is not transparent to the emission of fast charged particles needed for the time measurement. As we will see in sect. **5**, Γ_{π^-} goes down to the level of 10^{-4} due to the Pauli blocking. In sect. **6** we will see that the FSI probability for a proton emitted in a bare $1p$-induced NMWD is close to 100%; then only rescattered protons should possibly trigger the time measurement, with a consequent not acceptable time jitter.

In the following we review the existing published values of the measured lifetimes. For subsequent measurements from the same collaboration we will quote only the last published result; in case of several measurements from different groups we will quote the weighted average (w.a.). We will mention the laboratories at which the experiments were carried out, without specifying the experiment number, which can be found in the corresponding reference.

4˙2. *A review of existing data*

$^{3}_{\Lambda}$H. It is the lightest hypernucleus, characterized by a very small binding energy, BE $= (0.13 \pm 0.05)$ MeV [37]. It is thus expected that for such a system the Λ spends most of the time far from the deuteron core and then that $\tau(^{3}_{\Lambda}\mathrm{H})$ is very close to the free Λ value. MWD is expected to dominate over the NMWD and it may proceed through 2-, 3- and 4-body modes.

Early experiments were performed with visualizing techniques, namely emulsions [38-41] and He-filled bubble chambers [42-44]. The exposures were done with beams of K^- stopped or in flight at the CERN PS, the BNL AGS and the Argonne ZGS. 2- and 3-body MWD were examined. A common feature of all the measurements was the limited number of events satisfying the selection criteria, with consequent large errors.

At the JINR Nuclotron relativistic ion beams (^{3}He, ^{4}He, ^{6}Li and ^{7}Li) with 2.2–

5.1 AGeV energies on a polyethylene target were used successfully for producing light hyperfragments [45]. By measuring the recoil distance distribution with a Ne gas filled chamber a value of 240 ps with an error of $\sim 60\%$ was reported.

The interest for $\tau({}^{3}_{\Lambda}\mathrm{H})$ was very recently raised by the observation of the production of ${}^{3}_{\Lambda}\mathrm{H}$ and, even more important, of its antipartner $\overline{{}^{3}_{\Lambda}\mathrm{H}}$ in ultrarelativistic Au+Au collisions at RHIC by the STAR Collaboration [46]. The 2-body MWD was clearly observed, and the $\beta\gamma$-decay length allowed the determination of the lifetime, $\tau({}^{3}_{\Lambda}\mathrm{H}) = (182^{+89}_{-45} \pm 27)$ ps, with (157 ± 30) ${}^{3}_{\Lambda}\mathrm{H}$ and (70 ± 17) $\overline{{}^{3}_{\Lambda}\mathrm{H}}$ candidates.

Soon after another experiment with ions beams performed at GSI by the HypHi Collaboration [47] reported a determination of $\tau({}^{3}_{\Lambda}\mathrm{H})$. The experiment studied the projectile fragmentation reactions of ^{6}Li at 2 AGeV delivered on a carbon target. The invariant mass technique coupled to precise t.o.f. measurements allowed to select the 2-body MWD and to determine a value of $(183^{+42}_{-32\mathrm{stat}} \pm 37_{\mathrm{sys}})$ ps. We remark that in both experiments with heavy ions τ_Λ for the free Λ, produced abundantly in the same runs and selected with the same analysis criteria, was fully consistent with the Particle Data Group value [16].

A very recent analysis [48] of the statistical combination of all the aforesaid experimental lifetime estimations yielded a value of 216^{+19}_{-16} ps with a reduced χ^2 of 0.69. In this analysis the result from [45] was not taken into account. In the same paper a new insight into the $\tau({}^{3}_{\Lambda}\mathrm{H})$ estimation of [47] by a Bayesian approach was also presented, yielding a value of (217^{+19}_{-16}) ps. We notice also that a preliminary result by the STAR Collaboration with an improved statistical significance providing a quite lower value, $(123^{+26}_{-22\mathrm{stat}} \pm 10_{\mathrm{sys}})$ ps [49], was not considered. However, waiting for a definitive result from STAR, we use in the present review the value from ref. [48], (216^{+19}_{-16}) ps.

${}^{4}_{\Lambda}\mathrm{H}$. The experimental situation for the determination of the lifetime for this hypernucleus is similar to that of ${}^{3}_{\Lambda}\mathrm{H}$. The difference is that measurements in principle are easier, since the BE is higher ((2.08 ± 0.06) MeV [37]) and the 2-body MWD partial width is larger ($\sim 50\%$ [50]), thus allowing a better selection with the missing-mass method.

Earlier measurements with emulsions [38, 40, 51, 52] based on reduced numbers of events were affected by large errors, as for ${}^{3}_{\Lambda}\mathrm{H}$. The first experiment which proviced a value of 220 ps with a 20% error was the one at the JINR Nuclotron [45]. Nearly at the same time a value of 194^{+24}_{-26} ps was measured at the KEK PS by stopping a K^- beam in a liquid He (LHe) target and measuring the time delay of the π^- peak due to the MWD of ${}^{4}_{\Lambda}\mathrm{H}$ [53, 54].

Recently a value of $(140^{+48}_{-33\mathrm{stat}} \pm 35_{\mathrm{sys}})$ ps was reported by the HypHi Collaboration [47]. The combined analysis of all the above mentioned results yielded a value [48] of 192^{+20}_{-18} ps with a reduced χ^2 of 0.48 that we will take as the updated one. In the same paper [48] a revaluated value of 194^{+20}_{-18} ps for the HypHi determination is given as a result of a Bayesian approach.

As a final remark we recall that in the first experiment which pioneered the measurement of hypernuclear lifetimes as described in ref. [22] the authors notice that in the high missing-mass spectrum obtained with the ^{6}Li target the lifetime drops from (256 ± 20) ps for the ${}^{5}_{\Lambda}\mathrm{He}$ region (see later) to (160 ± 20) ps. The H hyperisotopes and ${}^{4}_{\Lambda}\mathrm{He}$ are the only hypernuclear systems that may populate this missing-mass region. ${}^{4}_{\Lambda}\mathrm{He}$ has a lifetime close to that of the free Λ (see later) and the configuration with ${}^{4}_{\Lambda}\mathrm{H}$ is much more favorite, as seen in the corresponding hyperfragment production [55]. The value should then correspond to the lifetime of ${}^{4}_{\Lambda}\mathrm{H}$ and agrees closely with the subsequent determinations.

$^{4}_{\Lambda}$He. The first measurements were obtained from emulsion data [38, 40] and are affected by large errors due to meagre statistics. The first experiment which provided a good result by using the time delay analysis was performed at the KEK PS with K^- stopped in a LHe target; the reported value for $\tau(^{4}_{\Lambda}\mathrm{He})$ is (256 ± 27) ps [56]. A value of (245 ± 24) ps was afterwards reported by ref. [23] with the same experimental technique but using K^- of 750 MeV/c and a 30.5 cm long LHe target. The w.a. value of (250 ± 18) ps is then adopted in this review.

$^{5}_{\Lambda}$He. Also for this hypernucleus the first data, of poor statistical significance, were obtained by emulsion experiments [38,40]. The first experiment which used the time delay analysis was performed at the BNL AGS by using the (K^-, π^-) reaction at 800 MeV/c on a ^{6}Li target. A value for $\tau(^{5}_{\Lambda}\mathrm{He})$ of (256 ± 21) ps was obtained [22]. It is consistent with the value of 278^{+11}_{-10} ps obtained subsequently at the KEK PS with a larger statistics by using the (π^+, K^+) reaction at 1.05 GeV/c [57]. The w.a. value of (273 ± 10) ps is finally adopted.

$^{9}_{\Lambda}$Be. In the first experiment perfomed at the BNL AGS by using the (K^-, π^-) reaction at 800 MeV/c on a carbon target [58], the time delay analysis was applied to the events selected in ranges of the excitation energy spectrum which showed three peaks. The first one was interpreted as the particle-hole shell-model configuration $(s(\Lambda),\ p-1(n))$, the ground state of $^{12}_{\Lambda}$C. The second one as the $(p(\Lambda),\ p-1(n))$, unbound and decaying strongly to ^{11}B plus a low-energy proton. Finally, the third one was tentatively identified as having the shell-model configuration $(s(\Lambda),\ s-1(n))$, whose break-up produced a stable hypernucleus decaying with a lifetime of (201 ± 31) ps. In the subsequent analysis by the same group [22] it was mentioned that such a hypernucleus could be $^{9}_{\Lambda}$Be, following theoretical predictions [59]. Such a hypothesis was accepted in the survey of hypernuclei's lifetimes presented in ref. [60].

$^{11}_{\Lambda}$B. The first measurement of the lifetime of $^{11}_{\Lambda}$B was performed in the previously mentioned experiment at the BNL AGS [58], $\tau(^{11}_{\Lambda}\mathrm{B}) = (192 \pm 22)$ ps. A subsequent experiment performed at the KEK PS by using the (π^+, K^+) reaction at 1.05 GeV/c on a Carbon target with a larger statistics yielded the value of (211 ± 13) ps [61]. The w.a. value of (206 ± 11) ps is finally adopted.

$^{12}_{\Lambda}$C. The first measurement of the lifetime of $^{12}_{\Lambda}$C was performed at the BNL AGS [58], $\tau(^{12}_{\Lambda}\mathrm{C}) = (211 \pm 31)$ ps. Then there was a series of several measurements at the KEK PS with improved statistics, which yielded the final result of $\tau(^{12}_{\Lambda}\mathrm{C}) = (212^{+7}_{-6})$ ps [36] which can be taken as fully representative of the experimental effort. The relevant delay spectrum is shown by fig. 8.

$^{16}_{\Lambda}$O. A lifetime measurement of $A \sim 16$ hypernuclei (mostly $^{16}_{\Lambda}$O?) was performed using a 2.1 GeV/nucleon ^{16}O beam on a (CH_2)n target at the LBL Bevalac [62]. Hypernuclear species could not be identified and the lifetime was extracted from the recoil distance distribution, measured with spark chambers. With only 22 events a lifetime of (86^{+33}_{-26}) ps was inferred, much smaller than the values for the neighbour $^{12}_{\Lambda}$C and $^{28}_{\Lambda}$Si. Though this measurement had the merit of being the first performed with relativistic ion beams, several experimental drawbacks, particularly the huge amount of background events, led to conclude that the value is not reliable.

$^{27}_{\Lambda}$Al. There is one measurement with the time delay technique performed on events produced by the (π^+, K^+) reaction at 1.05 GeV/c on a ^{28}Si target at the KEK PS [61]. The SKS spectrometer allowed to select in the missing-mass spectrum the p_Λ state decaying through proton emission to $^{27}_{\Lambda}$Al. The measured $\tau(^{27}_{\Lambda}\mathrm{Al})$ is (203 ± 10) ps.

$^{28}_{\Lambda}$Si. The only measurement so far performed was done at the KEK PS with the time delay technique on events produced by the (π^+, K^+) reaction at 1.05 GeV/c on a ^{28}Si target [61]. The measured $\tau(^{28}_{\Lambda}\mathrm{Si})$ is (206 ± 12) ps.

$_{\Lambda}$Fe. A measurement was performed at the KEK PS with the time delay technique on events produced by the (π^+, K^+) reaction at 1.05 GeV/c on a ^{56}Fe target [61]. The applied selection on the missing-mass spectrum ensured that the Λ was bound but not that the decay protons were emitted only by $^{56}_{\Lambda}$Fe, but also from $^{55}_{\Lambda}$Fe and $^{55}_{\Lambda}$Mn, present in the structure of the excited states. The measured lifetime for the complex of these hypernuclides, labelled $_{\Lambda}$Fe, is (215 ± 14) ps.

Heavy hypernuclear systems. As mentioned in subsec. **4**˙1, for heavy hypernuclei the application of direct timing methods, as adopted for light- and medium-A systems, is not feasible.

Attempts to overcome the problem of not having at disposal fast charged particles from the WD were done by detecting fragments from fission processes induced by the high-energy release due to the NMWD of the heavy hypernucleus. The high-A hypernuclei were produced by e^- beams at the Kharkov Linac on ^{209}Bi [63], by $\bar{p}$ annihilations at rest at the CERN LEAR on ^{209}Bi and ^{238}U [64] and by p-A collisions at the Jülich COSY on ^{197}Au, ^{209}Bi and ^{238}U [65]. A common feature of both $\bar{p}$-A and p-A reactions is that the hypernucleus is produced with a sizable energy, in particular for high-momentum p-A collisions, and then it recoils over a distance of some mm before decaying; the recoil shadow method [66], used in nuclear physics for the measurement of fission isomers, can thus be applied with good sensitivity to evaluate the lifetime.

However, the determination is not direct and it depends strongly on theoretical models which describe the time evolution of the system during the reaction: transport calculations for the initial fast non-equilibrium phase and statistical calculations for the final evaporation phase. These calculations give the mass A and the charge Z distribution of the hypernuclei which undergo delayed fission together with their individual, A- and Z-dependent, velocity distribution in the laboratory frame; a fit of the recoil distance distribution allows to extract the lifetime.

Following this procedure, from $\bar{p}$-A experiments $\tau(^{A}_{\Lambda}Z)$ values of (180 ± 40) ps have been obtained for the ^{209}Bi target and (130 ± 30) ps for the ^{238}U target [64], while from p-A experiments values of (130 ± 30) ps for the ^{197}Au target, (161 ± 16) ps for the ^{209}Bi target and (138 ± 18) ps for the ^{238}U target were reported [65].

It must be noted that, unlike (K^-, π^-) and (π^+, K^+) reactions, both $\bar{p}$-A and p-A production mechanisms do not allow to identify the decaying system; the A and Z values of the produced hypernuclei are, actually, obtained from the calculated (Z, A) distributions which span over 35-40 mass units and 8–10 charge units [65]. If we consider the overlap of the individual (Z, A) distributions for the three targets used in p-A experiments, it is possible to obtain a mean lifetime for hypernuclei with masses $A \sim$ 180–225, with a dispersion in charge $\Delta Z \sim 3$ for fixed A, of $\tau(^{A}_{\Lambda}Z) = (145 \pm 10)$ ps, while, by averaging over the results obtained in $\bar{p}$-A experiments on ^{209}Bi and ^{238}U, the value

TABLE I. – *Summary of* $\tau({}^{A}_{\Lambda}Z)$ *values for the hypernuclei discussed in this section. See text for more details.*

Hypernucleus	$\tau({}^{A}_{\Lambda}Z)$ (ps)	Γ_T/Γ_Λ
${}^{3}_{\Lambda}$H	216^{+19}_{-16}	$1.219^{+0.090}_{-0.107}$
${}^{4}_{\Lambda}$H	192^{+20}_{-18}	$1.37^{+0.13}_{-0.14}$
${}^{4}_{\Lambda}$He	250 ± 18	1.053 ± 0.076
${}^{5}_{\Lambda}$He	273 ± 10	0.963 ± 0.034
${}^{9}_{\Lambda}$Be	201 ± 31	1.31 ± 0.20
${}^{11}_{\Lambda}$B	206 ± 11	1.276 ± 0.070
${}^{12}_{\Lambda}$C	212^{+7}_{-6}	1.242 ± 0.040
${}^{16}_{\Lambda}$O	86^{+33}_{-26}	not reliable
${}^{27}_{\Lambda}$Al	203 ± 10	1.297 ± 0.064
${}^{28}_{\Lambda}$Si	206 ± 12	1.278 ± 0.074
${}_{\Lambda}$Fe	215 ± 14	1.224 ± 0.080
Heavy (w.a. for $180 < A < 238$)	146 ± 9	1.81 ± 0.12

$\tau({}^{A}_{\Lambda}Z) = (148 \pm 24)$ ps can be found, fully compatible; a global w.a. can be evaluated: $\tau({}^{A}_{\Lambda}Z) = (146 \pm 9)$ ps.

Table I summarizes the $\tau({}^{A}_{\Lambda}Z)$ values discussed in the previous subsections; in the third column the values of $\Gamma_T/\Gamma_\Lambda = (263.2 \pm 2.0)/\tau({}^{A}_{\Lambda}Z)$ (see eq. (15)) are reported. Figure 9 shows the trend of the experimental values of the hypernuclei lifetime as a function of A.

4˙3. *Comparison of measured hypernuclear lifetimes with theoretical predictions.* – A first calculation of hypernuclear lifetimes from ${}^{12}_{\Lambda}$C to ${}^{208}_{\Lambda}$Pb in the one-pion exchange (OPE) model approach (see later subsect. **6**˙5), including the $2N$-induced decay modes on strongly correlated *np* pairs was done in ref. [67]. The calculated values are shorter by 30–40% then the measured ones. A better agreement, with still a slight underestimation for the medium-A hypernuclei was obtained by the addition of $2\pi/\sigma$ and $2\pi/\rho$ exchange terms to the OPE exchange potential for the $1N$-induced NMWD [68], shown by the (green) dashed line in fig. 9. By adding further exchange terms, namely ω, K, $\rho\pi/a_1$ and $\sigma\pi/a_1$, a general overestimation with respect to the experimental values was obtained [69], as shown by the (blue) dotted line in fig. 9. This fact can be due, as remarked by the authors, to the circumstance, among others, that the $2N$-induced NMWD was not taken into account. The $2N$-induced was explicitly considered in ref. [19], in which exchange of mesons of the pseudoscalar and vector octets π, η, K, ρ, ω and K^* was taken into account for the weak transition potential, while for the N-N strong interaction the Bonn potential with the exchange of π, ρ, σ and ω was adopted. Calculations of the NMWD partial widths were performed from $A = 11$ to $A = 208$ hypernuclei. We derived from these calculations the lifetimes, by adding to the low-mass A hypernuclei

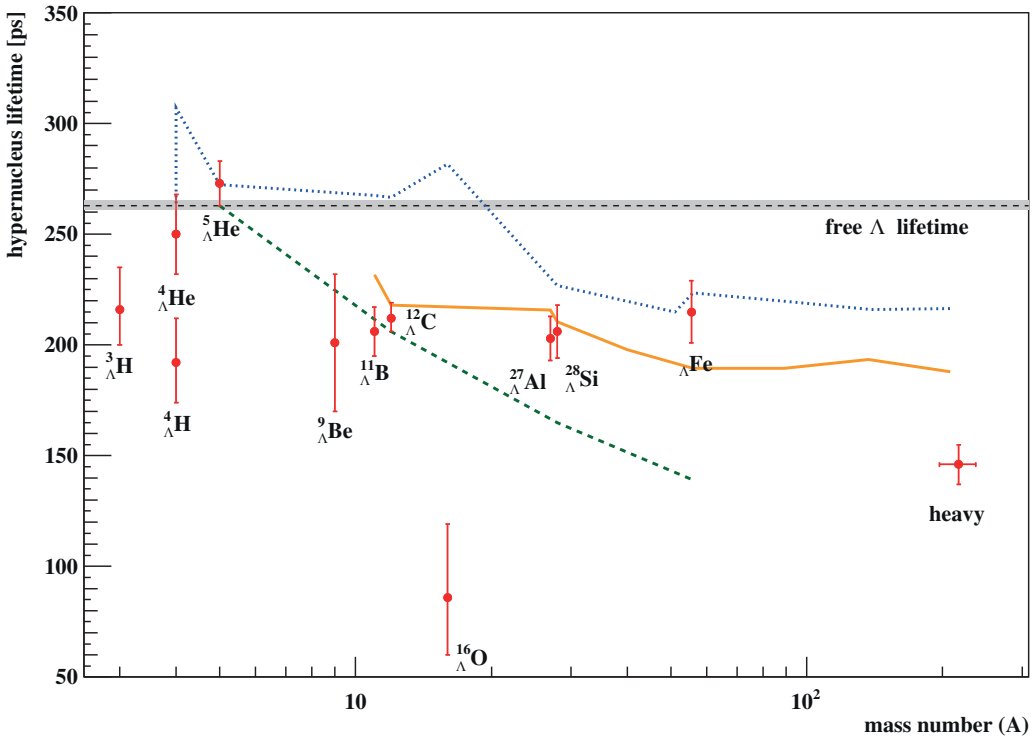

Fig. 9. – Experimental values of the lifetime of hypernuclei as a function of A (Log scale): weighted average values are used when several measurements are available for the same hypernucleus, as explained in the text. The dashed line represents calculations from ref. [68], the dotted line from ref. [69], the continuous line values obtained from ref. [19] with correction from ref. [70]. See text for more details.

the MWD widths calculated in ref. [70]. The result is shown by the continuous (orange) line in fig. 9; it is evident that this theoretical approach gives the best description of the experimental values in the $11 \leq A \leq 56$ mass range.

4˙4. *Future experimental efforts*. – From the above discussion it appears that the main efforts should be done on the measurement of the lifetimes of the hydrogen hyperisotopes and high-A systems.

The reliable technique of the time delayed spectra can be very hardly used for the hydrogen hyperisotopes since they cannot be produced from He targets in reactions employing only charged meson beams and ejectiles. When the high-intensity and high-resolution (HIHR) beam line at J-PARC, capable of producing up to 10^9 π^-/spill [71] will be operational, it should be possible to envisage the use of the (π^-, K^0) reaction on He targets to produce the hydrogen hyperisotopes. In order to achieve a resolution of 1.5 MeV FWHM, needed to isolate the ground state of $^{4}_{\Lambda}$H (BE = (2.08 ± 0.06) MeV [37]), the K spectrometer could have a global detection efficiency as low as 10^{-4}. A production rate of 10^4 $^{4}_{\Lambda}$H/day was evaluated, comfortable for the measurement of $\tau(^{4}_{\Lambda}\mathrm{H})$ [71]. A measurement of $\tau(^{3}_{\Lambda}\mathrm{H})$ seems very hard, since the BE of $^{3}_{\Lambda}$H is nearly an order of magnitude less than the resolution expected for the hypernuclear energy levels. In order to limit

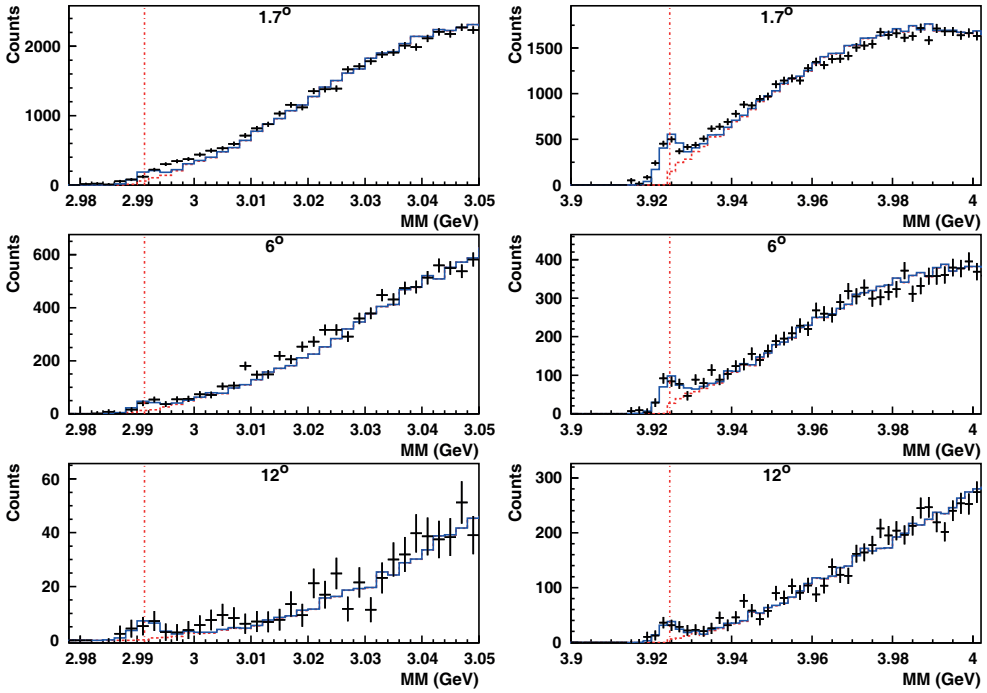

Fig. 10. – Missing-mass spectra for the $(e, e'K^+)$ reaction on ^{3}He (left) and ^{4}He (right) targets; vertical lines indicate the thresholds for quasi-free Λ production, continuous lines represent the distribution of simulated quasi-free Λ production background plus bound states formation. Reprinted with permission from ref. [72], © 2004, the American Physical Society.
http://dx.doi.org/10.1103/PhysRevLett.93.242501.

unavoidable contributions from the free Λ decay that could bias the result, it should be necessary to select the lower energy π^- from the 3-body decay but with the complication of a further reduction in the counting rate and a more sophisticated detector.

The recent advent of high-quality and high-intensity electron beams at JLab, coupled to the excellent energy resolutions so far achieved with dedicated spectrometers, offers a novel opportunity to produce the hydrogen hyperisotopes out from targets of the He isotopes by means of the $(e, e'K^+)$ reaction. A first study, performed with a spectrometer system featuring a final missing-mass resolution of 4 MeV [72] showed clearly signals corresponding to the production of ${}^{3}_{\Lambda}$H and ${}^{4}_{\Lambda}$H. Data were taken at an electron beam energy of 3.425 GeV and at 3 detection angles of the produced K^+; fig. 10 shows the obtained spectra. For the ^{4}He target a ${}^{4}_{\Lambda}$H peak corresponding to the production of the 0^+ ground state and 1^+ excited state at 1.04 MeV, not resolved, is well visible in all the three spectra just below the quasi-free ^{3}H-Λ production threshold of 3.925 GeV. It was found that the reduction of the production of ${}^{4}_{\Lambda}$H with respect to the Λ production from a proton target is of about 2 orders of magnitude. From fig. 10 it appears that within the experimental resolution there is a contribution from the quasi-free production of Λ's, dangerous if a measurement of the lifetime must be performed. As soon as the plan of upgrade in energy and quality of the electron accelerator complex will be achieved, by taking advantage of the excellent resolution of the present spectrometers for selecting

electroproduction of hypernuclei in the forward direction, $\sim 500\,\mathrm{keV}$ [73], it should be possible to get a time spectrum from the MWD of ${}^{4}_{\Lambda}\mathrm{H}$, background-free, containing several hundreds of events.

As a matter of fact, a new measurement of the ${}^{4}_{\Lambda}\mathrm{H}$ 0^+ ground state energy with a precision of the order of some 10 keV is planned [74] by using the ${}^{4}\mathrm{He}(e,e'K^+){}^{4}_{\Lambda}\mathrm{H}$ reaction and by exploiting the decay pion spectroscopy method (see subsect. **5**˙4). A simple barrel of scintillators or scintillating fibers around the target will allow the precise measurement of $\tau({}^{4}_{\Lambda}\mathrm{H})$. Since electroproduction has a large spin-flip probability in the forward direction [75] the excited state of the ${}^{4}_{\Lambda}\mathrm{H}$ system at 1.04 MeV should be populated preferentially. It decays by a fast γ-transition to the 0^+ ground state, from which the MWD finally occurs, and then no reductions of statistics should be expected.

The situation changes for the ${}^{3}\mathrm{He}$ target. Figure 10 shows that a signal corresponding to the production of ${}^{3}_{\Lambda}\mathrm{H}$ can be inferred by a weak shoulder in the spectrum at 1.7°, more visible at the other angles just below the ${}^{2}\mathrm{H}$-Λ threshold at 2.993 GeV. The reduction of the production of ${}^{3}_{\Lambda}\mathrm{H}$ with respect to the free Λ production ranges from 2 to 3 orders of magnitude, depending on the angle. If in addition we consider that the high-resolution spectrometer system for hypernuclear physics at JLab is optimized for production around 0° and the BE of ${}^{3}_{\Lambda}\mathrm{H}$ is only 130 keV, we may guess that the precise measurement is quite harder and would also necessitate of the detection of π^- from the 3-body decay with a dedicated set-up.

We may expect substantial improvements in the determination of $\tau({}^{3}_{\Lambda}\mathrm{H})$ by the analysis of the data that were and will be collected in relativistic ion collisions by the STAR Collaboration at RICH and by the ALICE Collaboration at LHC. We have seen in the previous subsect. **4**˙2 that STAR has already reported a preliminary quite low value for $\tau({}^{3}_{\Lambda}\mathrm{H})$ [49]. We may expect that such a value will be confirmed with possibly a reduced error thanks to a larger statistics.

Also the ALICE Collaboration has reported the observation of ${}^{3}_{\Lambda}\mathrm{H}$ and of its antipartner by analyzing data collected in the first run with Pb-Pb collisions at $\sqrt{s_{NN}} = 2.76\,\mathrm{TeV}$ in 2011 [76] and has measured a lifetime $\tau({}^{3}_{\Lambda}\mathrm{H}) = 181^{+54}_{-39\ \mathrm{stat}} \pm 33_{\mathrm{sys}}\,\mathrm{ps}$ [77]. In the third Pb-Pb run at $\sqrt{s_{NN}} = 5.5\,\mathrm{TeV}$, starting in 2018 with the upgraded version of the apparatus, in particular of the Inner Tracking System [78], an integrated luminosity one hundred times higher will be reached and a similar increase of the statistics of the data sample used to investigate ${}^{3}_{\Lambda}\mathrm{H}$ production will be achieved. Taking into account the different collision energy, a yield of $\sim 4.4 \cdot 10^4$ ${}^{3}_{\Lambda}\mathrm{H}$ is expected [79] and, due to quasi perfect colour transparency of the Pb-Pb interaction at $\sqrt{s_{NN}} = 5.5\,\mathrm{TeV}$, an equal yield of $\overline{{}^{3}_{\Lambda}\mathrm{H}}$ is foreseen. In this situation an improvement of the signal to noise (S/B) ratio of $\sim 42\%$ will be obtained for the evaluation of the yield, while for the determination of $\tau({}^{3}_{\Lambda}\mathrm{H})$ a reduction of a factor ~ 10 is expected on the statistical component of the error, and hopefully will permit to determine precisely the final value.

Finally it is possible that an upgraded version of the HypHi experiment [47] could improve the precision on the so far published values of the lifetimes of the hydrogen hyperisotopes.

For the measurement of the lifetime of high-A hypernuclei with the time delay spectra, we guess that the only possibility is to wait for the operation of the above mentioned beam line HIHR at J-PARC. The (π^+, K^+) reaction around $1.05\,\mathrm{GeV}/c$ on targets of La, Bi and Pb, arranged like in fig. 4 right, for a total thickness of 5 cm each along the incident beam direction should be used to produce the corresponding hypernuclear species. By assuming a differential cross section of $30\,\mu$barn/sr for the production of Λ-

bound states [80] a probability of 10^{-5} that a charged particle (p, π^-, e^-) produced in the WD of the hypernucleus should trigger the t.o.f. system and realistic other experimental features, we obtain around 90 events/day for target. As we will see in the following sects. **5** and **6**, reliable theoretical calculations show that the Pauli blocking effect for MWD is not fully effective and that some of the protons emitted in NMWD may leave the nucleus without suffering FSI effects. We have added electrons from the $\Lambda \to p + e^- + \bar{\nu_e}$ semileptonic decay (BR $= 8.32 \cdot 10^{-4}$) usually not considered, which is only partially Pauli blocked. Of course one has to wait for the operation of the beam line (backgrounds, time structure,...) before finalizing a proposal with the necessary experimental details.

5. – Mesonic weak decay

5˙1. *A compilation of existing data.* – There is a fairly good amount of data about $\Gamma_{\pi^-}/\Gamma_\Lambda$ in the case of *s*-, *p*- and *sd*-shell hypernuclei, for which the Pauli blocking effect leaves room for the process. The majority of experiments adopted the simple technique of selecting the π^- decay, by scintillator arrays (see fig. 4, right), in coincidence with a well-defined region of the hypernuclear excitation spectrum (see fig. 5). Energy distributions of the π^- decay have been produced only by the FINUDA experiment for four *p*-shell hypernuclei [30] and by ref. [36] for ${}^{12}_{\Lambda}$C. There are not so many data on $\Gamma_{\pi^0}/\Gamma_\Lambda$, due to the difficulty in detecting the π^0; they are limited to the $A = 4$, 5, 11 and 12 hypernuclear systems. The detection of the photons from the π^0 decay was performed with large arrays (128 elements for the LHe target [56], 176 for the active carbon target (plastic scintillator) [81]) of NaI(Tl) scintillators in the experiment with stopped K^- at KEK [27]. In experiments with K^- in flight at BNL [23] or with π^+ in flight at KEK [82] stacks of plastic scintillators like those sketched in fig. 4 right) were used to detect the photons from π^0 decay.

Table II summarizes the published data. In case of several values for the same hypernucleus we report the corresponding references, the laboratories where the measurements were done and the weighted average (w.a.). In case of subsequent reports from the same Collaboration we quote only the most recent one. In the case of $\Gamma_{\pi^0}/\Gamma_\Lambda$ we do not report values not directly measured but inferred by difference from other measured quantities using eq. (17), often with approximations based on theoretical assumptions.

Figure 11 shows the plots of the normalized MWD widths (w.a. or single values) as a function of A. The most visible effect is the expected decrease due to the Pauli blocking effect, modulated by quite strong variations due to the specific nuclear structure of the hypernucleus and of the daughter nucleus.

5˙2. *Comparison with theoretical predictions.* – The development of theoretical treatments to the MWD of hypernuclei is a paradigmatic case of the deep interplay between particle and nuclear physics aspects and of the usefulness of a close collaboration between experimentalists and theorists.

The start up of the theories of MWD is due to Dalitz [85], who introduced a phenomenological Lagrangian describing the elementary decay processes of the free Λ with the newly established properties ($\Delta I = 1/2$ rule, prevalence of the *s*-wave, parity-violating, spin–non-flip amplitude, π angular distribution dependence on Λ spin axis). Following this approach, it was possible to determine the ground state spin and parity of the hypernuclei observed in experiments with emulsions (see ref. [86] for a summary). Thanks to the advent of electronic experiments, capable of producing better quality data, the theoretical description was consequently improved by introducing the Pauli suppres-

TABLE II. – *Summary of published data on MWD widths direct measurements. For each measurement the corresponding reference and the Laboratory are indicated; in case of several measurements by different experiments for the same hypernucleus the w.a. is also calculated. See text for more details.*

	$\Gamma_{\pi^-}/\Gamma_\Lambda$ (ref., lab.)	$(\Gamma_{\pi^-}/\Gamma_\Lambda)_{\text{w.a.}}$	$\Gamma_{\pi^0}/\Gamma_\Lambda$ (ref., lab.)	$(\Gamma_{\pi^0}/\Gamma_\Lambda)$ (w.a.)	Remarks
${}^{4}_{\Lambda}$H	$1.00^{+0.12}_{-0.19}$ [56] KEK				
${}^{4}_{\Lambda}$He	0.33 ± 0.05 [56] KEK	0.304 ± 0.031	0.53 ± 0.07 [56] KEK	0.565 ± 0.051	
	0.289 ± 0.039 [23] BNL		0.604 ± 0.073 [23] BNL		
${}^{5}_{\Lambda}$He	0.44 ± 0.11 [22] BNL		0.201 ± 0.011 [82] KEK		
	0.340 ± 0.016 [57] KEK	0.342 ± 0.015			
	0.332 ± 0.069 [30] LNF				
${}^{7}_{\Lambda}$Li	0.353 ± 0.059 [30] LNF				π^- energy spectrum
${}^{9}_{\Lambda}$Be	0.178 ± 0.050 [30] LNF				π^- energy spectrum
${}^{11}_{\Lambda}$B	0.22 ± 0.05 [83] BNL		0.192 ± 0.056 [81] KEK		
	0.23 ± 0.06 [84] KEK	0.224 ± 0.023			
	0.212 ± 0.036 [26] KEK				
	0.249 ± 0.051 [30] LNF				π^- energy spectrum
${}^{12}_{\Lambda}$C	$0.052^{+0.063}_{-0.035}$ [22] BNL		0.165 ± 0.008 [81] KEK		
	0.14 ± 0.07 [84] KEK	0.118 ± 0.014	0.217 ± 0.073 [82] KEK	0.166 ± 0.008	
	0.123 ± 0.015 [36] KEK				π^- energy spectrum
${}^{15}_{\Lambda}$N	0.108 ± 0.038 [30] LNF				π^- energy spectrum
${}^{27}_{\Lambda}$Al	0.108 ± 0.038 [30] LNF				
${}^{28}_{\Lambda}$Si	0.046 ± 0.011 [26] KEK				
${}_{\Lambda}$Fe	< 0.015 (90% CL) [26] KEK				

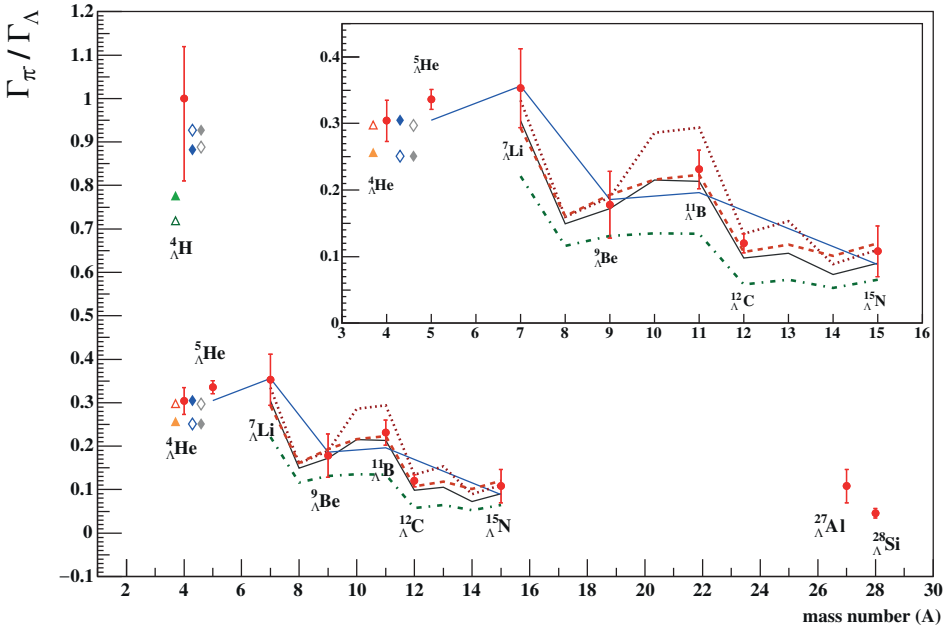

Fig. 11. – Normalized MWD widths as a function of A: w.a. values from table II are represented as full red circles. Theoretical calculations results are also indicated: black continuous line from ref. [70], brown dotted line from ref. [91] with the MSU group optical potential, green dashed line from ref. [91] with Whisnant optical potential, red dot-dashed line from ref. [91] with free-pion wave, blue continuous line from ref. [94], full green up-triangles from ref. [92] with one range Gaussian (ORG) potential, open green up-triangles from ref. [92] with Y-N G-matrix (YNG) potential, full orange triangle from ref. [95] with ORG potential, open red triangle from ref. [95] with YNG potential, full blue diamonds from ref. [96] with Isle potential, open blue diamonds from ref. [96] with single Gaussian potential. In the inset an expanded view of the region between $^{4}_{\Lambda}$He and $^{15}_{\Lambda}$N is presented.

sion effect, the MWD decay rate enhancement due to the pion polarization effect in the nuclear medium [87-90] and the final-state shell-structure dependence which strongly influences the charge status of the decay rates.

A significant improvement in MWD calculations was obtained by the introduction of the π^- nucleus optical potential which generates pion distorted waves that strongly affect the final results. Detailed calculations of the main observables in MWD (rates, energy spectra) were presented in refs. [70, 91-96]. In fig. 11 we have reported the values predicted by the theoretical calculations, which are in a remarkably nice agreement with the experimental ones.

5˙3. *MWD of s-shell hypernuclei and the central repulsion in the hyperon-nucleus potential.* – A motivation for performing precise measurements of the MWD partial widths for the s-shell $^{4}_{\Lambda}$H and for the He hyperisotopes ($^{4}_{\Lambda}$He, $^{5}_{\Lambda}$He) was represented by a possible verification of the existence of a central repulsion in the hyperon-nucleus mean potential. Several authors started from the realistic two-body YN interaction, in which the strength of the long-range attraction is much weaker than the NN one and is almost counterbalanced by the short-range repulsion; they finally argued that an inner repulsion

should be present in the Y-nucleus potentials deduced from the YN interaction with the folding procedure. The effect of such a repulsion should be more evident for s-shell hypernuclei; the hyperon would be pushed outward the nuclear core and consequently the overlap of the hyperon and of the nucleus wave functions should be much reduced.

The manifestation of the repulsive nuclear core was clearly assessed in the case of the Σ-hyperon through the observation of a narrow-width signal only for the ${}^{4}_{\Sigma}$He system [97-99]. All other nuclear systems containing a Σ exhibit a large width signal due to the ΣN-ΛN strong conversion which is suppressed in the ${}^{4}_{\Sigma}$He system, being the Σ pushed outward the nuclear core due to the inner repulsion. To verify the existence of a repulsive core also for Λ-nucleus potential it is necessary to look at the MWD rates, influenced by the Pauli principle suppression, which are sensitive to the overlap between the wave functions of the Λ and of the nuclear core; this overlap, in turn, reflects the potential shape felt by the Λ in nuclei.

A detailed overview of the theoretical efforts on this item, including comparison with the different decay widths for the MWD of ${}^{4}_{\Lambda}$H, ${}^{4}_{\Lambda}$He and ${}^{5}_{\Lambda}$He that were measured with considerable precision, can be found in refs. [13, 14]. We recall here the conclusion that only a Λ-nucleus potential having a central repulsive core and an outer attractive pocket, as introduced in refs. [95,96], was able to reproduce within 1σ all the experimental values of the different decay widths. The existence of an inner repulsive core in the Λ-nucleus was thus experimentally ascertained.

5˙4. *MWD of p-shell and heavier hypernuclei*. – We have already stressed that in hypernuclei the MWD is disfavoured by the Pauli principle, particularly in heavy systems. It is strictly forbidden in infinite nuclear matter at normal density, where the nucleon Fermi momentum is $\sim 270\,\mathrm{MeV}/c$, while in finite nuclei it can occur because of three important effects:

i) in hypernuclei the Λ has a momentum distribution, being confined in a limited spatial region, that allows larger momenta to be available to the final-state nucleon;

ii) the final state π feels an attraction by the nuclear medium, due to the p-wave part of the optical π-nucleus potential, which modifies the pion dispersion relation; for a fixed momentum, the outcoming pion carries an energy smaller than if it was free and the energy conservation increases the chance of the decay nucleon to be above the Fermi surface. Indeed, it has been argued that the pion distortion increases the MWD width by more than one order of magnitude (from some 10^{-5} to some 10^{-4}) for $A \sim 200$ hypernuclei with respect to the value obtained without the medium distortion [100];

iii) at the nuclear surface the local Fermi momentum can be smaller than $270\,\mathrm{MeV}/c$ and then the Pauli blocking should be less effective in suppressing the decay.

As can be seen in fig. 11, the MWD partial-decay rates decrease with increasing A, reaching values of less than 5% for ${}^{27}_{\Lambda}$Al and ${}^{28}_{\Lambda}$Si. Recently, the FINUDA Collaboration, besides reporting for the first time $\Gamma_{\pi^-}/\Gamma_{\Lambda}$ for the p-shell hypernuclei ${}^{7}_{\Lambda}$Li, ${}^{9}_{\Lambda}$Be and ${}^{15}_{\Lambda}$N and a further measurement for ${}^{11}_{\Lambda}$B, improved considerably the knowledge of the features of the MWD by showing the energy spectra of the emitted π^- too, measured with magnetic analysis [30]. A comprehensive account is given in ref. [15] and we recall here only some peculiar feature. Being characterized by a small Q-value, the MWD mode is strongly affected by the details of both the hypernucleus and the daughter

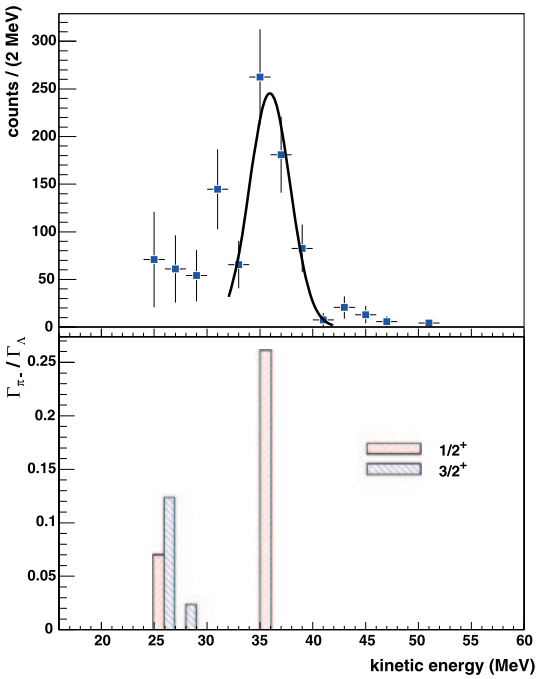

Fig. 12. – Upper part: kinetic energy spectrum of MWD π^- for ${}^{7}_{\Lambda}$Li. The solid curve is a Gaussian fit to the peak, to compare with theoretical predictions in the lower part. Lower part: calculated major decay rates to final ^{7}Be states from ref. [94], in red bars for ${}^{7}_{\Lambda}$Li ground-state spin-parity $1/2^+$, and in blue bars for ${}^{7}_{\Lambda}$Li ground-state spin-parity $3/2^+$. From ref. [30].

nucleus structure. Indeed, the theoretical calculations developed in refs. [70,95] evaluated the p-shell total and partial MWD rates by incorporating the pion FSI based on pion-nuclear distorted waves and by describing the structure of the nuclear core with the Cohen-Kurath spectroscopic approach [101,102]. It was found that for p-shell hypernuclei the total π^- decay rate is dominated by $\Lambda(1s) \to p(1p)$ transitions while only small contributions are given by higher-energy configurations of the final nuclear system, mainly through $\Lambda(1s) \to p(2s, 1d)$ transitions.

Recently, these calculations were revisited in ref. [94], following the same approach, and a new sum rule was introduced to encapsulate the suppressive effect of the Pauli principle on the total and partial π^- decay rates.

Figure 12 shows the π^- spectrum from the MWD of ^{7}Li (upper part) compared with the calculated decay rates to final ^{7}Be state [94] (lower part). These calculated rates are close to those obtained in ref. [70]. The correspondence of the structures identified in the experimental spectra with the rates for decays to different excited states of the daughter nucleus, assuming a $1/2^+$ initial spin-parity state, is clear. The peak structure corresponds to the production of ^{7}Be in its $3/2^+$ ground state and in its only bound $1/2^-$ excited state at 429 keV, not visible owing to the experimental resolution of 4.2 MeV FWHM. The part of the spectrum at lower energies is due to three-body decays. The shape of the spectrum confirms the spin assigned to the ground state of ${}^{7}_{\Lambda}$Li [103]. Indeed, only a $1/2^+$ spin-parity for ${}^{7}_{\Lambda}$Li ground state, shown by red bars, reproduces the fitted peak at $\sim$ 36 MeV, ascribed to the ^{7}Be ground state, and the excited state

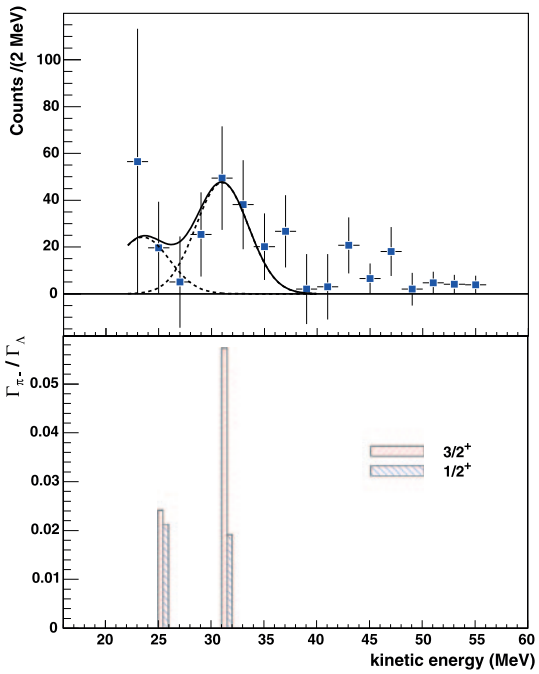

Fig. 13. – Upper part: kinetic energy spectrum of MWD π^- for ${}^{15}_{\Lambda}$N. The solid curve is a two-Gaussian fit to the peaks, to compare with theoretical predictions in the lower part; dashed curves are the single components. Lower part: calculated major decay rates to final ^{15}O states from ref. [94], in red bars for ${}^{15}_{\Lambda}$N ground-state spin-parity $3/2^+$, and in blue bars for ${}^{15}_{\Lambda}$N ground-state spin-parity $1/2^+$. From ref. [30].

at 429 keV. A $3/2^+$ spin-parity for ${}^{7}_{\Lambda}$Li ground state would imply a radically different spectral shape [70, 94], as indicated in fig. 12 by the blue bars.

Similar considerations were applied to the spectra for ${}^{9}_{\Lambda}$Be and ${}^{11}_{\Lambda}$B (shown in fig. 7). The case of ${}^{15}_{\Lambda}$N is somehow different and interesting as example of a possible spectroscopic tool. Figure 13 shows the experimental spectrum compared to calculated decay rates to ^{15}O final states [94]. In the experimental spectrum, the ^{15}O $1/2^-$ ground-state contribution stands out clearly, along with a hint for a secondary structure separated by $\sim$ 6 MeV. The fit to the lower-energy secondary structure is strongly influenced by the substantial error affecting the data point at the lowest energy. According to refs. [94,95] this secondary structure derives most of its strength from *sd*-states scattered around 6 MeV excitation, while the contribution of the $p^{-1}_{3/2}$ $p_{1/2}$ ^{15}O excited state at 6.176 MeV is negligible. Before the FINUDA measurement, the ground-state spin of ${}^{15}_{\Lambda}$N was not determined experimentally. The most recent theoretical study of hypernuclear spin-dependence [104] predicts $J^\pi({}^{15}_{\Lambda}\mathrm{N}_{\mathrm{g.s.}}) = 3/2^+$, setting the $1/2^+$ excited state of the ground-state doublet $\sim$ 90 keV above the $3/2^+$ state. However, the spin ordering could not be determined from the γ-rays de-excitation spectra measured on a ^{16}O target [105]. The prominence of the ${}^{15}\mathrm{O}_{\mathrm{g.s.}}$ in the spectrum of fig. 13 supports this $3/2^+$ theoretical assignment. Moreover, the total π^- decay rate of ${}^{15}_{\Lambda}$N agrees with calculations of refs. [94, 95] by assuming a $3/2^+$ ground-state spin-parity assignment. These two predictions disagree about a $1/2^+$ spin-parity assignment, and, following the most recent

calculation of ref. [94] for ${}^{15}_{\Lambda}$N, which corrects the previous ones [70, 95], a $1/2^+$ spin-parity is excluded and the assignment $J^\pi({}^{15}_{\Lambda}\mathrm{N}_{\mathrm{g.s.}}) = 3/2^+$ is made based mainly on the decay rate and the shape of the MWD spectrum.

It is then evident that the study of the MWD spectra has strong potentialities for the determination of the ground state spin-parity for strange nuclear systems up to *sd*-shell, for which the $\Gamma_{\pi^-}/\Gamma_\Lambda$ values are still known at a level of some percent. The spectroscopy of the π^- emitted in the decay process can help in fixing the spectroscopic configuration of the ground state and it becomes resolutive with respect to the γ-ray spectroscopy of low-lying excited states, when this latter is not able to determine the spin ordering. It represents a new version of the old technique based on the study of the angular distribution of the MWD π^-, which permitted the ground state spin-parity determination of light hypernuclei in emulsion experiments (see, *e.g.*, ref. [106]), based on the known properties of the free Λ WD.

5˙5. *Future experimental efforts*. – From the above discussion it appears that MWD of hypernuclei is quite well understood. It could be interesting to determine the MWD decay width for $A \sim 200$ hypernuclei, along with the measurement of their lifetime as described in the last part of subsect. **4**˙4.

It was realized that a better performance in spectroscopy of π^- from MWD of hyperfragments produced by electroproduction could be achieved at the continuous wave electron accelerators at JLab and Mainz, by taking advantage of the excellent spectrometers already in use. A proposal for an experimental setup aiming at a resolution of 100 keV, operating in Hall A of JLab, has been put forward [107,108]. The physical idea is that owing to large momentum transfer an electro-produced hypernucleus should have excitation energies well above the lowest particle emission threshold and then should fragment into lower mass clusters and nucleons. This fast process can lead to particle-stable hypernuclei (the old-hyperfragments seen in emulsions!) in a wide range of mass and of atomic number. MWD occurs from the ground state of these hyperfragments which are stopped in the production target. The momenta of the π^- from the two-body WD range from 100 to 140 MeV/c and they may permit the determination of the mass of the hyperfragment with a precision better than that achieved in emulsion experiments [108].

Very recently, the experimental proof of the soundness of the idea has been obtained at MAMI-C at Mainz: hyperfragments were electroproduced via the $(e, e'K^+)$ reaction on a Be target and they were detected with the Kaon Spectrometer (KaoS). KaoS has been setup by integrating the preexisting A1 apparatus [109] with a dedicated short orbit kaon spectrometer placed at 0° with respect to the e^- beam axis [110]. It is capable to detect kaons in the forward direction and then to tag events with strangeness production, while SpekA and SpekC, two of the three high-resolution spectrometers of the A1 apparatus, make possible to measure the momenta of π^- emitted in the two-body WD of the electroproduced hyperfragments. Stopped hyperfragments are identified by monochromatic peaks, that should permit the measurement of the mass with an expected precision of 50 keV/c^2. The monochromatic π^- peak at $\sim$ 133 MeV/c from the ${}^{4}_{\Lambda}\mathrm{H} \to {}^{4}\mathrm{He} + \pi^-$ decay, stemming from a flat background was clearly observed [111], making possible a new measurement of the ${}^{4}_{\Lambda}$H mass, an important piece of information in the long standing problem of the Charge Symmetry Breaking (CSB) in the $A = 4$ system. We may expect that the high-resolution pion decay spectroscopy of hyperfragments will be an important investment for hypernuclear physics in the next decade.

6. – Non-mesonic weak decay

6˙1. *Introductory remarks.* – A great deal of efforts was dedicated to NMWD of hypernuclei by both theorists and experimentalists in the last decades. The challenge was that of achieving an important physics result like the study of the ΛN-NN weak interaction, but facing a lot of difficulties that were encountered in all steps. A chronological description of the development of ideas and experimental achievements is perhaps more helpful for understanding the links between the various steps forward. Such an approach was adopted in a shortcut in ref. [86] and afterwards in ref. [15]. However, we think that nowadays a large part of the open problems is solved or at least understood and it is the time to address a systematic study of this challenging process. Then, we adopt a description not chronological but per items, being necessarily forced to say often "as we will see in the following section".

As anticipated at the end of sect. **2**, the observables that can be directly measured for a given hypernucleus are τ (and then Γ_T/Γ_Λ) and Γ_M. Γ_{NM} can be obtained in an indirect way by subtraction following eq. (15). Even if we neglect Γ_{2N} (this assumption can be applied perhaps only to ${}^{4}_{\Lambda}$He, as we will discuss in sect. **8**) it is necessary to have at least another measurement involving Γ_p and Γ_n in order to obtain their individual values and to compare them with theoretical estimations. The ratio Γ_n/Γ_p seems to be the most adequate. It is an important observable used to study the isospin structure of the NMWD, but for several decades it has been a puzzle. As a matter of fact, the most natural and simple model, the OPE, that we will briefly describe in subsect. **6**˙4, predicted low values (~ 0.1) for the ratio Γ_n/Γ_p whereas the experimental determinations, although affected by large errors, were higher by one order of magnitude. In the last decade, a great experimental effort was then devoted to the solution of the puzzle by dedicated measurements of the nucleon spectra and by their interpretation, in close collaboration with theoreticians.

6˙2. *Nucleon spectra from NMWD and determinations of* Γ_n/Γ_p. – Energy spectra of nucleons emitted in NMWD of several hypernuclei were measured with good precision and adequate statistics. We will show some of them, we discuss the main features and we outline briefly the attempts to determine from them Γ_n/Γ_p.

Figure 14 shows the spectrum of protons emitted in NMWD of ${}^{4}_{\Lambda}$He, obtained at the BNL AGS [23]. It has the shape of a broad peak centred around 80 MeV, very close to the value expected for the 3-body decay ${}^{4}_{\Lambda}\mathrm{He} \to d+p+n$ with no d recoil (84.1 MeV). It is important to note that the proton energy threshold is 30 MeV. We show it since it is the only experimental spectrum which closely carries the information on the bare spectrum emitted in the $1p$-induced NMWD process (7), without strong distortions from FSI and $2N$-induced NMWD. The measured neutron spectrum had little statistical significance, and only an upper limit of 0.19 (at 95% confidence level) for Γ_n/Γ_p could be deduced. We will return on this point in sect. **8**.

The SKS Collaboration at KEK produced a large amount of spectra of nucleons from NMWD with interesting interpretations and we will examine them briefly in the following. High-statistics proton energy distributions from NMWD of ${}^{12}_{\Lambda}$C, ${}^{28}_{\Lambda}$Si and ${}_{\Lambda}$Fe, with a 30 MeV threshold, were measured [26, 112] by means of the range arrays shown by fig. 4, left, and they are reported in fig. 15. The experimental spectra were compared with those calculated by means of a detailed model in which the proton energy spectra generated by $1N$-induced NMWD (the $1n$-induced produces secondary protons too) were summed incoherently for a given Γ_n/Γ_p ratio [113,114]. A possible contribution

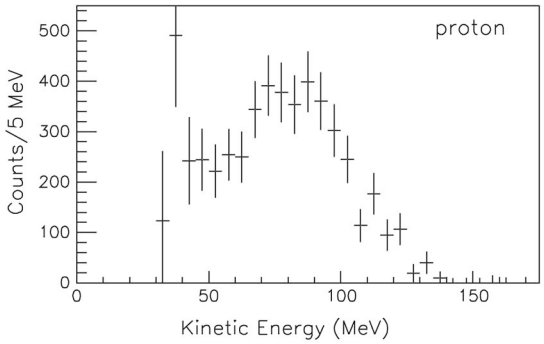

Fig. 14. – Proton kinetic energy spectra from WD of ${}^{4}_{\Lambda}$He. Adapted with permission from ref. [23], © 2007, the American Physical Society. http://dx.doi.org/10.1103/PhysRevC.76.035501.

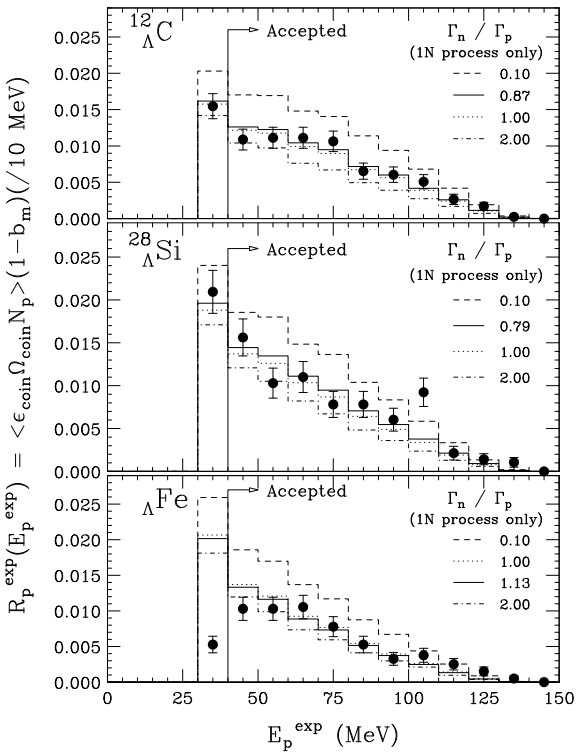

Fig. 15. – Comparison of the experimental data [26] and calculation from refs. [113, 114]. The horizontal axis is the observed energy by the decay counter. The vertical axis is normalized by the number of hypernuclear WDs. Reprinted with permission from ref. [26], © 2005, the American Physical Society. http://dx.doi.org/10.1103/PhysRevC.71.025203.

from the $2N$-induced NMWD, not yet observed experimentally, was also considered. FSI effects on the nucleons in the daughter nuclear system were taken into account resorting to an INC calculation. Experimental corrections were evaluated by means

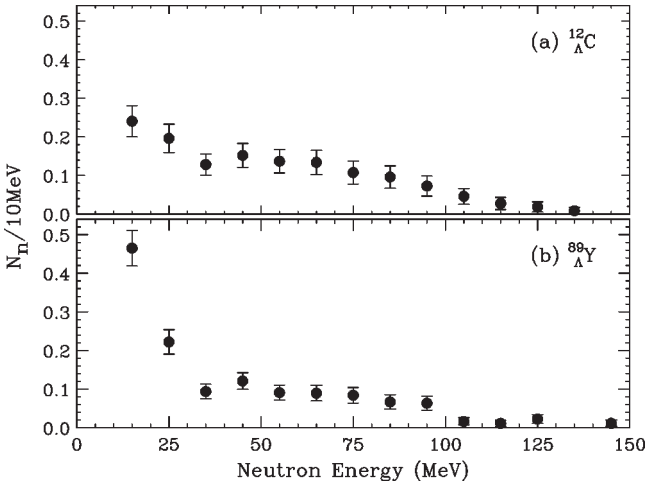

Fig. 16. – Neutron energy spectra per NMWD of (a) $^{12}_{\Lambda}$C and (b) $^{89}_{\Lambda}$Y. Reprinted with permission from ref. [116], © 2003, the American Physical Society.
http://dx.doi.org/10.1103/PhysRevC.68.065201.

of the GEANT simulation code [115]. The final values for the three hypernuclei were obtained by fitting the experimental spectra to the simulated ones, leaving the Γ_n/Γ_p ratio as a free parameter. The best fitting value obtained is reported in fig. 15 and it corresponds to the continuous line, whereas the other lines correspond to other values chosen for comparison. The result was encouraging since, though still affected by 30–40% errors, the reported values were in the 0.5–1.0 range for $^{12}_{\Lambda}$C and $^{28}_{\Lambda}$Si, considerably lower than the previous ones. An intrinsic weakness of the method of using only the proton spectra from NMWD was that it was depending on a theoretical model.

It became clear that a measurement of the neutron spectra from NMWD was needed. High-statistics spectra were obtained for $^{12}_{\Lambda}$C and $^{89}_{\Lambda}$Y [116] by surrounding the nuclear targets with four arrays of neutron detectors. Figure 16 shows the measured energy distributions; the threshold on the neutron detection was 10 MeV. A comparison of the two spectra indicates clearly the strong influence of FSI; above 30 MeV the yield of NMWD neutrons from $^{89}_{\Lambda}$Y is lower than that for $^{12}_{\Lambda}$C, whereas below 30 MeV it nearly doubles. This remark also explains why the measurement of lifetimes of hypernuclei exploiting the delay spectra method was stopped at $A = 56$. For heavier hypernuclei, like $^{89}_{\Lambda}$Y, FSI degrade the energy of protons so that they can hardly exit from the targets and trigger the t.o.f. system. It can be assumed that FSI affect the spectra of neutrons and protons from NMWD at the same extent, due to the charge symmetry of the NN scattering and then the distortions cancel out if we consider their ratio, at least at the first order. For $^{12}_{\Lambda}$C the yield of neutrons was compared to that of protons reported by ref. [112]. The N_n/N_p ratio between the neutron and proton numbers, corrected for acceptance and efficiency, was found to be (1.73 ± 0.22) corresponding to a Γ_n/Γ_p value of (0.51 ± 0.15). As we will see in subsect. **6**˙5, this result ruled out the original OPE model for NMWD in favour of more complex approaches.

Since this result was obtained by comparing data from different layouts, that could introduce systematic, not evaluated, errors a subsequent measurement was performed with higher statistics and detecting both nucleons simultaneously (but not in coinci-

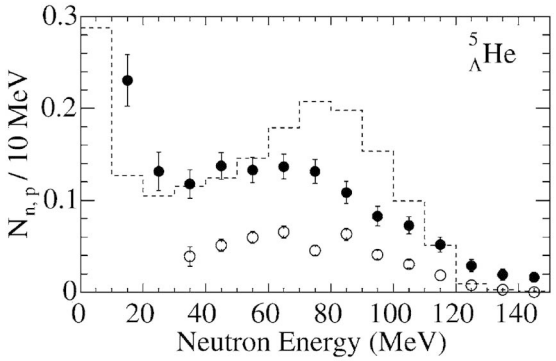

Fig. 17. – Neutron (filled circles) and proton (open circles) energy spectra per NMWD of $^{5}_{\Lambda}$He [117]. The dashed histogram shows the NMWD neutron spectrum of $^{5}_{\Lambda}$He calculated by [118]. Adapted from ref. [117].

dence) [117]. The set-up was basically the one represented by fig. 4, left, with the addition of a further range array, installed vertically on one side to increase the detection solid angle. Spectra were collected for $^{5}_{\Lambda}$He and $^{12}_{\Lambda}$C hypernuclei, typical of the *s*- and *p*-shells. Figure 17 shows the nucleon spectra for $^{5}_{\Lambda}$He. Due to the different thresholds (15 MeV for neutrons, 30 MeV for protons) the low-energy rise is not visible in the proton spectra. The dashed histogram represents a calculated neutron energy spectrum in which both FSI and $2N$-induced NMWD were taken into account and values of $\Gamma_n/\Gamma_p = 0.46$ and $\Gamma_{2N}/\Gamma_{1N} = 0.20$ were assumed [118]. It does not fit well the experimental spectrum; the main difference is that its maximum falls ~ 10 MeV higher than the measured one.

Since the FSI and $2N$-induced NMWD effects tend to enhance the low-energy region, a software threshold of 60 MeV was applied to reduce their importance and to deduce the ratios of the yields N_n/N_p. Values of $(2.17\pm0.15_{\rm stat}\pm0.16_{\rm sys})$ and $(2.00\pm0.09_{\rm stat}\pm0.14_{\rm sys})$ were found, respectively, for $^{5}_{\Lambda}$He and $^{12}_{\Lambda}$C. The last value is in agreement within the errors with the value from ref. [116]. Values of Γ_n/Γ_p between 0.5 and 0.6 were finally obtained.

The most complete set of energy distributions of protons from NMWD of hypernuclei (eight species in the range $5 \leq A \leq 16$) was recently provided by FINUDA [31, 32] and it would seem logical to include it in this subsection. However, since it allowed to deduce directly Γ_p/Γ_Λ with a dedicated analysis, we postpone its presentation to the next subsection.

We continue and we end this subsection with the discussion about the latest determinations of Γ_n/Γ_p based on the NN coincidence spectra analysis. The simultaneous measurement of both NMWD neutron and proton energy distributions turned out to be very important in clarifying the inconsistency of the old measurements. The assumption that the yield ratio N_n/N_p should give directly Γ_n/Γ_p since the FSI distortions are cancelled is valid only in a first approximation. Corrections based on FSI calculations and for possible contributions from $2N$-induced NMWD were still needed. A cleaner approach should be to measure the nucleon spectra in coincidence, even though with a drastic reduction of the statistics. Both the $\Lambda n \to nn$ and $\Lambda p \to np$ processes in nuclei are (quasi) two-body decay processes and then the two nucleons should have a clean back-to-back (b.t.b.) correlation, provided that both of them are not affected by FSI and do not originate from $2N$-induced NMWD. Experimentally the $1N$-induced processes could

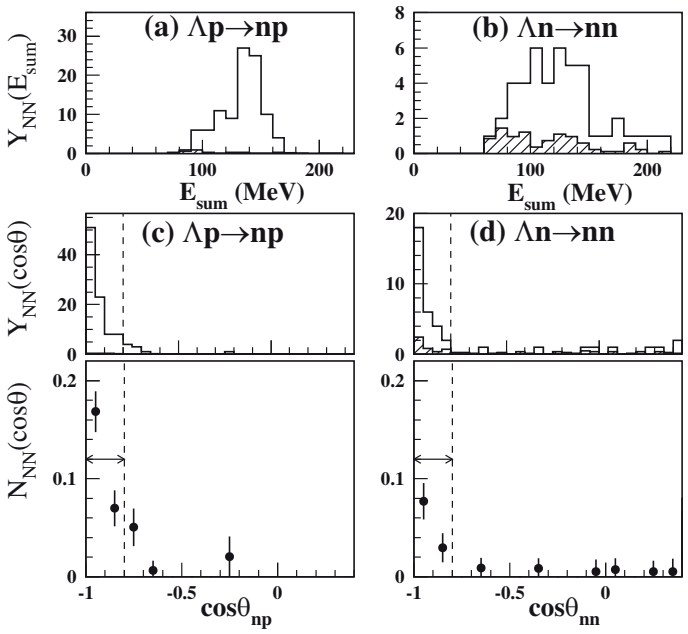

Fig. 18. – Nucleon-nucleon coincidence spectra for the NMWD of ${}^{5}_{\Lambda}$He. Reprinted with permission from ref. [119], © 2006, the American Physical Society. (a) and (b): *np* and *nn* pair raw yields as a function of the energy sum of the pair nucleons, before efficiency correction; a 30 MeV threshold was applied to both nucleons. (c) and (d): The upper panels show the opening angle dependence of the *np* and *nn* raw yields; the lower panels show the final angular spectra normalized for NMWD. http://dx.doi.org/10.1103/PhysRevLett.96.062301.

be clearly selected by measuring the yields of *np* and *nn* pairs in the b.t.b. configuration and by requiring that the sum of their kinetic energies correspond to the Q-value of the NMWD reaction. A measurement of N_{nn}/N_{np} under these constraints should provide a value of Γ_n/Γ_p, with only a small contamination from FSI and $2N$-induced processes.

A dedicated experiment was carried out at KEK and the first hypernucleus studied was the light one ${}^{5}_{\Lambda}$He, for which the FSI effects should be reduced [119]. The upper panels of fig. 18 shows the *np* and *nn* pair raw yields, Y_{np} and Y_{nn}, as a function of the sum of the kinetic energy of the nucleon pairs. In the energy sum spectrum of *np* pairs a clear peak around the Q-value of the NMWD process is visible. The analogous spectrum relative to the *nn* pair is broader, due to the limited energy resolution for neutrons, and contaminated by some background. The lower panels show the raw yields Y_{np} and Y_{nn} together with the efficiency corrected yields normalized per NMWD, N_{np} and N_{nn}, as a function of the opening angle between the two nucleons, θ_{np} and θ_{nn}. A nice angular correlation is evident, signature of the direct selection of the $1N$-induced processes. By applying the angular cut $\cos(\theta_{NN}) \leq -0.8$, shown by the vertical dashed lines in the lower panels, a final value $\Gamma_n/\Gamma_p = (0.45 \pm 0.11_{\mathrm{stat}} \pm 0.03_{\mathrm{sys}})$ was given. An analogous measurement for ${}^{12}_{\Lambda}$C, representative of p-shell hypernuclei, provided the value $\Gamma_n/\Gamma_p = (0.51 \pm 0.13_{\mathrm{stat}} \pm 0.05_{\mathrm{sys}})$ [120]. A large contribution to the errors was given by the efficiency for neutron detection. The assumption that the above values were free from ambiguities from FSI and $2N$-induced processes was questioned by the authors of

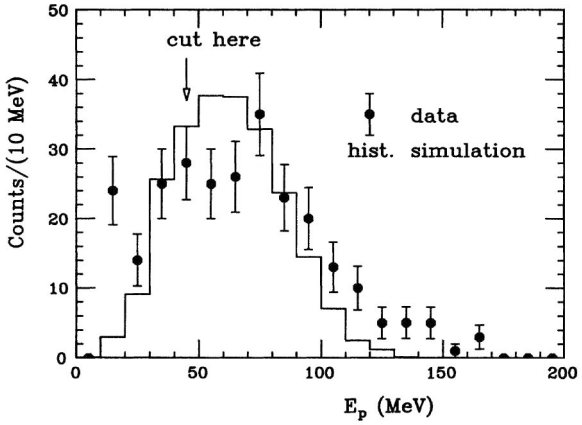

Fig. 19. – Proton-energy spectrum observed in the ${}^{12}_{\Lambda}$C ground-state region (full circles with error bars). Reprinted with permission from ref. [84], © 1995, the American Physical Society. http://dx.doi.org/10.1103/PhysRevC.52.2936.

ref. [118, 121], who calculated a reduction as large as 30% when the above effects were taken into account.

A final remark on the various experimental studies on nucleon spectra from NMWD is that they led to a realistic value of Γ_n/Γ_p, in agreement with the latest theoretical evaluations, but at the same time they recognized the importance of the $2N$-induced processes. The original idea of determining Γ_p and Γ_n through the measurement of Γ_{NM} and Γ_n/Γ_p, valid only in case that Γ_{2N} was negligible, was no longer suitable. Other approaches were necessary to determine Γ_p and Γ_n.

6˙3. *A compilation of existing data on proton-induced NMWD.* – The first experiment which reported a value for Γ_p/Γ_Λ was the already cited Moby Dick at BNL for the ${}^{5}_{\Lambda}$He hypernucleus [22]. The spectrum of protons was measured by a range array, with a resolution of $\sim 15\%$ and showed an indication for a maximum at an energy corresponding to that of the b.t.b. $1p$-induced NMWD, within the limits of the resolution and of the statistics. FSI were taken into account using a simplified INC model in which the nucleus was represented by a uniform spherical matter distribution of radius 2.1 fm and the mean free path for an outgoing nucleon from NMWD was 3 fm. A FSI probability of (0.3 ± 0.1) was estimated, which introduced a correction of 17% of the initial value of Γ_p/Γ_Λ, somewhat insensitive to the large uncertainty that was assigned to the FSI probability. The final value is reported in table III, along with all others that will be discussed in the following.

A measurement of Γ_p/Γ_Λ for the ${}^{11}_{\Lambda}$B and ${}^{12}_{\Lambda}$C hypernuclei was reported later in ref. [84]. The experiment was carried out at KEK with the spectrometer PIK, precursor of the SKS. The production reaction was (π^+, K^+) at $\sim 1.05\,\mathrm{GeV}/c$ on an active target constituted by a segmented scintillators array.

The energy of the decay charged particles was measured by two arrays of 16 NaI scintillators each, covered by plastic scintillators measuring ΔE and then allowing p.id. Figure 19 shows the proton energy spectrum observed from the ground state of ${}^{12}_{\Lambda}$C. The histogram shows also a simulation of the energy spectrum based on an INC calculation. The threshold was set at 45 MeV. It is interesting to note that the experimental spectrum

TABLE III. – *Summary of available Γ_p/Γ_Λ values for s- and p-shell hypernuclei: values, references and laboratories where the measurements have been performed are indicated in the second column. When several determinations have been obtained, the weighted average of the FSI corrected ones is indicated in the third column, while values without FSI correction are not considered. Comment on FSI treatment is reported in the fourth column.*

Hypernucleus	Γ_p/Γ_Λ (ref., lab.)	Γ_p/Γ_Λ (w.a.)	Remarks
${}^{4}_{\Lambda}$He	0.16 ± 0.02 [56] KEK		FSI corr. negligible
	0.180 ± 0.028 [23] BNL	0.167 ± 0.016	FSI corr. negligible
${}^{5}_{\Lambda}$He	0.21 ± 0.07 [22] BNL		FSI corrected
	0.22 ± 0.05 [32] LNF	0.217 ± 0.041	FSI corrected
${}^{7}_{\Lambda}$Li	0.28 ± 0.07 [32] LNF		FSI corrected
${}^{9}_{\Lambda}$Be	0.30 ± 0.07 [32] LNF		FSI corrected
${}^{11}_{\Lambda}$B	$0.30 \pm 0.07^{+0.08}_{-0.04}$ [81] KEK		not FSI corrected
	0.47 ± 0.11 [32] LNF	0.47 ± 0.11	FSI corrected
${}^{12}_{\Lambda}$C	$0.31 \pm 0.07^{+0.11}_{-0.04}$ [81] KEK		not FSI corrected
	0.45 ± 0.10 [122] KEK		FSI corrected
	0.65 ± 0.19 [32] LNF	0.49 ± 0.09	FSI corrected
${}^{13}_{\Lambda}$C	0.60 ± 0.14 [32] LNF		FSI corrected
${}^{15}_{\Lambda}$N	0.49 ± 0.11 [32] LNF		FSI corrected
${}^{16}_{\Lambda}$O	0.44 ± 0.12 [32] LNF		FSI corrected

shows a maximum around 75 MeV corresponding roughly to the expected value for $1p$-induced NMWD, in quasi b.t.b. kinematical configuration. The values reported for Γ_p/Γ_Λ on both hypernuclei, affected by quite large systematic errors, are not corrected for FSI, expected to be important for such medium-A systems. They are listed in table III but for homogeneity with other results they will not be used in the w.a. calculations.

The proton spectrum from NMWD of ${}^{4}_{\Lambda}$He was measured in the previously mentioned experiment with stopped K^- at KEK [56] by means of the array of 128 NaI scintillators, mentioned in subsect. **5**˙1. The threshold on the energy was 30 MeV and the spectrum had the quite regular shape of a broad peak centered around 80 MeV. From the shape of the spectrum and other quantitative estimations on the rates the authors concluded that effects due to FSI and $2N$-induced decays could be neglected in their evaluation of Γ_p/Γ_Λ, reported in table III, in the limits given by the statistics at disposal.

The same conclusion was reached by the experiment with K^- in flight at BNL [23]. The spectrum was already reported by fig. 11. Possible contributions from FSI and $2N$-induced NMWD were calculated using a simple model and the conclusion was that their effect on pertinent quantities, namely Γ_p/Γ_Λ listed in table III, was small and have thus little effect on the final interpretation of the data.

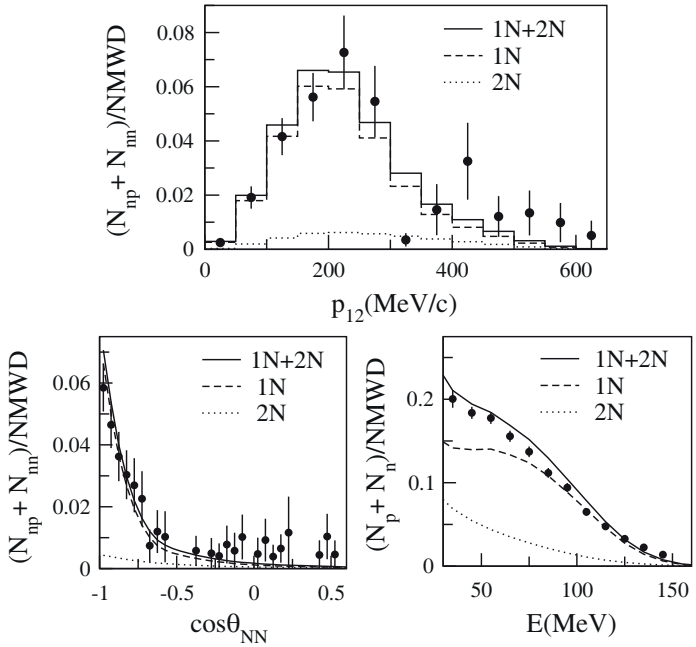

Fig. 20. – Total momentum p_{12} (upper panel), angular correlation (lower left panel) and normalized nucleon yield (lower right panel) for nn and np pairs from NMWD of ${}^{12}_{\Lambda}$C. Reprinted with permission from [122], © 2009, the American Physical Society. `http://dx.doi.org/10.1103/PhysRevLett.103.182502`. Experimental spectra are compared with those of INC ($1N + 2N$) (solid lines) with $\Gamma_{2N}/\Gamma_{nm} = 0.29$.

The SKS Collaboration at KEK, in successive steps aimed to clarify the links between their measured nucleon spectra, the values found for Γ_n/Γ_p and the importance of the $2N$-induced NMWD, noticed that experimental spectra of both protons and neutrons showed a quenching in the lower energy part with respect to what predicted for $1N$-induced NMWD including FSI. Since the three nucleons resulting from $1N$-induced decays with rescattering by FSI and those from $2N$-induced decays share the same phase space, it is impossible to disentangle them kinematically, but it is necessary to resort to an improved FSI calculation. To the purpose, the FSI strength of INC was renormalized by taking into account the measured inelastic total cross sections data for ${}^{12}\mathrm{C}(p,p')$ at 62 MeV [122]. By fitting simultaneously the experimental spectra of the sum of single n and p kinetic energy distributions, of the angular correlation, of the sum of the nn and np distributions and of the momentum sum correlation ($p_{12} = p_1 + p_2$) a value for Γ_{2N}/Γ_{NM} of (0.29 ± 0.13) was found, as shown in fig. 20; by combining it with $\Gamma_{NM}/\Gamma_\Lambda$ [57,82] the value $\Gamma_{2N}/\Gamma_\Lambda = (0.27 \pm 0.13)$ was deduced. Finally, a value of $\Gamma_p/\Gamma_\Lambda = (0.45 \pm 0.10)$ was found and it is reported in table III.

Soon afterwards, the FINUDA experiment obtained single proton energy spectra from NMWD of ${}^{5}_{\Lambda}$He, ${}^{7}_{\Lambda}$Li and ${}^{12}_{\Lambda}$C [123]. In spite ot the large mass number difference of these hypernuclei, they all show a similar shape, *i.e.* a peak around 80 MeV, corresponding to about a half the Q-value for the $\Lambda p \to np$ weak reaction, with a low-energy rise, due to the FSI and/or the $2N$-induced NMWD. If the low-energy rises were predominantly due to FSI effects, one should naturally expect that the broad peak structure at 80 MeV (coming from bare $\Lambda p \to np$ processes broadened by the Fermi motion of the interacting

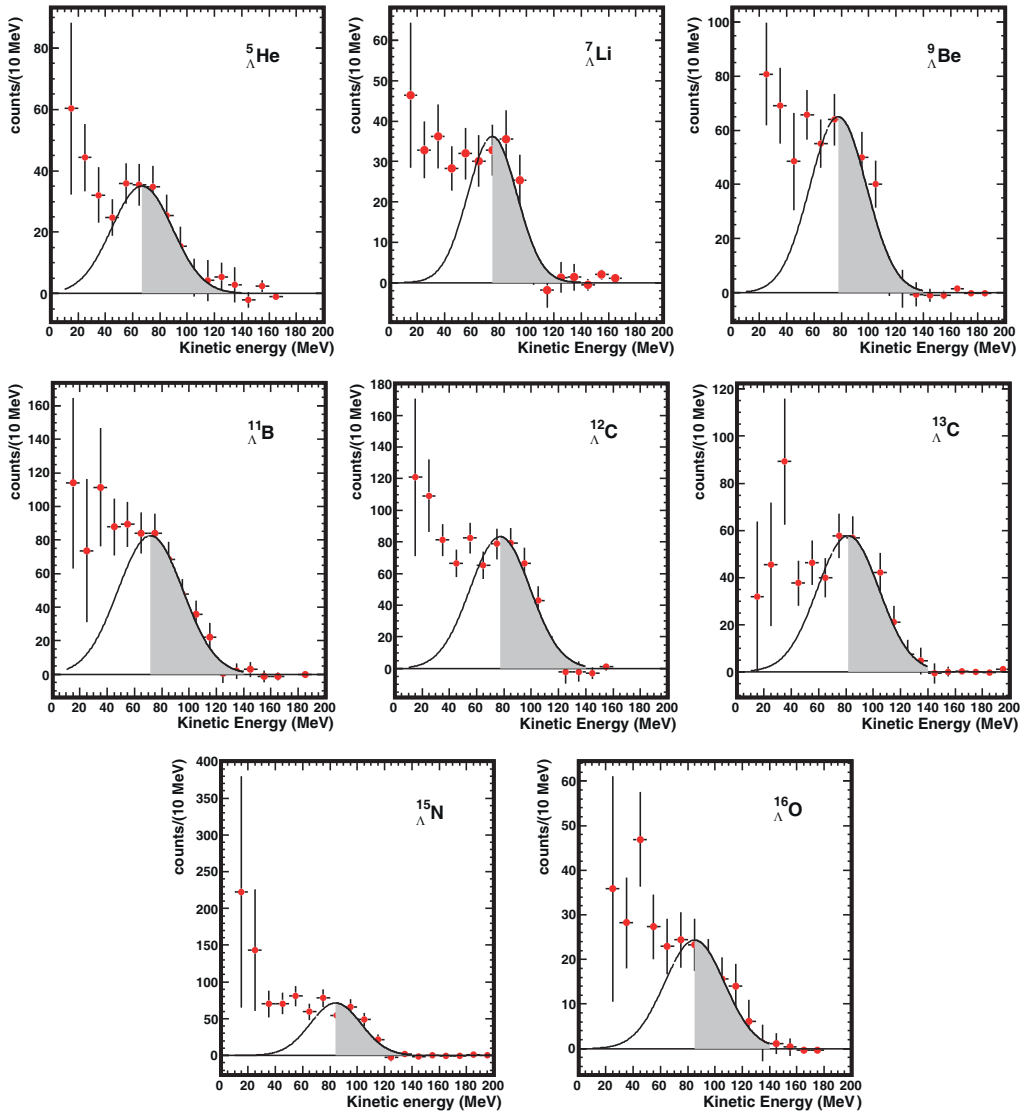

Fig. 21. – Proton kinetic energy spectra from the NMWD of (from left to right up and down rows): $^{5}_{\Lambda}$He, $^{7}_{\Lambda}$Li, $^{9}_{\Lambda}$Be, $^{11}_{\Lambda}$B, $^{12}_{\Lambda}$C, $^{13}_{\Lambda}$C, $^{15}_{\Lambda}$N and $^{16}_{\Lambda}$O. The curves represent the new analysis Gaussian fits to the spectra: the solid line part indicates the actual fit region, the dashed part indicates the one-proton–induced NMWD contribution to the lower-energy spectrum part. The filled area is the higher-energy half-Gaussian area, where the $2N$-induced NMWD is negligible. From ref. [32].

baryons) would be smeared out for heavier nuclei. As for the second effect, as already discussed, if the WD Q-value is shared by three nucleons, a low-energy rise may exist even for the very light s-shell hypernuclei.

As a second step, proton spectra from NMWD of $^{9}_{\Lambda}$Be, $^{11}_{\Lambda}$B, $^{13}_{\Lambda}$C, $^{15}_{\Lambda}$N and $^{16}_{\Lambda}$O were produced and analyzed [124]; the measured energy resolution was $\Delta E/E = 2\%$ at 80 MeV. Figure 21 shows all the final experimental spectra. We underline the circumstance that

the threshold for the proton energies was 15 MeV only, a half of that achieved in the previous best measurements. It was essential in determining Γ_{2N}/Γ_p. Despite the spectra are affected by considerable errors, in particular in the low-energy region, they confirm the clear systematic trend as a function of A (from 5 to 16): a peak around 80 MeV is broadened by the Fermi motion of the interacting baryons and more and more blurred as A increases. The peak is smeared, on its low-energy side, by a rise that can be ascribed to FSI and $2N$-induced NMWD. In conclusion the above spectra are a unique data bank for hypernuclei with A ranging from 5 to 16, from which several interesting considerations and conclusions were drawn.

The initial effort was that of developing a method for determining the contributions from the decay (10) without resorting to INC calculations, as in ref. [121,122]. The first step was to fit the eight experimental spectra of fig. 21 above 80 MeV ($\sim Q_{\mathrm{NMWD}}/2$) to Gaussians with free central values, widths and area; then the analysis continued following the scheme that will be outlined in subsect. **6**˙7. Some time later it was noticed [125] that the central values of these fitting Gaussians for ${}^{13}_{\Lambda}$C, ${}^{15}_{\Lambda}$N and ${}^{16}_{\Lambda}$O were significantly larger than those calculated following the relativistic kinematics with the exact Q-values for the considered eight decays, eq. (7), in the hypothesis of a b.t.b. emission of the proton-neutron pair with no recoil of the residual nucleus in its ground state.

It was then investigated [32] whether more suitable fits to all spectra could be obtained by shifting down the lower edge of the fitting interval of the experimental distributions to 70, 60 and finally 50 MeV. By looking at the reduced χ^2 of the values of the maxima of the corresponding fitting Gaussians with respect to those expected from the kinematics it was found that the most appropriate values for the maxima were those of the fitting Gaussians obtained starting from 70 MeV, shown in fig. 21. The widths found for ${}^{5}_{\Lambda}$He and ${}^{12}_{\Lambda}$C are consistent with those evaluated theoretically as due to the Fermi motion [118].

The number of protons N_p contained in the higher-energy half part of this fitting Gaussian was used for the determination of Γ_p/Γ_Λ for the eight studied hypernuclei. We have already mentioned that in order to deduce the absolute values of Γ_p/Γ_Λ from the measured proton spectra it is necessary to calculate as accurately as possible the effective influence of FSI. More in detail:

a) the real number of primary protons due to decays (7) and (10) is decreased due to FSI suffered by the proton;

b) there is an increase of the number of protons due not only to FSI of protons at higher energy in the spectrum, but also to FSI of higher-energy neutrons from (8);

c) quantum-mechanical interference effects may occur among protons of the same energy from the different sources (primary from (7) and (10), secondary from FSI).

All these effects may be evaluated by appropriate and precise INC calculations, as done in refs. [118, 121]. In ref. [32] the effect of FSI on the proton energy distributions was evaluated without using INC calculations but exploiting only experimental data and simple hypotheses.

By considering the portions of the spectra above the maximum found by the fit on data above 70 MeV (blue areas in fig. 21), the importance of the effect b) may be safely neglected, according to ref. [118]. The contribution of the decay (10) above 70 MeV is not larger than 5% of Γ_{NMWD} [118] and by considering the determination of Γ_{2N}/Γ_p provided by the same FINUDA experiment (that will be discussed in subsect. **6**˙7) it was concluded that the total amount of primary protons from (10) would not be larger than

2% of those from (7). Thus also the interference effect c) may be neglected. Effect a) was parametrized by means of the relationship

$$\frac{\Gamma_p}{\Gamma_\Lambda} = \frac{\Gamma_T}{\Gamma_\Lambda}\,\mathrm{BR}(p) = \frac{\Gamma_T}{\Gamma_\Lambda}\,\frac{2(N_p - N_{2N}) + \alpha(N_p - N_{2N})}{N_{\mathrm{hyp}}}\,, \tag{20}$$

where BR(p) is the branching ratio of (7), N_p is the number of protons in the higher-energy half part of the fitting Gaussian, N_{2N} the number of protons from (10) ($\sim 2\%$), N_{hyp} the number of produced hypernuclei, the factor 2 takes into account the total area of the Gaussians and α is a coefficient to be determined, which accounts for the number of protons moved below the central value of the fitting Gaussians due to FSI. More precisely $\alpha/(2+\alpha)$ is the fraction of protons affected by FSI.

To calculate α a method based only on the experimental values of Γ_T/Γ_Λ, Γ_M/Γ_Λ, Γ_n/Γ_p and $\Gamma_{2N}/\Gamma_\Lambda$ (see later) for ${}^{5}_{\Lambda}$He and ${}^{12}_{\Lambda}$C was adopted assuming a linear scaling law with A. The simple expression for α,

$$\alpha_A = (0.215 \pm 0.031) \cdot A, \tag{21}$$

was found, corresponding to 35% of the primary protons from NMWD lost (moved below the maximum value of the fitting Gaussian) for FSI in ${}^{5}_{\Lambda}$He and 63% in ${}^{16}_{\Lambda}$O.

Incidentally, we remark that if we assume the validity of eq. (21) not only for p-shell hypernuclei but for the full A range, for $A = 200$ we find $\alpha = 43$ and consequently more than 4% of the protons from NMWD would not be affected by FSI. This number is three orders of magnitude larger than that one indicated at the end of subsect. **4**˙4 and, even if only partially true, it should make easier the measurement of the lifetime of heavy hypernuclei.

It was then possible to evaluate by means of eq. (20) Γ_p/Γ_Λ for ${}^{5}_{\Lambda}$He and all studied p-shell hypernuclei: the errors, of the order of 20–25%, include all the contributions notably that on α, that is the main source for systematics. Table III summarizes the published data. In case of several values for a same hypernucleus we report the related reference, the laboratory where the measurement was done and the weighted average (w.a.) for homogenous results. Figure 22 shows the plot of the normalized 1p-induced NMWD widths (single values or w.a.) as a function of A. The most visible effect is an increasing trend, expected on the basis of the complementary decreasing behaviour of the MWD width (see fig. 8).

6˙4. *Data on* 1n*-induced NMWD*. – The determination of Γ_n/Γ_Λ is very hard to obtain. In addition to the difficulties so far described for the 1p-induced NMWD, there are the ones inherent to the detection of medium-energy neutrons (absolute efficiency determination, resolution, backgrounds). For these reasons the data are very scarce and of poor quality.

The first attempt was described in ref. [22] for ${}^{5}_{\Lambda}$He. A value of $\Gamma_n/\Gamma_\Lambda = (0.20 \pm 0.11)$ was reported, by detecting only (7.7 ± 3.3) neutron events, background corrected. By combining it with their already discussed value of Γ_p/Γ_Λ they found $\Gamma_n/\Gamma_p = (0.93 \pm 0.55)$. As we will discuss in detail in sect. **8**, this evaluation includes partially $\Gamma_{2N}/\Gamma_\Lambda$.

An attempt to observe neutrons emitted in the NMWD of ${}^{4}_{\Lambda}$He is presented in ref. [23]. Due to the high background, only an upper limit for Γ_n/Γ_Λ of 0.035 (at 95% confidence level) was obtained.

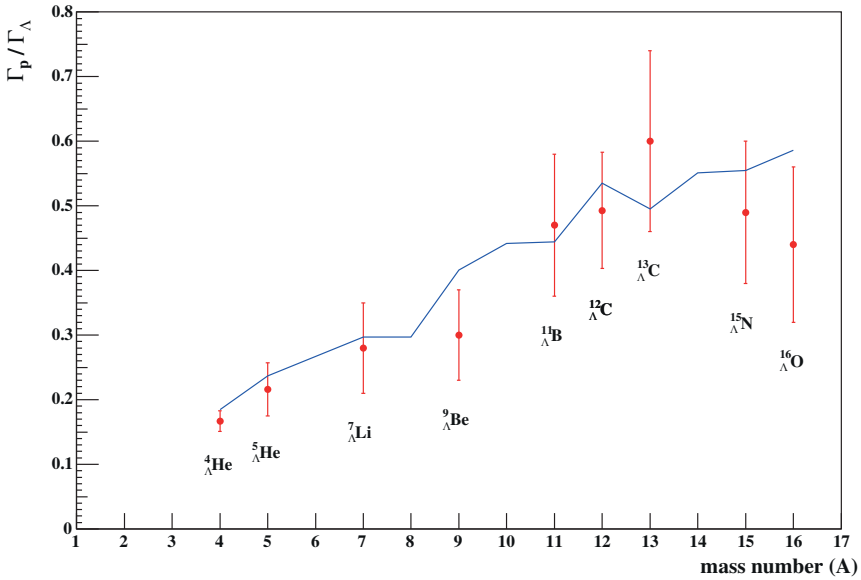

Fig. 22. – Normalized $1p$-induced NMWD widths as a function of A (full red circles): weighted average values are used when several results are available for the same hypernucleus. The continuous (blue) line indicates calculations from ref. [69].

At present the only experiment which reported a measurement of Γ_n/Γ_Λ for $^{12}_{\Lambda}$C is the last one from the SKS Collaboration at KEK [120]. The analysis of the neutron spectra performed following the same criteria as for the proton spectra led to determine a value $\Gamma_n/\Gamma_\Lambda = (0.23 \pm 0.08)$.

For some other hypernuclei, for which there is a set of data for all partial decay widths, except Γ_n/Γ_Λ, it is possible to evaluate it by subtraction, though with considerable errors. We will comment these results in sect. **8**.

6˙5. *Comparison with theoretical predictions.* – We mentioned in the Introduction the intuition that NMWD could occur as the result of the free space $\Lambda \to N\pi$ decay, in which the π was considered as virtual and then absorbed by a bound nucleon [9].

After about a decade Block and Dalitz [126] developed a phenomenological model of NMWD for s-shell hypernuclei in which some important characteristics, mainly the degree of validity of the $\Delta I = 1/2$ rule on the isospin change can be reproduced in terms of elementary spin-dependent branching ratios for the decays (7) and (8), by fitting the available experimental data. This analysis triggered the development of microscopic models of the $\Lambda N \to nN$ weak interaction.

The first one was the OPE model based on a $\Delta I = 1/2 \Lambda N \pi$ vertex, with the absorption of the virtual pion by another nucleon of the nuclear medium [127]. A peculiar difference between MWD and NMWD is that the last one is characterized by a larger momentum transfer ($\sim 400\,\mathrm{MeV}/c$ instead of $\sim 100\,\mathrm{MeV}/c$). Consequently it was expected that the details of the nuclear structure would not influence substantially the information on the four-baryon, strangeness changing weak interaction $\Lambda N \to nN$. A further difference was that the larger momentum transfer allowed to probe shorter distance interactions and to check the effects expected from the exchange of heavier mesons,

in a hadronic picture of the process, and/or the role of explicit quark/gluon degrees of freedom in baryon weak interactions.

In order to improve the OPE model, heavier mesons were introduced as mediators of the $\Lambda N \to nN$ interaction, starting from the ρ [128]. Only s-states were assumed together with the validity of the $\Delta I = 1/2$ rule, even though no experimental indication supported its validity for mesons heavier than the pion. In the following years the OPE evolved into the One-Meson-Exchange (OME), in which the π, ρ, K, K^*, ω and η mesons were considered in a nuclear matter calculation [129]. Shell model approaches were then considered [130,131] in terms of OME models including the mesons belonging to pseudoscalar and vector octets; more recently, also uncorrelated and correlated two-pion-exchange (TPE) terms were added to the OME potentials [132,133]. For most of the OME and OME+TPE calculations the $\Delta I = 1/2$ rule is assumed to be valid although, we repeat, it is justified only for the $\Lambda N\pi$ vertex. In the next subsection we shall briefly remind the present status of the studies on its validity in NMWD.

Recently, a complete calculation of NMWD widths for hypernuclei with A from 4 to 209 was presented in ref. [69]. A theoretical potential which contains π, $2\pi/\rho$, $2\pi/\sigma$, ω, K, $\rho\pi/a_1$ and $\sigma\pi/a_1$-meson exchanges between the Λ hyperon and the nucleon was used. The initial Λ-hypernucleus state was expressed in terms of the weak-coupling scheme in which a Λ-hyperon in the s-state couples to the lowest energy state of the core-nucleus. For p-shell hypernuclei, in which we are mainly interested in the comparison with the experimental data, the Λ-hyperon wave function was taken to be the solution of the density dependent Hartree-Fock equation [134]. For the nuclear core of the hypernucleus and the final nuclei the configuration-mixed shell model wave functions calculated with use of the Cohen-Kurath interactions [101] were used. In fig. 22 we have shown the comparison between the Γ_p/Γ_Λ calculated in ref. [69] with the experimental ones. A general agreement between the experimental data and the theoretical values is evident, but we must remark that the errors are quite large. Exceptions are ${}^{9}_{\Lambda}\mathrm{Be}$, for which the experimental value is lower by 1.5σ, and ${}^{16}_{\Lambda}\mathrm{O}$, lower by 1.3σ. The errors do not allow to put into evidence variations due to the nuclear structure of neighbour hypernuclei. Although of lesser importance with respect to those observed in MWD due to the higher momentum transfer, they are expected to show anymore, in particular on the Γ_n/Γ_p values.

Quark models were suggested as theoretical approaches of the short range part of the $\Lambda N \to nN$ weak interaction. A hybrid quark-hadron model was considered in refs. [135, 136]: two separate mechanisms with different interaction ranges were taken into account. The long-range term ($r \geq 0.8\,\mathrm{fm}$) was described by the OPE with the $\Delta I = 1/2$ rule, while the short-range interaction was described by a six-quark cluster model including both $\Delta I = 1/2$ and $\Delta I = 3/2$ contributions. Subsequently, a direct-quark (DQ) model combined with the OPE description was adopted to calculate the $1N$-induced NMWD widths [137]. In the DQ model the ΛN and NN short-range repulsion originates from quark exchange between baryons and from gluon exchange between quarks, and contains both $\Delta I = 1/2$ and $\Delta I = 3/2$ transitions; the last one was found to provide a significant contribution in the $J = 0\,\Lambda N \to nN$ channel. The approach was furthermore extended to incorporate a OME model containing π, K and σ exchange [138,139]. A further method of calculating the NMWD widths making use of the nuclear matter formalisms will be outlined in subsect. **6**˙7.

6˙6. *Violation of the* $\Delta I = 1/2$ *rule in NMWD?* – The $\Delta I = 1/2$ isospin rule was established empirically following the analysis of several non-leptonic strangeness changing

processes, namely the K, Λ and Σ decays in free space. It is well established phenomenologically, but it is still unknown whether the large suppression of the $I = 3/2$ amplitudes with respect to the $I = 1/2$ ones holds as a general feature of all non-leptonic weak processes. A possible relevance of $\Delta I = 3/2$ terms in hypernuclear NMWD would represent the first evidence for a $\Delta I = 1/2$ rule violation in non-leptonic strangeness changing interactions. We remark that the $\Lambda N \to nN$ process has an important short-range part due to the higher momentum transfer, not accessible to non-leptonic strangeness changing decays of free $S = -1$ particles which follow the $\Delta I = 1/2$ rule. Indeed, while the MWD involves only the $\Lambda N\pi$ vertex, which in free space respects the $\Delta I = 1/2$ rule, the NMWD involves also mesons heavier than the pion in the Λ vertices, with weak interaction couplings not available to the free decays. Nowadays, no experimental indication supports nor excludes the validity of the $\Delta I = 1/2$ rule for these couplings and indirect information could come from hypernuclear NMWD. Moreover, it has been suggested that several weak $\Lambda N \to NN$ amplitudes are dominated by direct-quark processes in which no intermediate meson is involved [137, 140]. Such direct processes may not obey the $\Delta I = 1/2$ rule.

To exploit at best this important option of really using hypernuclei as a laboratory to study interactions not otherwise allowed in free space it is useful to select simple systems, like the s-shell hyperisotopes of H and He (${}^{3}_{\Lambda}$H, ${}^{4}_{\Lambda}$H, ${}^{4}_{\Lambda}$He, ${}^{5}_{\Lambda}$He). For them the ΛN initial system is in the $L = 0$ relative angular-momentum state and it is possible to use the simple phenomenological model of Block-Dalitz [126]. Such an approach allows one to easily extract information on the spin-isospin dependence of the $\Lambda N \to nN$ process directly from data on s-shell hypernuclei. For them the neutron- and proton-induced decay widths are obtained in terms of a few spin- and isospin-dependent rates for the elementary process $\Lambda N \to nN$. The relationship among the elementary rates is strongly affected by the isospin change experienced in the NMWD, both $\Delta I = 1/2$ and $\Delta I = 3/2$ being in principle possible.

Detailed descriptions of the Block-Dalitz model can be found in refs. [11,13,15] and we report here only the most relevant conclusions that were drawn from the existing data. Various equalities and inequalities among the hypernuclear decay rates were obtained in the limit of pure $\Delta I = 1/2$ transitions. Before commenting them we would like to underline that the NMDW of s-shell hypernuclei is certainly the easiest to be studied theoretically, but the hardest to be measured. We have already often mentioned that for s-shell hypernuclei MWD dominates (see fig. 8); furthermore, the H hyperisotopes are hard to be produced abundantly by exclusive experiments, as discussed in subsect. **4**˙4.

A first attempt to verify the validity of the $\Delta I = 1/2$ rule by using the existing, poor quality, data on various exclusive channels of NMWD of s-shell hypernuclei was performed in ref. [141]. A suggestion that a large violation of the $\Delta I = 1/2$ rule could be observed in NMWD of s-shell hypernuclei was put forward. However, due to the large errors affecting the experimental data that were considered, ranging from 38% to 59%, the result could not be considered as definitive. As a matter of fact, an analysis of more recent experimental data, performed in ref. [142] always with the phenomenological Block-Dalitz model, reinforced the previous doubts. It was concluded that the large error bars do not allow to draw definitive conclusions about the possible violation of the $\Delta I = 1/2$ rule and the spin dependence of the Block-Dalitz transition rates. The data turned out to be consistent with the hypothesis of validity of the $\Delta I = 1/2$ rule at the level of 60%. In other words, the $\Delta I = 1/2$ rule could be excluded only at the 40% confidence level. This result is not changed much if some present data, more precise, are used. Among the different equalities and inequalities concerning exclusive NMWD

channels which can be obtained in the limit of pure $\Delta I = 1/2$ transitions the most interesting one, from a theoretical point of view, looks $\Gamma_n({}^4_\Lambda\mathrm{He})/\Gamma_p({}^4_\Lambda\mathrm{H})$ which should be equal to 2. We have seen in subsect. **6**˙4 that only an upper limit was set on Γ_n/Γ_Λ for ${}^4_\Lambda$He [23] which is compatible with zero. We have no experimental information on Γ_p/Γ_Λ for ${}^4_\Lambda$H. New, ambitious and hard experiments are planned to that purpose at J-PARC and will be outlined in subsect. **6**˙10.

6˙7. *Experimental indications for the* $2N$*-induced NMWD.* – In subsect. **6**˙2 we have mentioned the subsequent steps performed by the SKS Collaboration in improving the quality and the theoretical interpretation of the nucleon spectra, both single and in coincidence, from the decay of selected hypernuclei, mainly ${}^{12}_\Lambda$C. $1N$- and $2N$-induced NMWD processes were described by phase space arguments, without resorting to any WD model, while an INC code was used to incorporate nucleon FSI effects. We recall that without the $2N$-induced process a quenching of the measured nucleon spectra was observed with respect to the calculated spectra and was interpreted as the effect of the $2N$-induced NMWD. It was argued that the values of Γ_{2N} could be deduced from the measured single-nucleon spectra by considering this rate as a free parameter in fitting the single-nucleon spectra, measured with high statistics. A contribution as large as 0.4 for Γ_{2N}/Γ_{NM} was inferred [143]. A quite lower value, $\Gamma_{2N}/\Gamma_{NM} = (0.27 \pm 0.13)$ was found in the complete analysis summarized in subsect. **6**˙3 and in fig. 20, in which both single and coincidence nucleon spectra from ${}^{12}_\Lambda$C were analyzed simultaneously with a renormalized INC model calculation [122].

An upper limit for Γ_{2N}/Γ_{NM} of 0.24 (at 95% CL) was found for ${}^4_\Lambda$He [23]. Though consistent with the SKS value, it is not clear whether the speculations on the importance of the $2N$-induced process may be applied to a system as light as ${}^4_\Lambda$He.

The FINUDA experiment adopted a completely different approach to determine Γ_{2N}/Γ_{NM}. Starting from the measured inclusive single-proton spectra from NMWD of ${}^5_\Lambda$He, ${}^7_\Lambda$Li, ${}^9_\Lambda$Be, ${}^{11}_\Lambda$B, ${}^{12}_\Lambda$C, ${}^{13}_\Lambda$C, ${}^{15}_\Lambda$N and ${}^{16}_\Lambda$O, a technique was introduced to disentangle the contribution coming from the $2N$-induced decays from the $1p$-induced decays affected by FSI. The original method was first exploited and described in ref. [124], with a first set of values for Γ_{2N}/Γ_{NM} for the above hypernuclei. A further improvement was developed in ref. [32], in which slightly modified values for Γ_{2N}/Γ_{NM} were determined; they will be quoted in the following. The systematic analysis over the mass number range $A = 5$–16 covered by the FINUDA measurements was exploited and only simple assumptions were made in the calculations. Each of the eight experimental spectra, shown by fig. 21, was fitted, from 70 MeV proton kinetic energy onward, with a Gaussian function with free central value and width in order to determine, by its mean value, the energy corresponding to the maximum of the $1p$-induced contribution. The spectrum was then divided into two regions, one below the mean value, with area A_{low}, and one above the mean value, with area A_{high} (blue area in fig. 21). It was assumed that the first part is populated by $1p$-induced decays, $2N$-induced decays and FSI processes, while the second part has contributions from $1p$-induced processes and FSI; the $2N$-induced decays contribution can be neglected since, as we have already mentioned in subsect. **6**˙3, it accounts for only 5% of the total $2N$-induced strength [118]. A_{low} and A_{high} can be written as

$$A_{\mathrm{low}} = N(\Lambda p \to Np)/2 + N(\Lambda np \to nnp) + N_{p\,\mathrm{FSI\,low}}, \tag{22}$$

$$A_{\mathrm{high}} = N(\Lambda p \to Np)/2 + N_{p\,\mathrm{FSI\,high}}, \tag{23}$$

where $N(\Lambda p \to Np)$ is the total number of $\Lambda p \to Np$ decays (which are assumed to be

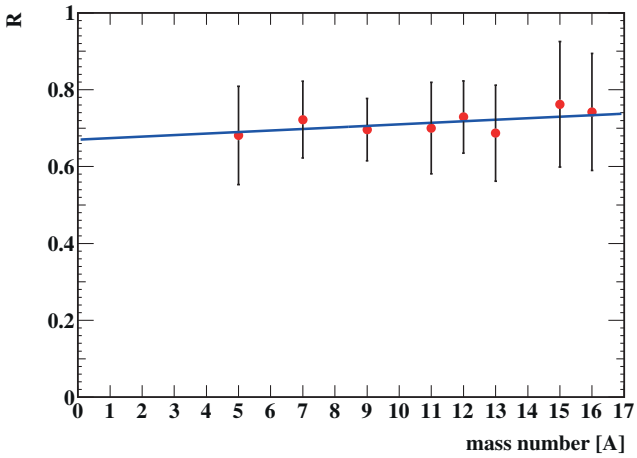

Fig. 23. – $R = A_{\rm low}/(A_{\rm low} + A_{\rm high})$ values as a function of A for ${}^{5}_{\Lambda}$He, ${}^{7}_{\Lambda}$Li, ${}^{9}_{\Lambda}$Be, ${}^{11}_{\Lambda}$B, ${}^{12}_{\Lambda}$C, ${}^{13}_{\Lambda}$C, ${}^{15}_{\Lambda}$N and ${}^{16}_{\Lambda}$O. The blue line is a linear fit to the data; see text for more details.

evenly distributed in the Gaussian peak, *i.e.* half in $A_{\rm low}$ and half in $A_{\rm high}$), $N(\Lambda np \to nnp)$ is the total number of $\Lambda np \to nnp$ decays (which are assumed to occur only in $A_{\rm low}$), $N_{p\,\mathrm{FSI\,low}}$ ($N_{p\,\mathrm{FSI\,high}}$) is the difference between the number of protons detected in the region below (beyond) the peak of the spectrum and the (unknown) number of primary protons which originate from the $1N$- and $2N$-induced WDs in the same region. We remark the similitude between the definitions of $N_{p\,\mathrm{FSI\,high}}$ in eq. (23) and of α in eq. (20). As a matter of fact it is easy to see that $N_{p\,\mathrm{FSI\,high}} = -N_p\ \alpha/2$. In eq. (20) α was explicitly deduced since it was necessary to obtain absolute values for Γ_p/Γ_Λ for each hypernucleus, whereas in the case of the Γ_{2N}'s only relative values were deduced, with a simpler approach.

For each hypernucleus of mass number A the ratio

$$R(A) = \frac{A_{\rm high}(A)}{A_{\rm low}(A) + A_{\rm high}(A)} \tag{24}$$

was evaluated. Figure 23 shows the A-dependence of data for $R(A)$ obtained for the 8 studied hypernuclei. Taking into account that, following INC models, nucleon FSI effects can be assumed to be proportional to A and that both Γ_{2N}/Γ_{NM} and Γ_n/Γ_p in the studied A range may be considered constant [11], the ratio $R(A)$ is expected to have a linear behaviour like $R(A) = a + bA$. The best linear fit is reported in fig. 23, with values $a = (0.67 \pm 0.14)$, $b = (0.004 \pm 0.013)$ and $\chi^2/ndf = 0.225/6$. It was finally shown that

$$\frac{\Gamma_{2N}}{\Gamma_p} = \frac{(R(A) - bA) - 0.5}{1 - (R(A) - bA)}\,, \tag{25}$$

providing a w.a. ($A = 5$–16) for $\Gamma_{2N}/\Gamma_p = (0.50 \pm 0.24_{\rm stat} \pm 0.04_{\rm sys})$ and $\Gamma_{2N}/\Gamma_{NM} = (0.25 \pm 0.12_{\rm stat} \pm 0.02_{\rm sys})$ by using the value $\Gamma_n/\Gamma_p = (0.48 \pm 0.08)$, w.a. of the data taken from refs. [119, 120].

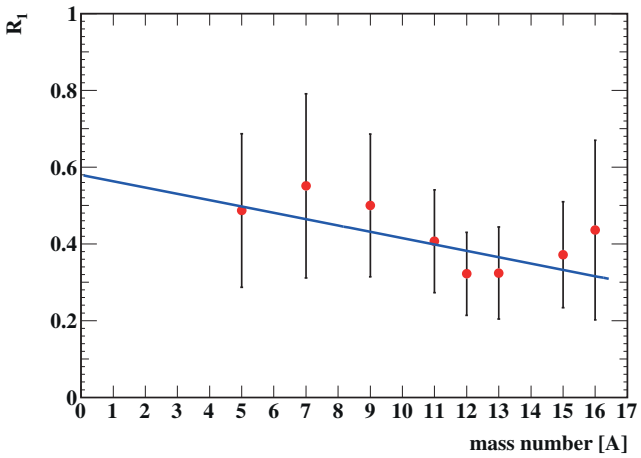

Fig. 24. – $R_1 = N_n(E_p \leq (\mu - 20\,\mathrm{MeV}), \cos\theta(np) \geq -0.8)/Np(E_p > \mu)$ values as a function of A for ${}^{5}_{\Lambda}$He, ${}^{7}_{\Lambda}$Li, ${}^{9}_{\Lambda}$Be, ${}^{11}_{\Lambda}$B, ${}^{12}_{\Lambda}$C, ${}^{13}_{\Lambda}$C, ${}^{15}_{\Lambda}$N and ${}^{16}_{\Lambda}$O from ref. [32]. The blue line is a linear fit to the data; see text for more details.

In a second approach [31] Γ_{2N}/Γ_p was determined by considering both protons and neutrons emitted in coincidence with the π^- from the formation reaction of hypernuclei. To this purpose np events were considered for each hypernucleus, with a proton of energy lower than an adequate threshold, $E_p^{\mathrm{thr}} = \mu - 20\,\mathrm{MeV}$, where μ was the mean value of the Gaussians used in the proton inclusive spectra analysis, and a restriction on the opening angle between the two nucleons $\cos(\theta_{np}) \geq -0.8$. In such a way neutrons from $2N$-induced processes were selected and could be counted for. With the applied selections, events due to the $1N$-induced process would be excluded and only a small contribution of FSI should be present. A ratio $R_1(A)$ was defined as

$$R_1(A) = \frac{N_{np}(E_p \leq E_p^{\mathrm{thr}}, \cos\theta_{np} \geq -0.8)}{N_p(E_p\,\mu)} = \frac{0.8N(\Lambda np \to nnp) + \mathrm{FSI}_{np}}{0.5N(\Lambda p \to np) + \mathrm{FSI}_p}, \tag{26}$$

where $N_{np}(E_p \leq E_p^{\mathrm{thr}}, \cos\theta_{np} \geq -0.8)$ is the number of neutrons in coincidence with a proton of energy lower than $\mu - 20\,\mathrm{MeV}$ and forming an angle with the proton direction such as $\cos(\theta_{np}) \geq -0.8$, while N_p is the number of protons with energy larger than μ (blue areas in fig. 21); FSI_{np} and FSI_p indicate the residual effect of FSI processes on the corresponding samples. The factor 0.8 is due to the selections applied in the analysis. Figure 24 shows the dependence of $R_1(A)$ on the hypernuclear mass number.

Also in this case, it is possible to apply the same considerations on the A-dependence of FSI and Γ_{2N} used in the study of the single proton spectra. In fig. 24 the ratio (26) shows a decreasing trend. This is consistent with the simple hypothesis that $R_1(A)$ is linearly correlated with the width of the $2N$-induced rate, which is in the first approximation independent from A [11], with a small contribution due to FSI which, again in a first approximation, increases linearly with A. By a simple linear fit to (a + bA), shown in fig. 24, the values $a = (0.58 \pm 0.23)$, $b = (-0.017 \pm 0.090)$ with $\chi^2/\mathrm{ndf} = 1.045/6$ were

found. By indicating with Γ_{np} the width of the np-induced decay (10) of the hypernucleus it is possible to write

$$\frac{\Gamma_{2N}}{\Gamma_p} \simeq \frac{\Gamma_{np}}{\Gamma_p} = \frac{R_1(A) - bA}{1.6} = \frac{a}{1.6} = 0.36 \pm 0.14_{\text{stat}}{}^{+0.05}_{-0.04\text{sys}}. \tag{27}$$

The first approximate equality was assumed taking into account that the microscopic calculation [18] predicts $\Gamma_{np} : \Gamma_{pp} : \Gamma_{nn} = 0.83 : 0.12 : 0.05$ and that the total error quoted in eq. (27) is bigger than the contribution of $(\Gamma_{pp} + \Gamma_{nn})$.

Furthermore, using $\Gamma_n/\Gamma_p = (0.48 \pm 0.08)$ as in ref. [23] and 0.83 for the contribution of Γ_{np} to Γ_{2N}, a value of $\Gamma_{2N}/\Gamma_{\text{NMWD}} = (0.20 \pm 0.08_{\text{stat}}{}^{+0.04}_{-0.03\text{sys}})$ is found. This value supports the recent theoretical predictions ($\Gamma_{2N}/\Gamma_{\text{NMWD}} = 0.26$ [19]), the experimental result from SKS [36] for ${}^{12}_{\Lambda}$C (0.29 ± 0.13) and the one from FINUDA with the above-described analysis of the inclusive proton spectra $(0.25 \pm 0.12_{\text{stat}} \pm 0.02_{\text{sys}})$.

6˙8. *Direct experimental evidence of the* $2N$*-induced NMWD.* – Even though the assessment of the existence of $2N$-induced NMWD, inferred from different experiments with different techniques, leads to the same results within the (large) errors, some scepticism could remain. The smoking gun proof, *i.e.* the measurement of a triple (n, n, p) coincidence, in well defined and clean kinematics, of the three outgoing nucleons from the decay of a hypernucleus in its ground state was lacking.

Among the capabilities of the FINUDA detector, there was that of permitting the full reconstruction of very rare multi-tracks events, resembling to some extent the old emulsion technique. This possibility was due to the excellent stability of the detector over periods of several months and to the absence of severe backgrounds and it was exploited for discovering the superheavy hyperisotope ${}^{6}_{\Lambda}$H [35] and for the search of completely reconstructed $2N$-induced events [144] outlined in the following.

Over the full data sample, 101 (π^-, n, p) coincidence events have been found with the analysis selection on E_p and $\cos(\theta_{np})$ described in the previous subsection. This sample was well enriched (by a factor ~ 2.5) in events coming supposedly from the $2N$-induced NMWD. Taking into account a $\Gamma_{2N}/\Gamma_{\text{NMWD}}$ value of 0.2, the enrichment factor and the global neutron detection efficiency of the apparatus, it was expected to find ~ 2.5 $(\Lambda + (np) \to nnp)$ NMWD events. One event was found on a ^{7}Li target, satisfying the selection criteria and with an additional neutral particle in the final state. For this event the missing momentum was evaluated according to the hypothesis of a decay at rest of the hypernucleus and the missing mass of the reaction was calculated. The angular correlation among the three nucleons and between the π^- and the proton was then considered to define exclusively the final state of the decay process. Column two in table IV reports the kinematics while fig. 25 displays the event in the ρ-ϕ plane of the apparatus.

The statistical uncertainties on the angles between the tracks (rows 6, 7, 8 and 9 of table IV) have been evaluated with Gaussian error propagation taking into account the spatial resolution of the subdetectors. The event on ^{7}Li target exhibits a total kinetic energy of the three nucleons $T_{n1\ n2\ p} = (178 \pm 23)\,\text{MeV}$ and a missing mass of $(3710 \pm 23)\,\text{MeV}/c^2$. In the first two columns of table V the possible final-state configurations following the $2N$-induced NMWD of ^{7}Li to bound or partially bound residual nuclear systems are listed, together with the corresponding expected missing mass. The configuration containing ^{4}He has the smallest missing mass due to the high binding energy of the nucleus ($\sim 28\,\text{MeV}$). The missing-mass value measured in the

TABLE IV. – *Kinematics of the three* $\Lambda(np) \to nnp$ *candidate events observed by FINUDA:* p_{π^-} *indicates the momentum of the hypernucleus formation* π^-*,* T_p *the p kinetic energy,* T_{n1} *the kinetic energy of one of the neutrons,* T_{n2} *the kinetic energy of the second one,* $\theta_{n1\ n2}$ *the angle between the two n's,* $\theta_{n1\ p}$ *the angle between the first n and the p,* $\theta_{n2\ p}$ *the angle between the second n and the p,* $\theta_{\pi^-\ p}$ *the angle between the formation* π^- *and the p,* p_{miss} *the missing momentum of the final state, corresponding to the recoil momentum of the residual nucleus in a 4-body final state, and missing mass the missing mass for the decay of the hypernucleus from its ground state. From ref.* [144].

Target	^{7}Li	^{7}Li	^{9}Be
p_{π^-} (MeV/c)	276.9 ± 1.2	276.5 ± 1.2	286.7 ± 1.2
T_p (MeV)	51.11 ± 0.85	90.83 ± 0.50	71.77 ± 0.80
T_{n1} (MeV)	110 ± 23	21.0 ± 2.0	20.2 ± 2.5
T_{n2} (MeV)	16.9 ± 1.7	35.3 ± 3.6	31.5 ± 4.2
$\theta_{n1\ n2}$ (deg)	94.8 ± 3.8	126.5 ± 5.4	133.6 ± 7.5
$\theta_{n1\ p}$ (deg)	102.2 ± 3.4	53.5 ± 4.3	128.5 ± 5.5
$\theta_{n2\ p}$ (deg)	154 ± 19	124.6 ± 3.9	95.4 ± 3.6
$\theta_{\pi^-\ p}$ (deg)	33.4 ± 3.7	121.7 ± 3.2	159.3 ± 5.9
$p_{\rm miss}$ (MeV/c)	217 ± 44	447 ± 18	253 ± 18
Missing mass (MeV/c^2)	3710 ± 23	3720.3 ± 4.7	5617.3 ± 5.0

event is compatible within the global resolution at the 0.76 σ level with the ^{4}He final state and within (1.62–1.65) σ with the other two states, thus favouring the hypothesis of the first configuration.

Since the topology of the event suggested the possibility of a $1p$-induced decay followed by a nn scattering, a careful kinematical analysis was done and led to conclude that such occurrence could be excluded with a confidence level higher than 99% (normal test). This interesting observation stimulated the search for additional events by relaxing some of the selection criteria, namely the cut imposed on the proton kinetic energy, and 307 (π^-, n, p) events were thus found. Asking in addition for the presence of a neutral particle, detected in coincidence, two more events were found, one again from a ^{7}Li target and one from ^{9}Be target. Both (π^-, n, n, p) events fulfill the condition that the total kinetic

TABLE V. – *Column one: undetected nuclear systems for the* $2N$*-induced decay of* ${}^7_\Lambda$Li*; column two: missing mass with respect to the detected* $(n1, n2, p)$ *system; column three: undetected nuclear systems for the* $2N$*-induced decay of* ${}^9_\Lambda$Be*; column four: missing mass with respect to the detected* $(n1, n2, p)$ *system. From ref.* [144].

${}^7_\Lambda$Li	Missing mass (MeV/c^2)	${}^9_\Lambda$Be	Missing mass (MeV/c^2)
^{4}He	3727.4	^{6}Li	5601.5
^{3}He+n	3748.0	^{5}Li+n	5607.2
^{3}H+p	3747.2	^{4}He+d	5603.0
		^{3}He + ^{3}H	5617.3

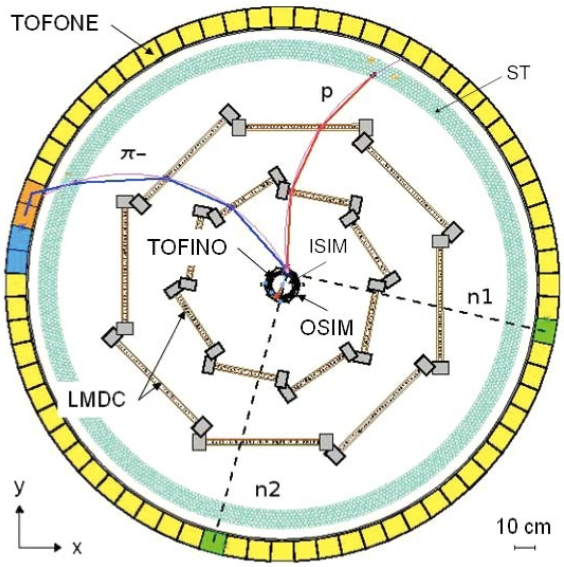

Fig. 25. – Triple coincidence (p, n, n) event coming from ^{7}Li target detected with the FINUDA spectrometer. Reprinted from ref. [144], © 2012, with permission from Elsevier.

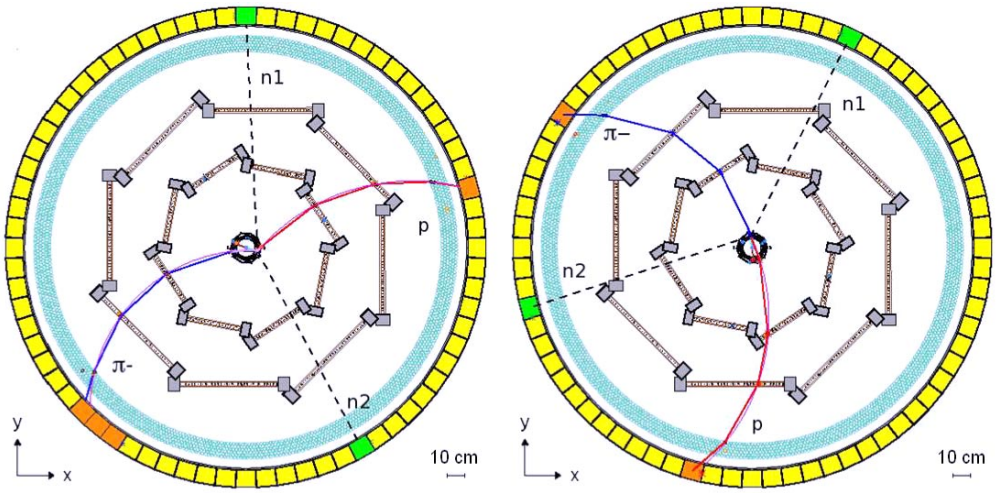

Fig. 26. – Four-particle coincidence (π^-, p, n, n) event coming from ^{7}Li target (on the left) and from ^{9}Be target (on the right) detected by FINUDA. Reprinted from ref. [144], © 2012, with permission from Elsevier.

energy of the three nucleons $\leq 195\,\mathrm{MeV}$ to fit the Q-value of the $2N$-induced NMWD (kinematics reported in table IV, columns 3 and 4). Extensive and accurate Monte Carlo simulations of possible sources of backgrounds that could mimic the observed topologies and kinematics led to exclude this possibility with a confidence level larger than 99%.

In the second event on ^{7}Li target (third column of table IV and fig. 26, left), a total kinetic energy of the three nucleons $T_{p\ n1\ n2} = (147.1 \pm 4.2)\,\mathrm{MeV}$ and a missing

mass of $(3720.3 \pm 4.7)\,\mathrm{MeV}/c^2$ were measured. The missing-mass value of the event is compatible within 1.5 σ with the ^{4}He final state and within (5.7–5.9) σ with the other two states, clearly favouring a ^{4}He exclusive reaction. Also in this case the occurrence of a rescattering of the energetic proton was excluded by the topological and the kinematical analysis and this event can be also attributed to the exclusive ${}^{7}_{\Lambda}\mathrm{Li} \to {}^4\mathrm{He} + n + n + p$ decay.

Finally, concerning the event on ^{9}Be target (fourth column of table IV and fig. 26, right), a total kinetic energy of the three nucleons $T_{p\ n1\ n2} = (123.5 \pm 4.9)\,\mathrm{MeV}$ and a missing mass of $(5617.3 \pm 5.0)\,\mathrm{MeV}/c^2$ have been obtained. Columns three and four of table V list the possible final-state configurations for the $2N$-induced NMWD of ${}^{9}_{\Lambda}\mathrm{Be}$ to bound or partially bound residual nuclear systems and the corresponding missing mass. The configuration with ^{6}Li is the only possible four-body final state and has the smallest missing mass due to the BE of the ^{6}Li nucleus, even smaller than that of the configuration with ^{4}He due to the small BE of the partner deuteron; the mirror ${}^3\mathrm{He} + {}^3\mathrm{H}$ configuration features the largest missing-mass value. The measured missing mass is compatible to less than 0.1 σ with the ${}^3\mathrm{He} + {}^3\mathrm{H}$ final state, to 2.1 σ with the ${}^5\mathrm{Li} + n$ state, to 2.9 σ with the ${}^4\mathrm{He} + d$ state and to 3.2 σ with the ^{6}Li final state. The kinematics of the event excludes the possibility of a $1p$-induced NMWD followed by a NN scattering with a confidence level $> 90\%$ (normal test) and it was concluded that the third event could be attributed to the exclusive ${}^{9}_{\Lambda}\mathrm{Be} \to {}^3\mathrm{He} + {}^3\mathrm{H} + n + n + p$ decay.

The three events discussed above represent the first direct experimental evidence of (n, n, p) triplets following the NMWD of hypernuclei, very likely $2N$-induced processes. We have seen before that from a quantum-mechanical point of view it is not possible to disentangle $2N$-induced NMWD events from spurious $1N$-induced with FSI, sharing the same phase space. However, the importance of the two contributions can be varied by selecting specific kinematical configurations. It is the case for the three discussed events. The probability that they could be due to FSI effects may be deduced from the quoted errors, as it has been evaluated for each event. The exiguousness of the sample prevented attempts to make reliable calculations of $\Gamma_{2N}/\Gamma_\Lambda$ with definite numbers. However, we remark that out of the three events, two were attributed to the exclusive NMWD ${}^{7}_{\Lambda}\mathrm{Li} \to {}^4\mathrm{He} + n + n + p$. The structure of ${}^{7}_{\Lambda}\mathrm{Li}$ is usually described as a core nucleus ^{6}Li plus a Λ, moreover it is well known that ^{6}Li can be understood as a quasi-molecule $(\alpha + d)$ [34] and finally ^{4}He is a strongly bound nucleus. All these circumstances explain why ${}^{7}_{\Lambda}\mathrm{Li}$ is a hypernucleus well suited to observe the exclusive $2N$-induced NMWD.

6˙9. *Theoretical predictions of the $2N$-induced NMWD.* – The finite nucleus shell-model and quark-model based calculations described in subsect. **6**˙7 restricted their analyses to $1N$-induced NMWD. A third method made use of a nuclear matter formalism. This is a many-body technique, first introduced in refs. [89, 90] in which the calculation is performed in infinite nuclear matter and then is extended to finite nuclei through the local density approximation. The method provides a unified picture of both MWD and NMWD channels. In nuclear matter one has to evaluate the Λ self-energy Σ^*, which provides the various decay widths through the relation $\Gamma_i = -2\ \mathrm{Im}\Sigma^*$.

In the first nuclear matter calculations, developed for the evaluations of the $2N$-induced decay rates, a phenomenological approach was used [17, 67]. In these works the Feynman diagrams contributing to the $2N$-induced NMWD were not explicitly evaluated, but an approximate evaluation was done by using the experimental data on pion absorption in nuclei. Additionally, in ref. [67], an argument for the phase-space available for the $2p2h$ configuration was introduced, with the result that the $2N$-induced decay

was providing a non negligible contribution to the total NMWD width. In accordance with a quasi-deuteron approximation, well known in describing the pion absorption in nuclei, the rate was assumed to be a decay induced by a correlated *np* pair, *i.e.* $\Gamma_2 = \Gamma_{np}$.

More recently, the nuclear matter formalism was extended to finite hypernuclei by the local density approximation [18,19]. This microscopic calculation considered all channels (9), (10), (11) of the $2N$-induced NMWD and the predictions on the relative importance of the three channels were used in experimental approximations, as previously discussed. In particular, Pauli exchange (ground state correlation) contributions were evaluated and the results showed that Pauli exchange terms and ground-state correlations are very important for a detailed calculation of all the NMWD rates and that, as expected, the $2N$-induced decay is dominated by the $I_3 = 0$ component of the NN pair. Unfortunately, these detailed predictions are not yet verified experimentally, due to the large errors still present in the data. We may remark that the main predictions of the $2N$-induced NMWD, namely its existence and a contribution of 20–30% to the total NMWD rate, are verified but the detailed information on the various features predicted theoretically must wait for more performing and dedicated experiments. We observed in subsect. **4**˙3 that nuclear matter formalism inspired calculations of the lifetime of medium-heavy hypernuclei provided a good approximation of the experimental data in the $A = (11–56)$ mass range.

6˙10. *Future experimental efforts.* – Two proposals were presented and approved at J-PARC Hadron Experimental Facility (HEF) about NMWD studies. The first one, E18 [145], aims to improve by a factor 10 the statistics previously achieved by the SKS Collaboration on all channels of NMWD of ${}^{12}_{\Lambda}$C as summarized in ref. [36]. ${}^{12}_{\Lambda}$C (and ${}^{11}_{\Lambda}$B) will be produced on a multiple-layered CH target via the (π^+, K^+) reaction at $1.05\,\mathrm{GeV}/c$. An increase of statistics of an order of magnitude will be reached by the sinergic effect of an increase in the total number of π^+ delivered on the target and an increase of the solid angle of detection for the nucleons. The new layout will consist in six equal modules composed by many segmented scintillators, that will be arranged as faces of an hexagonal prism. The scintillators will detect and will measure the energy of neutrons by t.o.f. and of protons by the range depth method. Since the localization of both nucleons will be determined by means of the signals from the photomultipliers facing each end of the scintillators slabs the expected resolution on the proton energy will be $\sim 5\%$. The experiment aims to achieve a statistical error on the measurement of Γ_n/Γ_p of 10% and of the order of 100 triple coincidences of the three nucleons from the $2N$-induced NMWD of ${}^{12}_{\Lambda}$C and it should start its data taking quite soon.

The aim of the second proposal, E22 [71], is the exclusive study of the NMWD in $A = 4$ hypernuclei, with the final goal of investigating the validity of the $\Delta I = 1/2$ rule, that we have discussed in subsect. **6**˙6. The proposal deals in two separate measurements, the first one achievable at the start-up of the intensive experimentation phase at the HEF, the second as a long range program. The initial measurements will consist in the determination of Γ_p and Γ_n for the decay of ${}^{4}_{\Lambda}$He. The hypernucleus will be produced by the (π^+, K^+) reaction on a LHe target at $\sim 1.05\,\mathrm{GeV}/c$. The target will be placed inside a Cylindrical Drift Chamber (CDC), already built for the experiment E15. Neutrons and protons from the NMWD will be detected by four arrays of scintillators measuring the energy of the protons by range and of the neutrons by t.o.f., arranged around the CDC. The CDC will be used for the tracking of the charged particles, pions and protons, emitted in the WD of ${}^{4}_{\Lambda}$He. It is interesting to note that a careful tracking of the π^- is very important for eliminating the background coming from the b.t.b. pairs of neutrons

that are produced from the stopping of the π^- in the materials of the apparatus and that could mimic the b.t.b. pairs of neutrons from the NMWD. In subsect. **6**˙4 we have seen that for Γ_n only an upper limit was given up to now and it is then consistent with zero. By assuming for Γ_n a value of 0.01 and for Γ_p the value reported in table IV, ~ 1300 np pairs and 75 nn pairs are expected. The existing value of Γ_n/Γ_p for ${}^4_\Lambda$He, with its large error, was used in ref. [141] in the first attempt of testing the validity of the $\Delta I = 1/2$ rule. The expected strong reduction in the error will improve the reliability of the test.

We have seen in subsect. **6**˙6 that the most direct test of the $\Delta I = 1/2$ rule is given by the value of the ratio $\Gamma_n({}^4_\Lambda\mathrm{He})/\Gamma_p({}^4_\Lambda\mathrm{H})$ and the measurement of the denominator could be attempted by using the (π^-, K^0) reaction on a LHe target. Comfortable counting rates will be achievable only by using the HIHR beam line at J-PARC, which is a long-range program. The detector should be essentially the same used for the measurement of $\Gamma_n({}^4_\Lambda\mathrm{He})$.

7. – Unusual decays of hypernuclei

Under this classification we consider the MWD with a π^+ in the final state and the NMWD in which nuclear aggregates (d, t, ...) are emitted, with frequencies larger than expected from simple mechanisms. Considering the case of π^+ in the final state, it is quite straightforward to expect its appearance as the result of a two-step process due to a charge exchange $\pi^0 p \to \pi^+ n$ reaction inside the parent nucleus induced by a π^0 emitted in a $\Lambda \to n\pi^0$ WD. Following calculations, we do not expect that the related Γ_{π^+} should be higher than 1% of Γ_{π^0} and that it could then affect the physical conclusions so far reached on MWD. The same holds for the emission of d, t, ... due to the pick-up of nucleon(s) produced in a $1N$- or even $2N$-induced NMWD.

However, some peculiar cases deserve a more careful attention. The first one is the anomalously high rate of π^+ emitted in the MWD of ${}^4_\Lambda$He. For ${}^4_\Lambda$He the ratio $R(\pi^+/\pi^-)$ defined as the ratio of all π^+ decay modes to all π^- decay modes was found as lying in the range $(5.4^{+1.5}_{-1.7} \div 6.9^{+1.8}_{-2.1})\%$ in ref. [146, 147] and equal to $(4.3 \pm 1.7)\%$ [148]. A value for $R(\pi^+/\pi^-)$ of $(5 \pm 2)\%$ may then be inferred from these bubble chamber experiments. A first theoretical approach considering two step processes concluded that even a 1% value for R could not be accounted for [149]; an updated value of 1.2% was given in ref. [150]. A plausible explanation for the high value of $R(\pi^+/\pi^-)$ in ${}^4_\Lambda$He was put forward in ref. [151]. It is pointed out that the wave function of the ${}^4_\Lambda$He hypernucleus has the unique property of having a large probability for a component with a virtual Σ^+. A virtual transition $\Lambda p \to \Sigma^+ n$ may occur, followed by a three-body mechanism of the type $\Sigma^+ + N \to N + n + \pi^+$, able to restore on-shell the full process $\Lambda N p \to N n n \pi^+$, thus sometimes referred to as nucleon-induced pionic emission. This hypothesis is further reinforced by the observation that the spectrum of π^+ emitted in the decay is roughly (owing to the poor statistics) flat, suggesting a predominant s-wave emission of the π^+, as expected from the three-body decay mechanism.

At this point we cannot refrain from observing that it is a further case for which the $S = -1$ $A = 4$ system exhibits unusual features. In this review it appears from the second and third items of sect. **4**˙2 that the lifetime of ${}^4_\Lambda$H is smaller by $\sim 30\%$ than that of the hyperisobar ${}^4_\Lambda$He, the last one being consistent with that of the free Λ, as expected. Afterwards, we pointed out in subsect. **5**˙3 that ${}^4_\Sigma$He is the only Σ hypernucleus till now identified, due to the suppression of the $\Sigma N \to \Lambda N$ conversion. In subsect. **5**˙5 we recalled the problem of the CSB, again explained by a large $\Sigma\Lambda$ coupling. A comprehensive theoretical approach accounting for all these anomalies would be welcome.

The NMWD of the light hypernuclei ${}^{4}_{\Lambda}$He and ${}^{5}_{\Lambda}$He in two-body channels is considered a rare process because of the large momentum transfer and of the possible two-step mechanisms involved. It can occur through the following reactions:

$$ {}^{4}_{\Lambda}\mathrm{He} \to d + d, \tag{28} $$

$$ {}^{4}_{\Lambda}\mathrm{He} \to p + t, \tag{29} $$

$$ {}^{4}_{\Lambda}\mathrm{He} \to n + {}^{3}\mathrm{He}, \tag{30} $$

and

$$ {}^{5}_{\Lambda}\mathrm{He} \to d + t. \tag{31} $$

Early observations of two-body NMWD of hypernuclei are very scarce and date back to bubble chamber and emulsion experiments [148, 152]. The only existing calculations for the ${}^{4}_{\Lambda}$He two-body NMWD rates was performed long ago in ref. [153] and only one theoretical evaluation for the expected decay rates of ${}^{5}_{\Lambda}$He exists [154].

More recently, the decays (25), (26) and (28) have been searched for [155] by taking advantage of the peculiar features of the FINUDA spectrometer described in sect. **3**: large solid angle coverage, good p.id. properties and good momentum resolution for charged particles. ${}^{4}_{\Lambda}$He was produced as hyperfragment following the interaction of a K^- with all the various stopping nuclear targets used in the data takings; a coincidence with a π^- of momentum larger than $200\,\mathrm{MeV}/c$ was required. ${}^{5}_{\Lambda}$He was isolated in the events from the ^{6,7}Li stopping targets using the narrow selections on the momentum spectra of π^- described in refs. [30, 123]. The reactions (25), (26) and (28) were identified by the b.t.b. topology of the final charged particles produced with typical high momenta ($p_d = 570\,\mathrm{MeV}/c$ for (28), $p_p = 508\,\mathrm{MeV}/c$ for (29) and $p_d = 597\,\mathrm{MeV}/c$ for (31)).

For reaction (31) a BR of $(2.8 \pm 1.4) \cdot 10^{-3}$ was obtained, in rough agreement with the theoretical expectation of two orders of magnitude less than Γ_{NM}. For reactions (28) and (29) yields averaged over all the used nuclear targets were reported: $Y({}^{4}_{\Lambda}\mathrm{He} \to d+d) = (2.82 \pm 0.62) \cdot 10^{-5}/K^-_{\mathrm{stop}}$, $Y({}^{4}_{\Lambda}\mathrm{He} \to p+t) = (5.42 \pm 3.43) \cdot 10^{-5}/K^-_{\mathrm{stop}}$. To have a guess of an order of magnitude of the BRs for the ${}^{4}_{\Lambda}$He rare decays, we may assume that the yield of production of ${}^{4}_{\Lambda}$He following the stopping of K^- in the nuclear targets is $10^{-2}/K^-_{\mathrm{stop}}$, taking the values for the yields of production of the mirror hyperfragment ${}^{4}_{\Lambda}$H [50]. BRs for the decays (28) and (29) should then also be two orders of magnitude smaller than Γ_{NM}.

There are no experiments planned on this item. However tens of events for the decays (28) and (29) can be expected to be observed in the CDC of the E22 experiment approved at J-PARC, mentioned in subsect. **6**˙10.

8. – Full pattern of the partial weak decay widths for some hypernuclei

8˙1. *Existing data for some s- and p-shell hypernuclei.* – We have seen that, at present, only for ${}^{12}_{\Lambda}$C there is an experimental full pattern of the partial WD widths, summarized in ref. [36]. In the various subsections of this review we have collected all the experimental data relevant to the different channels. It is clear that there is a nearly full absence of data for Γ_n/Γ_Λ, and data for $\Gamma_{\pi^0}/\Gamma_\Lambda$ are available only for ${}^{4}_{\Lambda}$He, ${}^{5}_{\Lambda}$He, ${}^{11}_{\Lambda}$B and ${}^{12}_{\Lambda}$C. This is not surprising since the neutral channels of the WD are the hardest to measure.

TABLE VI. – *Summary of WD amplitudes available for* ${}^{4}_{\Lambda}$He, ${}^{5}_{\Lambda}$He, ${}^{11}_{\Lambda}$B, ${}^{12}_{\Lambda}$C *hypernuclei for which* Γ_T/Γ_Λ, $\Gamma_{\pi^0}/\Gamma_\Lambda$, $\Gamma_{\pi^-}/\Gamma_\Lambda$, Γ_p/Γ_Λ *have been determined. The w.a. of values for* ${}^{4}_{\Lambda}$He *from refs.* [23,56] *are indicated in column 2; the values for* ${}^{5}_{\Lambda}$He, ${}^{11}_{\Lambda}$B, ${}^{12}_{\Lambda}$C *from ref.* [156] *are reported in columns 3, 4 and 5; the complete set of* Γ*'s obtained by ref.* [36] *for* ${}^{12}_{\Lambda}$C *is reported in column 6. See text for more details.*

	${}^{4}_{\Lambda}$He [23,56]	${}^{5}_{\Lambda}$He [156]	${}^{11}_{\Lambda}$B [156]	${}^{12}_{\Lambda}$C [156]	${}^{12}_{\Lambda}$C [36]
Γ_T/Γ_Λ	1.056 ± 0.076	0.962 ± 0.034	1.274 ± 0.072	1.241 ± 0.041	1.241 ± 0.041
$\Gamma_{\pi^-}/\Gamma_\Lambda$	0.304 ± 0.031	0.342 ± 0.015	0.228 ± 0.027	0.120 ± 0.014	0.123 ± 0.015
$\Gamma_{\pi^0}/\Gamma_\Lambda$	0.563 ± 0.051	0.201 ± 0.011	0.192 ± 0.056	0.1656 ± 0.0080	0.165 ± 0.008
Γ_p/Γ_Λ	0.167 ± 0.016	0.217 ± 0.041	0.47 ± 0.11	0.493 ± 0.088	0.45 ± 0.10
$\Gamma_{2N}/\Gamma_\Lambda$		0.078 ± 0.034	0.169 ± 0.077	0.178 ± 0.076	0.27 ± 0.13
Γ_n/Γ_Λ	$\leq 0.01^{+0.04}_{-0.01}$	0.125 ± 0.066	0.21 ± 0.16	0.28 ± 0.12	0.23 ± 0.08
Γ_n/Γ_p	$\leq 0.06^{+0.28}_{-0.06}$	0.58 ± 0.32	0.46 ± 0.37	0.58 ± 0.27	0.51 ± 0.14

We may then try to reconstruct the full pattern of the WD channels for these hypernuclei by evaluating Γ_n/Γ_Λ by difference with all the other widths. The errors inherent to this difference procedure are high, but we could check in any case if the results, in particular those on Γ_n/Γ_p, are consistent with the direct measurements (${}^{5}_{\Lambda}$He and ${}^{12}_{\Lambda}$C) and the theoretical evaluations. We will use the w.a. or the single values of Γ_T/Γ_Λ, $\Gamma_{\pi^-}/\Gamma_\Lambda$, $\Gamma_{\pi^0}/\Gamma_\Lambda$ and Γ_p/Γ_Λ given in tables I, II and III.

Table VI summarizes the results for ${}^{4}_{\Lambda}$He [23,56], ${}^{5}_{\Lambda}$He, ${}^{11}_{\Lambda}$B and ${}^{12}_{\Lambda}$C [156] in columns 2–5, respectively. Column 6 reports the results for ${}^{12}_{\Lambda}$C from ref. [36] for comparison.

Let us add a few comments on the results for each hypernucleus. For ${}^{4}_{\Lambda}$He a possible significant contribution of the $2N$-induced NMWD was excluded by both experiments [23] and [56]. Since a significant contribution from this process was found for the neighbour hypernucleus ${}^{5}_{\Lambda}$He by ref. [32], we tried to apply the same procedure to the proton spectra reported in refs. [23, 56]. However, due maybe to the higher threshold on the proton energy (30 MeV instead of 15 MeV) we did not find any appreciable contribution. A simple explanation for such an effect could be due to the fact that in both hypernuclei all the baryons lie in the s-state and this circumstance simplifies the discussion. We have already seen that the interaction with an (np) pair gives the main contribution. Thus by simple combinatorial arguments we may estimate that the $2N$-induced NMWD in ${}^{4}_{\Lambda}$He is reduced by a factor ~ 6 with respect to ${}^{5}_{\Lambda}$He.

For the upper limit on Γ_n/Γ_Λ and Γ_n/Γ_p of ${}^{4}_{\Lambda}$He we have reported in table VI the values from ref. [56], which are not directly measured but determined by fitting the experimental proton energy distribution to the simulated proton energy one with Γ_n/Γ_p as a free parameter. Higher values for the upper limits at 95% CL ($\Gamma_n/\Gamma_\Lambda \leq 0.035$, $\Gamma_n/\Gamma_p \leq 0.19$) were found in ref. [23] with a direct experimental procedure.

A first attempt to determine the full pattern of WD widths for ${}^{5}_{\Lambda}$He was done by ref. [22]. Γ_T/Γ_Λ, Γ_p/Γ_Λ, Γ_n/Γ_Λ and $\Gamma_{\pi^-}/\Gamma_\Lambda$ were directly measured, $\Gamma_{\pi^0}/\Gamma_\Lambda$ was inferred by difference; we recall that the existence of $\Gamma_{2N}/\Gamma_\Lambda$ was not yet anticipated theoretically at the time of the experiment. Due to this lack of information a value for $\Gamma_n/\Gamma_p = 0.93 \pm 0.55$ was calculated. Taking advantage of the very recent determination of $\Gamma_{2N}/\Gamma_\Lambda$ (27) and of the confirmation of the value of Γ_p/Γ_Λ, both reported in ref. [32],

it was possible to calculate Γ_n/Γ_Λ by difference [156] using eq. (17), making also use of the precise values of Γ_M/Γ_Λ given in table III. In conclusion, for the first time the full pattern of partial decay widths for WD of ${}^{5}_{\Lambda}$He, given in the second column of table VI was presented. A value $\Gamma_n/\Gamma_p = (0.64 \pm 0.33)$ is found, the large error being due to the subtraction procedure used in the determination of Γ_n/Γ_Λ. It is consistent with the value $(0.45 \pm 0.11_{\rm stat} \pm 0.03_{\rm sys})$ obtained with the direct measurement discussed in subsect. **6**·3 [119].

A first attempt to obtain all the partial decay widths for WD of ${}^{11}_{\Lambda}$B (and ${}^{12}_{\Lambda}$C) was performed by ref. [84]. However only $\Gamma_{\pi^-}/\Gamma_\Lambda$ and Γ_p/Γ_Λ were directly measured. Furthermore, the value for Γ_p/Γ_Λ was not corrected for FSI, as visible also in table III. The FSI correction may amount up to 100%, as it can be seen from eq. (21). The recent evaluation of Γ_p/Γ_Λ accounting for FSI and of $\Gamma_{2N}/\Gamma_\Lambda$ given in ref. [32], allowed to obtain for the first time [156] the full map of the partial decay widths for ${}^{11}_{\Lambda}$B reported in the third column of table VI. The values of Γ_n/Γ_Λ and consequently of Γ_n/Γ_p are affected by large errors. However it is encouraging the fact that the last one is consistent with the recent theoretical evaluation of 0.502 given by ref. [69].

In order to have a consistency check of the procedure adopted to determine the full pattern of WD widths for ${}^{5}_{\Lambda}$He and ${}^{11}_{\Lambda}$B, it was applied it also for ${}^{12}_{\Lambda}$C. Data from tables I, II, III, $\Gamma_{2N}/\Gamma_\Lambda$ from ref. [32] were used and Γ_n/Γ_Λ was obtained by subtraction. They are reported in column 5 of table VI. Column 6 gives the values reported by ref. [36]. An overall agreement within the errors is apparent and provides support for the validity of the method. Table VI summarizes then our present knowledge of the importance of the various WD widths for two Hypernuclei of the *s*-shell and two of the *p*-shell.

8·2. *Future experimental efforts*. – It would be very interesting to have a complete map of the partial decay widths for *s*- and *p*-shell hypernuclei with a precision on each channel better than or of the order of 5%. To our knowledge there are not at present plans for such an experimental program and we would like to discuss briefly a possible experiment able to achieve this goal by taking advantage of the major instrumental facilities existing or planned at J-PARC.

The production reaction of hypernuclei which seems more useful should be (π^+, K^+) at around 1.05–1.1 GeV/c in the forward direction, well known and exploited in past experiments. The spectrometer system ensuring a missing-mass selection with a resolution of the order of 2–3 MeV could be the old SKS or the new S-2S in construction [157]. The solenoidal CDC spectrometer [158] should be installed around the targets system, located along the beam axis, taking advantage from the internal hollow hole of the CDC, with a diameter of 16 cm. The purpose is that of obtaining the full pattern of the decay widths for ${}^{5}_{\Lambda}$He, ${}^{7}_{\Lambda}$Li, ${}^{9}_{\Lambda}$Be, ${}^{11}_{\Lambda}$B, ${}^{12}_{\Lambda}$C, ${}^{15}_{\Lambda}$N and ${}^{16}_{\Lambda}$O in a unique run.

The experience achieved with the FINUDA experiment will be quite helpful to the purpose. Only four nuclear targets will be necessary; as shown in ref. [31, 32], adequate selections on the excitation energy spectra obtained with ^{7}Li target allow to isolate ${}^{5}_{\Lambda}$He and ${}^{7}_{\Lambda}$Li, with ^{12}C target ${}^{11}_{\Lambda}$B and ${}^{12}_{\Lambda}$C, with ^{16}O target ${}^{15}_{\Lambda}$N and ${}^{16}_{\Lambda}$O. Since an important requirement will be that of a threshold as low as possible (15–20 MeV) for protons from NMWD, each target slab should not be thicker than 2 mm, and tilted by 15–20 degrees with respect to the beam axis, as done in previous experiments [26] in order to maximize the thickness seen by the beam particles and minimize that seen by the charged particles emitted in the decay. Three slabs for each ^{7}Li, ^{9}Be and ^{16}O (water or heavy water) will ensure a target thickness larger than 1 gr/cm^2 for hypernuclei production. Each of the nine thin slabs should be interleaved with eight 1 mm thick plastic CH_2 scintillators,

acting as active ^{12}C targets and allowing the identification of the slab in which the interaction occurred by means of $\mathrm{d}E/\mathrm{d}x$. Such an identification is necessary in case of WD with final neutral particles.

This venetian blind arrangement of targets should be no longer than 40 cm, compared with the 80 cm length of the CDC. An angular portion of the CDC (π or $4/3\pi$) should be used for the determination of the momenta of the charged particles (π^-, protons) by magnetic analysis in the 0.7 T field of the solenoid in which the detector is installed. They encounter on their path only the 1 mm thick CFRP cylinder of the inner wall of the CDC. The remaining angular portion of the inner hole of the CDC detector should be instrumented with a Pb converter about 1 radiation length thick for photons of ~ 100 MeV. The converter should be sandwiched between two layers of thin plastic scintillators; this arrangement would be able to identify the π^0 from MWD. The inner layer, with excellent timing properties, will permit the measurement of the lifetime of the different hypernuclei. This way Γ_T, Γ_{π^0}, Γ_{π^-}, Γ_p and Γ_{2N} will be directly measured, Γ_n determined indirectly by difference. A cross check on Γ_n would be obtained by the direct measurement of neutrons with the segmented plastic scintillator barrel enclosing the CDC. The detection efficiency will be low due to the reduced thickness (3 cm).

Let us calculate the order of magnitude of expected events and then the statistical precision (s.p.) that we may expect from such an arrangement. We assume for simplicity for all hypernuclei $\Gamma_T/\Gamma_\Lambda = 1.15$, $\Gamma_p/\Gamma_\Lambda = 0.5$, $\Gamma_n/\Gamma_\Lambda = 0.25$, $\Gamma_{2N}/\Gamma_\Lambda = 0.2$, $\Gamma_{\pi^-}/\Gamma_\Lambda = 0.1$, $\Gamma_{\pi^0}/\Gamma_\Lambda = 0.1$. We assume furthermore a beam intensity of 10^8 π^+/spill, which looks a realistic guess of the improvements of the machine in the forthcomings years from the present value of some 10^7 π^+/spill. We may then expect more than 10^4 hypernuclei/day produced in their ground or low-lying excited states, for each of the seven hypernuclear species above mentioned. Assuming realistic values for the solid angles and detection efficiencies, in 10 days of run we expect 10^4 protons from $1N$-induced NMWD (s.p. on Γ_p/Γ_Λ and on Γ_T/Γ_Λ of 1%), $\sim 4 \cdot 10^3$ protons from $2N$-induced NMWD (s.p. on $\Gamma_{2N}/\Gamma_\Lambda$ of 2%), $\sim 10^3$ π^- (s.p. on $\Gamma_{\pi^-}/\Gamma_\Lambda$ of 3%) $\sim 4 \cdot 10^2$ π^0 (s.p. on $\Gamma_{\pi^0}/\Gamma_\Lambda$ of 5%). By difference Γ_n/Γ_Λ could be deduced with a s.p. of 6%, comparable to the s.p. hopefully achievable with the direct detection of ~ 300 neutrons. The numbers on the expected statistical errors look quite comfortable, but great care should be devoted to the importance of possible systematic errors, mainly those related to the extraction of Γ_p/Γ_Λ and Γ_{2N}/Γ_p from the inclusive proton spectra, as described in subsects. **6**˙3 and **6**˙7.

9. – Asymmetry in NMWD of polarized hypernuclei

Hypernuclei can also be produced in polarized states [159, 160]. The production reaction (π^+, K^+) at 1.05 GeV/c with the π^+ selected at forward angles ($2^\circ \leq \theta_{K^+\mathrm{Lab}} \leq 15^\circ$) was the only one so far exploited to produce hypernuclear states with a substantial amount of spin-polarization, preferentially aligned with the axis normal to the reaction plane, usually referred to as polarization axis [161, 162]. The origin of hypernuclear polarization is twofold, as discussed in refs. [159, 160]. The distortions of the initial and final meson waves produce a small positive polarization of the hypernuclear orbital angular momentum up to production angles $\theta_{K^+\mathrm{Lab}} \leq 15^\circ$. At smaller angles the main source of polarization is due to the spin-flip interaction term in the elementary associated production reaction $\pi^+ n \to \Lambda K^+$, which interferes constructively with the spin–non-flip amplitude. In the typical kinematical configurations in which the experiments were carried out the polarization of the Λ spin in the free reaction is ~ 0.75. The distribution of nucleons (in particular protons, easier to detect) produced in $1N$-induced NMWD

of polarized hypernuclei shows an angular asymmetry. It is measured by the difference between the number of protons emitted along the polarization axis and that of the protons outgoing in the opposite direction. It was shown [163, 164] that the proton asymmetry is due to the interference between the parity-violating and parity-conserving $\Lambda N \to nN$ transition amplitudes with different values of the isospin of the final NN pair. Asymmetry studies could also provide the relative phases of the decay amplitudes, *i.e.* on the dynamics of the hypernuclear decay.

Experimentally the so-called asymmetry parameter $a_\Lambda^M(J)$ is given by

$$a_\Lambda^M(J) = \frac{1}{P_\Lambda(J)} \frac{I^M(0°, J) - I^M(180°, J)}{I^M(0°, J) + I^M(180°, J)}, \tag{32}$$

in which I^M is the observed proton intensity and $P_\Lambda(J)$ the polarization of the Λ spin in the Hypernucleus. It should be noticed that eq. (32) is an approximation of the exact expressions used to define the intrinsic asymmetry parameter a_Λ, which is not an observable due to FSI effects. A more complete discussion on this item may be found in ref. [15].

Measurements of $a_\Lambda^M(J)$ are very hard. In addition to all the difficulties mentioned in sect. **6** and to the large statistical error expected by the use of eq. (32) there is the further error linked to the determination of $P_\Lambda(J)$. All the experiments on the asymmetry of NMWD of polarized hypernuclei were performed at the KEK PS. The first attempt to measure $a_\Lambda^M(J)$ is due to the authors of ref. [161]. The quite large value of (-1.3 ± 0.4) was observed for NMWD of the polarized ${}^{11}_{\Lambda}\mathrm{B}$ and ${}^{12}_{\Lambda}\mathrm{C}$ hypernuclei by using the ${}^{12}\mathrm{C}(\pi^+, K^+)$ reaction at $1.05\,\mathrm{GeV}/c$. Triggered by this unexpected result a new experiment was carried out on the *s*-shell hypernucleus ${}^{5}_{\Lambda}\mathrm{He}$. The well known ${}^{6}\mathrm{Li}(\pi^+, K^+\mathrm{p}){}^{5}_{\Lambda}\mathrm{He}$ reaction at $1.05\,\mathrm{GeV}/c$ was used to produce polarized ${}^{5}_{\Lambda}\mathrm{He}$. The value for $P_\Lambda(J)$ was measured [165] by observing the asymmetric emission of π^- in its MWD and by assuming that the pion asymmetry in the MWD of ${}^{5}_{\Lambda}\mathrm{He}$ coincides with the value measured in the free $\Lambda \to \pi^- p$ decay. The observed polarization was consistent with a theoretical calculation [166]. The experimental value for the asymmetry parameter found finally [162] was (0.24 ± 0.22), *i.e.* positive and close to zero, in strong disagreement with the first result on the ${}^{11}_{\Lambda}\mathrm{B}$ and ${}^{12}_{\Lambda}\mathrm{C}$ hypernuclei.

This puzzling situation led to perform a further experimental effort at the KEK PS to measure the asymmetry parameter for ${}^{5}_{\Lambda}\mathrm{He}$ and ${}^{12}_{\Lambda}\mathrm{C}$ with improved accuracy. Since for ${}^{12}_{\Lambda}\mathrm{C}$ the small value of Γ_{π^-} and of the asymmetry parameter made a direct measurement of $P_\Lambda(J)$ very difficult, it was evaluated theoretically by a delicate analysis based on the Distorted-Wave Impulse Approximation [166, 167]. The final values for the asymmetry parameter [168, 169] are $(0.07 \pm 0.08_{\mathrm{stat}}{}^{+0.08}_{-0.00\mathrm{sys}})$ for ${}^{5}_{\Lambda}\mathrm{He}$ and $(-0.16 \pm 0.28_{\mathrm{stat}}{}^{+0.18}_{-0.00\mathrm{sys}})$ for ${}^{12}_{\Lambda}\mathrm{C}$, both consistent with zero.

A significant theoretical effort was done on the evaluation of the asymmetry parameter starting from the various assumptions developed for explaining the main features of NMWD, summarized in subsect. **6**˙5. A short account of the results from these efforts is given in ref. [15] and we recall here that most of them predicted quite large negative values for the asymmetry parameters of ${}^{5}_{\Lambda}\mathrm{He}$ and ${}^{12}_{\Lambda}\mathrm{C}$. Only the approaches based on chirally motivated two-pion-exchange mechanisms [133] and in particular a more recent and different one [170] based on the use of correlated meson-pair and on the exchange of the axial-vector a_1-meson were successful in predicting very low values for the asymmetry parameter. The difficulty in measuring such a vanishing small value of an observable

already difficult to be determined experimentally has discouraged the experimentalists to plan further experiments, to our knowledge.

10. – Summary and conclusions

After more than six decades from the discovery of hypernuclei we may assert that the full pattern of hypernuclear WDs is qualitatively understood from the experimental side. It took quite a long time due to the inherent difficulty of the experimentation, which couples technologies and methods typical of the high-energy physics with those typical of nuclear physics. A great help to this achievement was given by the constant interest and stimulus of the theoreticians, which elaborated detailed and precise predictions many years, often decades, in advance to the experimental observations. Hypernuclear physics may be considered as an outstanding proof of the validity of the close collaboration between experimentalists and theorists.

There are however still some items that remain not well understood and need experimental verification. The first one is related to the simplest inclusive observable of the hypernuclear WDs, the lifetime of a hypernucleus compared to the lifetime of the free Λ. For the hydrogen hyperisotopes ${}^{3}_{\Lambda}\mathrm{H}$ and ${}^{4}_{\Lambda}\mathrm{H}$ it is significantly lower than that of the free Λ, in contrast to what happens for the helium hyperisotopes ${}^{4}_{\Lambda}\mathrm{He}$ and ${}^{5}_{\Lambda}\mathrm{He}$, for which it coincides within the errors with that of the free Λ. At the opposite side of the mass number scale, the measured lifetime of heavy ($A > 200$) hypernuclei, though determined by indirect methods, seems significantly lower than the constant value observed for medium-A systems. For the hydrogen hyperisotopes running or planned experiments could provide an answer, for the heavy hypernuclei the direct measurements look hard but feasible. However they are not yet proposed.

Another long standing problem (five decades!) in hypernuclear physics is a possible violation of the $\Delta I = 1/2$ rule in the NMWD of hypernuclei. The present data on the $1N$-induced NMWD of s-shell Hypernuclei, affected by large errors, did not provide a convincing answer to this interesting item. A long range program is planned at J-PARC to clarify in an unambiguous way the situation (experiment P22).

A third hot point is the determination of the $2N$-induced NMWD width with a reduced error. The introduction of such a decay channel was essential for the solution of the long-standing puzzle of the Γ_n/Γ_p value. Different experimental approaches have verified the existence of such a process, however with huge errors (larger than 40%). An experiment at J-PARC, P18, has been approved and will run soon with the aim of measuring the $2N$-induced NMWD width for the typical hypernucleus ${}^{12}_{\Lambda}\mathrm{C}$ with a precision of 10%.

One could think that the completion of these experiments would be the end of the experimentation on the hypernuclear WD, since they will allow a reasonable understanding of the process. The file could be closed. However another way of thinking could be that it is the starting point for another campaign of experiments. In all research or review papers on WD of hypernuclei (including the present one) it is stated, more or less with the same words, that the NMWD of hypernuclei is the unique physical process able to give information on the four baryon weak interaction. This new file has to be open. Theorists and experimentalists should define, on the grounds of the knowledge so far acquired, which are the systems to be considered and the observables to be measured and at which precision to give a convincing answer to the above fundamental question. From the experimental side the J-PARC accelerator complex and associated detector facilities looks adequate to achieve this goal.

* * *

We are grateful to Prof. A. Bettini for the opportunity of summarizing the present situation about experimental studies on hypernuclei weak decays.

REFERENCES

[1] Rochester G. D. and Butler C. C., *Nature*, **160** (1947) 855.
[2] Nambu Y., Nishijima K. and Yamaguchi Y., *Prog. Theor. Phys.*, **6** (1951) 615.
[3] Pais A., *Phys. Rev.*, **86** (1952) 663.
[4] Danysz M. and Pniewski J., *Philos. Mag.*, **44** (1953) 348.
[5] Gell-Mann M., *Phys. Rev.*, **92** (1953) 833.
[6] Hashimoto O. and Tamura T., *Prog. Part. Nucl. Phys.*, **57** (2006) 564.
[7] Millener D. J., *Lect. Notes Phys.*, **724** (2007) 31.
[8] Tamura H. *et al.*, *Nucl. Phys. A*, **835** (2010) 3.
[9] Cheston W. and Primakoff H., *Phys. Rev.*, **92** (1953) 1537.
[10] Cohen J., *Prog. Part. Nucl. Phys.*, **25** (1990) 139.
[11] Alberico W. M. and Garbarino G., *Phys. Rep.*, **369** (2002) 1.
[12] Alberico W. M. and Garbarino G., in *Proceedings of the International School of Physics "Enrico Fermi", Course CLVIII "Hadron Physics"* edited by Bressani T., Wiedner U. and Filippi A. (IOS Press, Amsterdam; SIF, Bologna) 2005, p. 125.
[13] Outa H., in *Proceedings of the International School of Physics "Enrico Fermi", Course CLVIII "Hadron Physics"* edited by Bressani T., Wiedner U. and Filippi A. (IOS Press, Amsterdam; SIF, Bologna) 2005, p. 219.
[14] Parreno A., *Lect. Notes Phys.*, **724** (2007) 141.
[15] Botta E., Bressani T. and Garbarino G., *Eur. Phys. J. A*, **48** (2012) 41.
[16] Particle Data Group (Olive K. A. *et al.*), *Chin. Phys. C*, **30** (2014) 090001.
[17] Alberico W. M., De Pace A., Ericson M. and Molinari A., *Phys. Lett. B*, **256** (1991) 134.
[18] Bauer E. and Garbarino G., *Nucl. Phys. A*, **828** (2009) 29.
[19] Bauer E. and Garbarino G., *Phys. Rev. C*, **81** (2010) 064315.
[20] Bressani T., in *Advances in Nuclear Physics and Related Areas*, edited by Lalazzisis G. and Massen S. E. (Art of Text, Thessaloniki) 2005, p. 94.
[21] Bressani T., in *Proceedings of the International School of Physics "Enrico Fermi", Course CLXVII "Strangeness and Spin in Fundamental Physics"* edited by Anselmino M., Bressani T., Feliciello A. and Ratcliffe Ph. G. (SIF, Bologna and IOS Press, Amsterdam) 2008, p. 3.
[22] Szymanski J. J. *et al.*, *Phys. Rev. C*, **43** (1991) 849.
[23] Parker J. D. *et al.*, *Phys. Rev. C*, **76** (2007) 035501.
[24] Fukuda T. *et al.*, *Nucl. Instrum. Methods A*, **361** (1995) 485.
[25] Hotchi H. *et al.*, *Phys. Rev. C*, **64** (2001) 044302.
[26] Sato Y. *et al.*, *Phys. Rev. C*, **71** (2005) 025203.
[27] Tamura H. *et al.*, *Prog. Theor. Phys. Suppl.*, **117** (1994) 1.
[28] FINUDA Collaboration (Agnello M. *et al.*), *Phys. Lett. B*, **622** (2005) 35.
[29] Feliciello A., *Riv. Nuovo Cimento*, **32** (2009) 147.
[30] FINUDA Collaboration (Agnello M. *et al.*), *Phys. Lett. B*, **681** (2009) 139.
[31] FINUDA Collaboration (Agnello M. *et al.*), *Phys. Lett. B*, **701** (2011) 556.
[32] FINUDA Collaboration (Agnello M. *et al.*), *Phys. Lett. B*, **738** (2014) 499.
[33] FINUDA Collaboration (Agnello M. *et al.*), *Phys. Rev. Lett.*, **94** (2005) 212303.
[34] FINUDA Collaboration (Agnello M. *et al.*), *Nucl. Phys. A*, **775** (2006) 35.
[35] FINUDA Collaboration (Agnello M. *et al.*), *Phys. Rev. Lett.*, **108** (2012) 042501.
[36] Bhang H. *et al.*, *J. Kor. Phys. Soc.*, **59** (2011) 1461.
[37] Juric M. *et al.*, *Nucl. Phys. B*, **52** (1973) 1.
[38] Prem R. J. and Steinberg P. H., *Phys. Rev.*, **136** (1964) B1803.

[39] Keyes G. *et al.*, *Phys. Rev. Lett.*, **20** (1968) 819.
[40] Phillips R. E. and Schneps J., *Phys. Rev.*, **180** (1969) 1307.
[41] Bohm G. *et al.*, *Nucl. Phys. B*, **16** (1970) 46.
[42] Block M. M. *et al.*, *Proceedings of the Siena International Conference on Elementary Particles*, 1963, edited by Bernardini G. and Puppi G. P. (Editrice Compositori, Bologna) 1963, p. 62.
[43] Keyes G. *et al.*, *Phys. Rev. D*, **1** (1970) 66.
[44] Keyes G. *et al.*, *Nucl. Phys. B*, **67** (1973) 269.
[45] Avramenko S. *et al.*, *Nucl. Phys. A*, **547** (1992) 95c.
[46] STAR Collaboration, *Science*, **328** (2010) 58.
[47] Rappold C. *et al.*, *Nucl. Phys. A*, **913** (2013) 170.
[48] Rappold C. *et al.*, *Phys. Lett. B*, **728** (2014) 543.
[49] Zhu Y., *Nucl. Phys. A*, **904** (2013) 551c.
[50] Tamura H. *et al.*, *Phys. Rev. C*, **40** (1989) R479.
[51] Crayton N. *et al.*, *Proceedings of the 11th International Conference on High Energy Physics, CERN* (1962), p. 460.
[52] Kang Y. W. *et al.*, *Phys. Rev.*, **139** (1965) B401.
[53] Outa H. *et al.*, *Nucl. Phys. A*, **547** (1992) 109c.
[54] Outa H. *et al.*, *Nucl. Phys. A*, **585** (1995) 109c.
[55] FINUDA Collaboration (Agnello M. *et al.*and Gal A.), *Nucl. Phys. A*, **881** (2012) 269.
[56] Outa H. *et al.*, *Nucl. Phys. A*, **639** (1998) 251c.
[57] Kameoka S. *et al.*, *Nucl. Phys. A*, **754** (2005) 173.
[58] Grace R. *et al.*, *Phys. Rev. Lett.*, **55** (1985) 1055.
[59] Bandō H., Yamada T. and Žofka J., *Phys. Rev. C*, **36** (1987) 1640.
[60] Bhang H. C. *et al.*, *Nucl. Phys. A*, **639** (1998) 269c.
[61] Park H. *et al.*, *Phys. Rev. C*, **61** (2000) 054004.
[62] Nield K. J. *et al.*, *Phys. Rev. C*, **13** (1976) 1263.
[63] Noga V. I. *et al.*, *Sov. J. Nucl. Phys.*, **43** (1986) 856.
[64] Armstrong T. A. *et al.*, *Phys. Rev. C*, **47** (1993) 1957.
[65] Cassing W. *et al.*, *Eur. Phys. J. A*, **16** (2003) 549.
[66] Metag V. *et al.*, *Nucl. Instrum. Methods*, **114** (1974) 445.
[67] Ramos A., Oset E. and Salcedo L. L., *Phys. Rev. C*, **50** (1994) 2314.
[68] Itonaga K. *et al.*, *Nucl. Phys. A*, **639** (1998) 329c.
[69] Itonaga K. and Motoba T., *Prog. Theor. Phys. Suppl.*, **185** (2010) 252.
[70] Motoba T. and Itonaga K., *Prog. Theor. Phys. Suppl.*, **117** (1994) 477.
[71] Ajimura S. *et al.*, *J-PARC proposal*, **P22** (2006) http://j-parc.jp/researcher/Hadron/en/Proposal_e.html.
[72] Dohrmann F. *et al.*, *Phys. Rev. Lett.*, **93** (2004) 242501.
[73] Garibaldi F. *et al.*, *Nucl. Phys. A*, **914** (2013) 34.
[74] Nakamura S. N., *EPJ Web of Conferences*, **66** (2014) 01020.
[75] Cotanch S. R. and Hsiao S. S., *Nucl. Phys. A*, **450** (1986) 419.
[76] Lea R. for the ALICE Collaboration, *Nucl. Phys. A*, **914** (2013) 415.
[77] ALICE Collaboration (J. Adam *et al.*), arXiv:1506.08453.
[78] ALICE Collaboration (Abelev B. *et al.*), *J. Phys. G*, **41** (2014) 087002.
[79] ALICE Collaboration (Abelev B. *et al.*), *J. Phys. G*, **41** (2014) 087001.
[80] Ajimura S. *et al.*, *Nucl. Phys. A*, **585** (1995) 173.
[81] Sakaguchi A. *et al.*, *Phys. Rev. C*, **43** (1991) 73.
[82] Okada S. *et al.*, *Nucl. Phys. A*, **754** (2005) 178.
[83] Montwill A. *et al.*, *Nucl. Phys. A*, **234** (1974) 413.
[84] Noumi H. *et al.*, *Phys. Rev. C*, **52** (1995) 2936.
[85] Dalitz R. H., *Phys. Rev.*, **112** (1958) 605.
[86] Davis D. H., *Nucl. Phys. A*, **754** (2005) 3.
[87] Bandō H. and Takaki H., *Prog. Theor. Phys.*, **72** (1984) 106.
[88] Bandō H. and Takaki H., *Phys. Lett. B*, **150** (1985) 409.

[89] Oset E. and Salcedo L. L., *Nucl. Phys. A*, **443** (1985) 704.
[90] Oset E. *et al.*, *Phys. Rep.*, **188** (1990) 79.
[91] Motoba T., Itonaga K. and Bandō H., *Nucl. Phys. A*, **489** (1988) 683.
[92] Motoba T., Bandō H., Fukuda T. and Žofka J., *Nucl. Phys. A*, **534** (1991) 597.
[93] Bandō H., Motoba T. and Žofka J., in *Perspectives of Meson Science* edited by Yamazaki T. T., Nakai K. and Nagamine K. (North Holland, Amsterdam) 1992, p. 571.
[94] Gal A., *Nucl. Phys. A*, **828** (2009) 72.
[95] Motoba T., *Nucl. Phys. A*, **547** (1992) 115.
[96] Kumagai-Fuse L., Okabe S. and Akaishi Y., *Phys. Lett. B*, **345** (1995) 386.
[97] Hayano R. S. *et al.*, *Phys. Lett. B*, **231** (1989) 355.
[98] Outa H. *et al.*, *Prog. Theor. Phys. Suppl.*, **117** (1994) 177.
[99] Nagae T. *et al.*, *Phys. Rev. Lett.*, **80** (1998) 1605.
[100] Oset E. *et al.*, *Prog. Theor. Phys. Suppl.*, **117** (1994) 461.
[101] Cohen D. and Kurath S., *Nucl. Phys.*, **73** (1965) 1.
[102] Cohen D. and Kurath S., *Nucl. Phys. A*, **101** (1967) 1.
[103] Sasao J. *et al.*, *Phys. Lett. B*, **579** (2004) 258.
[104] Millener D. J., *Nucl. Phys. A*, **804** (2008) 84.
[105] Ukai M. *et al.*, *Phys. Rev. C*, **77** (2008) 054315.
[106] Davis D. H. *et al.*, *Nucl. Phys.*, **41** (1963) 73.
[107] Tang L. *et al.*, *Exp. Proposal*, **E-08-012** (Jefferson Lab.) 2007.
[108] Tang L., *Int. J. Mod. Phys. E*, **19** (2010) 2638.
[109] A1 Collaboration (Blomqvist K. I. *et al.*), *Nucl. Instrum. Methods Phys. Res. A*, **403** (1998) 263.
[110] A1 Collaboration (Achenbach P. *et al.*), *Eur. Phys. J. ST*, **198** (2011) 307.
[111] A1 Collaboration (Esser A. *et al.*), *Phys. Rev. Lett.*, **114** (2015) 232501.
[112] Hashimoto O. *et al.*, *Phys. Rev. Lett.*, **88** (2000) 042503.
[113] Ramos A., Vicente-Vacas M. J. and Oset E., *Phys. Rev. C*, **55** (1997) 735.
[114] Ramos A., Vicente-Vacas M. J. and Oset E., *Phys. Rev. C*, **66** (2002) 039903.
[115] CERN Program Library Entry W5013, GEANT.
[116] Kim J. H. *et al.*, *Phys. Rev. C*, **68** (2003) 065201.
[117] Okada S. *et al.*, *Phys. Lett. B*, **597** (2004) 249.
[118] Garbarino G., Parreno A. and Ramos A., *Phys. Rev. C*, **69** (2004) 054603.
[119] Kang B. H. *et al.*, *Phys. Rev. Lett.*, **96** (2006) 062301.
[120] Kim M. J. *et al.*, *Phys. Lett. B*, **641** (2006) 28.
[121] Bauer E., Garbarino G., Parreno A. and Ramos A., *Nucl. Phys. A*, **836** (2010) 199.
[122] Kim M. *et al.*, *Phys. Rev. Lett.*, **103** (2009) 182502.
[123] FINUDA Collaboration (Agnello M. *et al.*), *Nucl. Phys. A*, **804** (2008) 151.
[124] FINUDA Collaboration (Agnello M. *et al.* and Garbarino G.), *Phys. Lett. B*, **685** (2010) 247.
[125] Bufalino S., *Nucl. Phys. A*, **914** (2013) 160.
[126] Block M. M. and Dalitz R. H., *Phys. Rev. Lett.*, **11** (1963) 96.
[127] Barclay Adams J., *Phys. Rev.*, **156** (1967) 1611.
[128] McKellar B. J. H. and Gibson B. F., *Phys. Rev. C*, **30** (1984) 322.
[129] Dubach J. F., *Nucl. Phys. A*, **450** (1986) 71.
[130] Parreno A., Ramos A. and Bennhold C., *Phys. Rev. C*, **56** (1997) 339.
[131] Parreno A. and Ramos A., *Phys. Rev. C*, **65** (2002) 015204.
[132] Jido D., Oset E. and Palomar J. E., *Nucl. Phys. A*, **694** (2001) 525.
[133] Chumillas C., Garbarino G., Parreno A. and Ramos A., *Phys. Lett. B*, **657** (2007) 180.
[134] Itonaga K., Ueda T. and Motoba T., *Phys. Rev. C*, **65** (2002) 034617.
[135] Cheung C. Y., Heddle D. P. and Kisslinger L. S., *Phys. Rev. C*, **27** (1983) 335.
[136] Heddle D. P. and Kisslinger L. S., *Phys. Rev. C*, **33** (1986) 608.
[137] Inoue T., Oka M., Motoba T. and Itonaga K., *Nucl. Phys. A*, **633** (1998) 312.
[138] Sasaki K., Inoue T. and Oka M., *Nucl. Phys. A*, **669** (2000) 331.

[139] Sasaki K., Inoue T. and Oka M., *Nucl. Phys. A*, **678** (2000) 455.
[140] Sasaki K., Izaki M. and Oka M., *Phys. Rev. C*, **71** (2005) 035502.
[141] Schumacher R. A., *Nucl. Phys. A*, **547** (1992) 143.
[142] Alberico W. M. and Garbarino G., *Phys. Lett. B*, **486** (2000) 362.
[143] Bhang H. *et al.*, *Eur. Phys. J. A*, **33** (2007) 259.
[144] FINUDA Collaboration (Agnello M. *et al.*), *Nucl. Phys. A*, **881** (2012) 322.
[145] Bhang H. *et al.*, *J-PARC proposal*, **P18** (2006) http://j-parc.jp/researcher/Hadron/en/Proposal_e.html.
[146] Mayeur C. *et al.*, *Nuovo Cimento*, **44** (1966) 698.
[147] Bohm G. *et al.*, *Nucl. Phys. B*, **9** (1969) 1.
[148] Keyes G. *et al.*, *Nuovo Cimento A*, **31** (1976) 401.
[149] Dalitz R. H. and von Hippel F., *Nuovo Cimento*, **34** (1964) 799.
[150] Cieply A. and Gal A., *Phys. Rev. C*, **55** (1997) 2715.
[151] Gibson B. F. and Timmermans R., *Nucl. Phys. A*, **639** (1998) 341c.
[152] Coremans G. *et al.*, *Nucl. Phys. B*, **16** (1970) 209.
[153] Rayet M., *Nuovo Cimento B*, **42** (1966) 238.
[154] Thurnauer P. G., *Nuovo Cimento*, **26** (1962) 869.
[155] FINUDA Collaboration (Agnello M. *et al.*), *Nucl. Phys. A*, **835** (2010) 439.
[156] Botta E., Bressani T., Bufalino S. and Feliciello A., *Phys. Lett. B*, **748** (2015) 86.
[157] Nagae T., *Few-Body Sys.*, **54** (2013) 785.
[158] Agari K. *et al.*, *Prog. Theor. Exp. Phys.*, **2012** (2012) 02B011.
[159] Bandō H., Motoba T., Sotona M. and Žofka J., *Phys. Rev. C*, **39** (1989) 587.
[160] Kishimoto T., Ejiri H. and Bandō H., *Phys. Lett. B*, **232** (1992) 24.
[161] Ajimura S. *et al.*, *Phys. Lett. B*, **282** (1992) 293.
[162] Ajimura S. *et al.*, *Phys. Rev. Lett.*, **84** (2000) 4052.
[163] Bandō H., Motoba T. and Žofka J., *Int. J. Mod. Phys. A*, **5** (1990) 4021.
[164] Nabetani H., Ogaito T., Sato T. and Kishimoto T., *Phys. Rev. C*, **60** (1999) 017001.
[165] Ajimura S. *et al.*, *Phys. Rev. Lett.*, **80** (1998) 3471.
[166] Itonaga K., Motoba T., Richter O. and Sotona M., *Phys. Rev. C*, **49** (1994) 1045.
[167] Motoba T. and Itonaga K., *Nucl. Phys. A*, **577** (1994) 293c.
[168] Maruta T. *et al.*, *Nucl. Phys. A*, **754** (2005) 168.
[169] Maruta T. *et al.*, *Eur. Phys. J. A*, **33** (2007) 255.
[170] Itonaga K., Motoba T., Ueda T. and Rijken Th. A., *Phys. Rev. C*, **77** (2008) 044605.